# FLOOD PROPAGATION ASSESSMENT FOR DEVELOPING A LOCATION-SPECIFIC FLOOD FORECASTING METHODOLOGY IN A FLOODPLAIN

by

**ASHIK IQBAL**

MASTER OF SCIENCE IN WATER RESOURCES DEVELOPMENT

Institute of Water and Flood Management

BANGLADESH UNIVERSITY OF ENGINEERING AND TECHNOLOGY

November 2021

**Flood Propagation Assessment for Developing a Location-Specific Flood Forecasting Methodology in a Floodplain**

A Thesis submitted by

**ASHIK IQBAL**

Student ID: 1018282024

Session: October 2018

In partial fulfillment of the requirements for the degree of

**MASTER OF SCIENCE IN WATER RESOURCES DEVELOPMENT**



Institute of Water and Flood Management

BANGLADESH UNIVERSITY OF ENGINEERING AND TECHNOLOGY

November 2021

**BANGLADESH UNIVERSITY OF ENGINEERING AND TECHNOLOGY**

**INSTITUTE OF WATER AND FLOOD MANAGEMENT**

The thesis titled "**Flood Propagation Assessment for Developing a Location-Specific Flood Forecasting Methodology in a Floodplain**" submitted by Ashik Iqbal, Roll No: 1018282024, Session: October 2018, has been accepted as satisfactory in partial fulfillment of the requirement for the degree of Master of Science in Water Resources Development on 27 November, 2021.
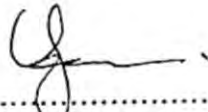
**BOARD OF EXAMINERS**

.......................................
Dr. Mohammad Shahjahan Mondal
Professor
Institute of Water and Flood Management, BUET, Dhaka-1000.
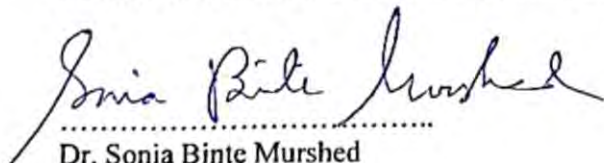
Chairman

(Supervisor)

.......................................
Dr. Mohammad Shahjahan Mondal
Professor and Director
Institute of Water and Flood Management, BUET, Dhaka-1000.

Member

(Ex-Officio)

.......................................
Dr. Muhammad Shah Alam Khan
Professor
Institute of Water and Flood Management, BUET, Dhaka-1000.

Member

.......................................
Dr. Sonia Binte Murshed
Assistant Professor
Institute of Water and Flood Management, BUET, Dhaka-1000.

Member

.......................................
Dr. Robin Kumar Biswas
Superintending Engineer
Bangladesh Water Development Board,72 Green Road, Dhaka-1215.

Member

(External)

ii

# CANDIDATE'S DECLARATION

It is hereby declared that this thesis or any part of it has not been submitted elsewhere for the award of any degree or diploma.

……………………..

(Ashik Iqbal)

Student ID: 1018282024

Session: October 2018

Date: 27 November 2021

*Dedicated*

*to*

*MY BELOVED FAMILY*

# ACKNOWLEDGEMENT

# ABSTRACT

Monsoon flooding inundates a substantial part of Bangladesh, where 80% of the areas are floodplains. Sirajganj, located beside the Jamuna River in northwestern Bangladesh, is home to many communities living in the low-lying unprotected floodplains. The Ranigram village of Sirajganj has a hydraulic connection with the Jamuna River and is flooded almost every year. Proper assessment of the flooding process in inundated areas is a prerequisite for appropriate flood forecasting. The Flood Forecasting and Warning Center (FFWC) of the Bangladesh Water Development Board (BWDB) provides information on the river stage at some locations along the major rivers in Bangladesh. FFWC provides the forecasts by rainfall-runoff modeling and one-dimensional (1D) hydrodynamic modeling using MIKE 11 software which does not provide any flood information for the floodplain localities. Consequently, people of the localities cannot take necessary precautions before the floodwater enters their localities as they do not get any proper location-specific forecasts. This study explores how flood propagates in the floodplain, determines the water level variation in the floodplain concerning the Jamuna River stage, and develops a 2D model to forecast the flood in the floodplain of a riverside area in Sirajganj where there is an interaction between the locality and the river.

Water level gauges were installed at strategically selected locations in Ranigram, and flood data were collected during the 2018 and 2020 monsoons. A statistical equation of floodplain water level is derived from the river water level for the 2018 data and is validated with the observed data of 2020. With the $R^2$, NSE, MSE and RMSE analyses, the observed floodwater level in Ranigram shows an excellent dynamic relation with the water level at Sirajganj on the Jamuna River. A 2D hydrodynamic model is developed with HEC-RAS using a high-resolution Digital Terrain Model (DTM) generated with surveyed bathymetry and Unmanned Aerial Vehicle (UAV)-based data, and is calibrated and validated with the observed water level data and satellite-based flood images. The model performance is also assessed with globally available WorldDEM$^{TM}$, ALOS PALSAR, SRTM, MERIT and ASTER Digital Elevation Models (DEMs). The 2D model incorporated with high-resolution UAV-based DTM is found to better represent the flood scenario in the locality. The results of the flood arrival time, duration, maximum flood extent and depth are extracted from the model. In the 2D model, the boundary condition is developed from the FFWC's forecasted water level in the Jamuna River and

the result of the model represents the forecasted flood scenario in the Ranigram area for the corresponding FFWC forecast. This developed methodology can be helpful in forecasting floods in any riverside locality using the FFWC forecasted data. It will thus help the local people to take the necessary precautions before floodwater enters their lands. Furthermore, the outcomes of this study will be helpful in forecasting and assessing flood risk and damage for the floodplain areas.

# TABLE OF CONTENTS

# LIST OF FIGURES

# LIST OF TABLES

# ABBREVIATION AND ACRONYM

| | |
|---|---|
| BMD | Bangladesh Meteorological Department |
| BWDB | Bangladesh Water Development Board |
| FFWC | Flood Forecasting and Warning Center |
| LGED | Local Government Engineering Department |
| NGO | Non-Governmental Organization |
| RIMES | Regional Integrated Multi-hazard Early Warning System |
| FAP | Flood Action Plan |
| FC | Flood Control |
| FCD | Flood Control and Drainage |
| G-K Project | Ganges-Kobadak Irrigation Project |
| DND | Dhaka-Narayanganj-Demra Project |
| UP | Union Parishad |
| RL | Reduced Level |
| USACE | United States Army Corps of Engineers |
| HEC | Hydrologic Engineering Centre |
| HEC-RAS | Hydrologic Engineering Center - River Analysis System |
| ESRI | Environmental Systems Research Institute |
| USGS | United States Geological Survey |
| NASA | National Aeronautics and Space Administration |
| ASF | Alaska Satellite Facility |
| GIS | Geographic Information System |
| RS | Remote Sensing |
| SAR | Synthetic Aperture Radar |
| 1D | One Dimensional |
| 2D | Two Dimensional |
| TIN | Triangulated Irregular Network |
| DEM | Digital Elevation Model |
| DTM | Digital Terrain Model |
| DSM | Digital Surface Model |
| SRTM | Shuttle Radar Topography Mission |

| | |
|---|---|
| ALOS | Advanced Land Observing Satellite |
| MERIT | Multiple-Error-Removed-Improved-Terrain |
| ASTER | Advanced Spaceborne Thermal Emission and Reflection Radiometer |
| UAV | Unmanned Aerial Vehicle |
| RTC | Radiometric Terrain Correction |
| PWD | Public Works Datum |
| GCP | Ground Control Points |
| WGS84 | World Geodetic System |
| NSE | Nash Sutcliffe Efficiency |
| MAE | Mean Absolute Error |
| RMSE | Root Mean Square Error |

# CHAPTER ONE
## INTRODUCTION

## 1.1 Background of the Study

Bangladesh has 80% of floodplain land area that is considered flood-prone, and in average flood years, about 20% of the land area (31,000 km$^2$) is flooded (Mirza, 2002). Monsoon flooding from the river inundates a substantial part, especially the northern part of Bangladesh, every year from early July to late September (Khan, 2008). Many communities reside in the low topographical non-protected area of the riverside that is flooded by the river overtopping water. Such communities are entirely exposed and vulnerable even to flood events with low associated return periods. They are the first to be affected during floods and cannot take enough precautions before the floodwater enters the locality (Mirza, 2002). The people of these areas often build their houses on elevated mounds as an indigenous technique to save their houses from flood exposure (Brammer, 2010).

Due to climate change and riverbed siltation, flood events are becoming increasingly unpredictable and severe every year, and so the historical practice of living with water is being threatened by rising flood impacts (Biswas, 2008; Mondal et al., 2018). In addition, the encroachment of wetlands and floodplains and the inadequate drainage capacity may increase the flood process's severity at the local level (Islam et al., 2010; Miller and Hutchins, 2017; Avinash, 2014). Bangladesh faces many challenges in flood management (Ali et al., 2018), where the implementation gap and poor planning and design of flood mitigation measures make the management system inadequate and ineffective (Vaz, 2000; Brammer, 2010). Nevertheless, a proper assessment of flooding is first necessary for selecting and taking effective measures.

One of the most efficient non-structural flood impact mitigation measures is flood forecasting and early warning systems (Subramanya, 2008). Proper assessment of the flooding process in inundated areas is a prerequisite for proper flood forecasting. The Flood Forecasting and Warning Center (FFWC) of the Bangladesh Water Development Board (BWDB) provides information on the river stage at critical locations along the

major rivers in Bangladesh. The FFWC has developed danger levels for different locations to indicate the magnitudes of the expected flood conditions (FFWC, 2018). FFWC provides forecasts by rainfall-runoff modeling and 1-D hydrodynamic modeling using MIKE 11 software (FFWC, 2018). These forecasted water levels primarily indicate major events when evacuation and temporary relocation might be needed.

Sirajganj Sadar Upazila (sub-district) has hydraulic interaction with the Jamuna River and is flooded every year due to the overtopping of the river (Islam et al., 2010). Many riverside areas and communities are not considered for protection from flooding with the embankment, and they suffer from the loss of houses and livelihoods (Ali et al., 2018). The flood information provided by FFWC is only based on the river stage, but there is no flood information for the locality. People of the locality do not get any proper location-specific flood information with indicative lead time. Nevertheless, better insight into the flood extent and depth distribution in the area is essential for safety that impacts livelihoods since insight into local flood conditions is essential for appropriate responses (Hassan and Shah, 2008). If the flood propagation process is appropriately understood, the consequent hazards for the flood in the locality can be forecasted; thus, the necessary measures can be taken.

Two-dimensional hydrodynamic modeling is an effective method for gaining insight into the propagation of floods (Meire et al., 2010). The 2D flood modeling is useful for representing mixed flow regimes, highly dynamic food waves, abrupt contraction and expansions, tidally influenced conditions, general wave propagation modeling, and super-elevation around bends (HEC, 2018). The 2D flood model requires an accurate representation of the floodplain and is sensitive to the quality of the utilized Digital Elevation Model (DEM) (Saksena and Merwade, 2015; Jain et al., 2018). Such models typically rely on remote sensing data with subsequent coarse digital elevation models (Rahman 2015; Jain et al. 2018; Masood and Takeuchi, 2011). Such practices are adequate for predicting the flood extent for relatively large areas (Jain et al., 2018; Yalcin, 2020) but often lack the level of details needed for sub-critical floods at the scale of local communities.

In order to fulfill the gaps and use for forecasting, a fit-for-purpose flood modeling should be developed at a level of detail that can give accurate flood information fulfilling the needs of local end-users.

**1.2  Objectives of the Study**

The main objective of this study is to analyze floods and develop a flood propagation model to forecast flood in the floodplain of a riverside area where there is an interaction between the locality and the river.

The specific objectives of the study are:

1. To find out the flood propagation in a floodplain of the Jamuna River through statistical relation with the river stage.
2. To develop a two-dimensional hydrodynamic model of flood propagation and calibrate and validate the model.
3. To simulate floods with different types and resolutions of DEMs for getting a more reliable model that can be useful for forecasting floods in the locality.

**1.3  Rationale of the Study**

The present FFWC forecasting information can provide a picture of the flood risk in the river, but cannot provide location-specific forecasts in the community. Most people in the riverside locality are not educated to analyze the river forecast into their community forecasting (Ali et al., 2018). The location-specific forecast will help them to decide when to cut the crop, when to evacuate their houses, etc. Many 2D modeling approaches have been undertaken, which mostly cannot provide detailed information because of its low-resolution data. So, with high-resolution data, a fit-for-purpose flood model is very much necessary for the vulnerable riverside community.

Thus, this study is expected to provide a methodology on how current FFWC's river forecasts by combining a two-dimensional hydrodynamic model can be useful for forecasting floods at the local level. This methodology can be used anywhere in the floodplain and the location-specific forecasting will help the local people and authorities to carry out flood management measures and programs more effectively.

## 1.4    Limitations of the study

The regular floodwater depth collection in the floodplain was a big challenge during the 2020 flood season, and hence there was less frequent data for model validation. The char area in between Ranigram and the Jamuna River is not considered in the HEC-RAS model. As it was very costly to create high-resolution Unmanned Aerial Vehicle (UAV)-based Digital Terrain Model (DTM) for large areas, the char area, which does not have any intervention or abrupt topographical features, was not considered in the study. If we can afford DTM of more areas, the river water level station can also be included in the 2D model domain, which will add more value to the model's accuracy.

## 1.5    Structure of the Thesis

This thesis has been divided into six chapters. The major contents of each chapter are outlined below.

**Chapter One** discusses a brief background and rationale of this study, along with the major objective and expected outcome of the study.

**Chapter Two** reviews the relevant literature. This chapter contains a review of the flood hazard in Bangladesh, flood management practices, and flood forecasting systems. A brief description on the HEC-RAS model for flood propagation modeling has been also discussed. Different kinds of literature from local and abroad have been reviewed in the preparation of the thesis.

**Chapter Three** includes a description of the study area. This chapter covers the general location, insight of the specific study area, and the flood occurring scenario inside the study area.

**Chapter Four** describes the materials used and the methodology employed to carry out the research work in detail. This chapter discusses secondary data sources and detailed processes of primary flood data collection. The chapter introduces all the materials and tools used for the study. The chapter also broadly describes the steps of DTM generation and model development.

**Chapter Five** describes the results of the study and provides relevant discussion. It contains a detailed representation of the analysis by graphs and maps. It also contains the calibration and validation of the model and the procedure for the developed methodology for location-specific flood forecasting in a floodplain.

**Chapter Six** provides the conclusions of the thesis work and a few recommendations for future research work. It also recommends some prospective practices to test the improvement and align with the FFWC established model.

# CHAPTER TWO
# LITERATURE REVIEW

## 2.1 Floods in Bangladesh

Bangladesh is a riverine country and as a result, flood is one of the most common natural disasters that affect the livelihood of people of the almost entire area. Bangladesh happens to lie in the downstream of three of the largest river systems in the world, the Ganges, the Brahmaputra, and the Meghna, which (and other minor rivers) make the entire country a very large floodplain (Mozumder, 2005). Overflowing rivers annually flood about one-fifth to one-third of the country during monsoon (June to September) when the rainfall within the country is also very high (Mirza, 2002). Bangladesh ranks high in the list of vulnerable countries in South Asia, the most vulnerable region of the world to climate change impacts (Khan, 2008).

## 2.1.1 Types of Flooding in Bangladesh

Many of the local areas are adjacent to rivers; during excessive rainfall, water cannot drain out, and if the water level in the river is high, they cause flooding in the surrounding areas by overtopping. Hence, local areas in Bangladesh are vulnerable to both riverine and urban floods. Five main types of natural floods occur in Bangladesh: river flood, rainfall flood, flash flood, tidal flood, and storm surge flood. Figure 2.1 shows the locations of Bangladesh with dominating flood type.

### 2.1.1.1 Rainfall Flooding

During an extreme rainfall event, when water cannot drain out from the urban area because of low runoff rate and so gets staged inside the area, it causes waterlogging which is known as rainfall flooding. It also occurs in the floodplains where natural drainage systems have been disturbed due to human interferences, mainly due to the construction of unplanned rural roads and illegal occupation of river courses (Rahman and Salehin, 2013). When intense rainfall occurs in those areas, the natural drainage system cannot carry the run-off generated by the rain and causes temporary inundation in many localities. The type and amount of precipitation, prolonged rainfall, soil and

underlying rock in the area, land use, human interventions, drainage basin shape, and drainage density are the main factors affecting rainfall flooding (Mirza, 2002). This kind of rain-induced flood has increased in urban areas. Urban rainfall flooding causes widespread devastation, economic damages, and loss of human lives.

### 2.1.1.2 Storm Surge Flooding

A storm surge is a rise in sea level that occurs during tropical cyclones, intense storms. The storms produce strong winds that push the water into shore, which lead to flooding. This makes storm surges very dangerous for coastal regions. This kind of flood mainly occurs along the coastal areas of Bangladesh, which has a coastline of about 800 km along the northern part of the Bay of Bengal (Agrawala et al., 2003). In the case of super cyclones hitting the coast of Bangladesh, the maximum height of the surges was 10-15 m, which causes flooding in the entire coastal belt (Gallien et al., 2011).

### 2.1.1.3 Tidal Flooding

Tidal flooding is the temporary inundation of low-lying areas adjacent to tidal rivers during exceptionally high tide events, like at the full and new moons. The year's highest tides may be known as the perigean spring tide, during the months from June to September in Bangladesh when the sea is in spate due to southwesterly monsoon wind (Sumaiya, 2017). The incidence of this kind of flooding is now on the increase.

### 2.1.1.4 Flash Flooding

Flash flood is the rapid rise in water levels that results in flooding followed by a relatively rapid recession. Flash floods can occur within a period between a few minutes to a few hours. Often with high velocities, the floods damage crops, properties, and fish stocks of the wetland. This type of flood occurs mainly in some northernmost areas, north-central part, north-eastern part, and south-eastern Bangladesh (Munir and Iqbal, 2016). In northernmost, north-central, and north-eastern parts, land areas lie mostly at foothills but most of the hilly catchments are in India. If it rains heavily in the Indian parts of the catchments, the run-off quickly accumulates and flows to Bangladesh. Flash flood starts occurring in these areas from mid-April, i.e., before the onset of the southwesterly monsoon (Munir and Iqbal, 2016).

### 2.1.1.5   Riverine Flooding

A flood occurs when a river or stream is filled, overflows its banks, and then water moves onto the floodplain and slows down. River floods occur when water normally flowing in the channel overflows its bank and spreads out onto the surrounding land. It is one of the most common forms of natural disaster in Bangladesh. Usually, 25-30% of the area of Bangladesh is inundated during the monsoon season along the river (Hossain, 2003). In case of extreme flood events, 50-70% of the country is inundated, extending the areas far beyond the riverbanks (Shaibur et al., 2017).

Heavy rainfall in the upstream basin, levee breach, ice melt, river damming, riverbed aggradation, deforestation, and climate change are the leading causes of riverine flooding.

River foods have profound effects. The floodwater drowns human beings and animals. It damages buildings, roads, bridges, and crops. River floods displace large amounts of sediment. This river sediment mixes with agricultural land and replenishes valuable topsoil components (Biswas, 2008). This action also increases the elevation of lands. Humans, houses, agriculture, livestock, roads, and transport are the worst affected due to such floods. The damage from a river flood can be widespread as the overflow affects smaller rivers in downstream, often causing dams and dikes to break and swamp nearby areas.
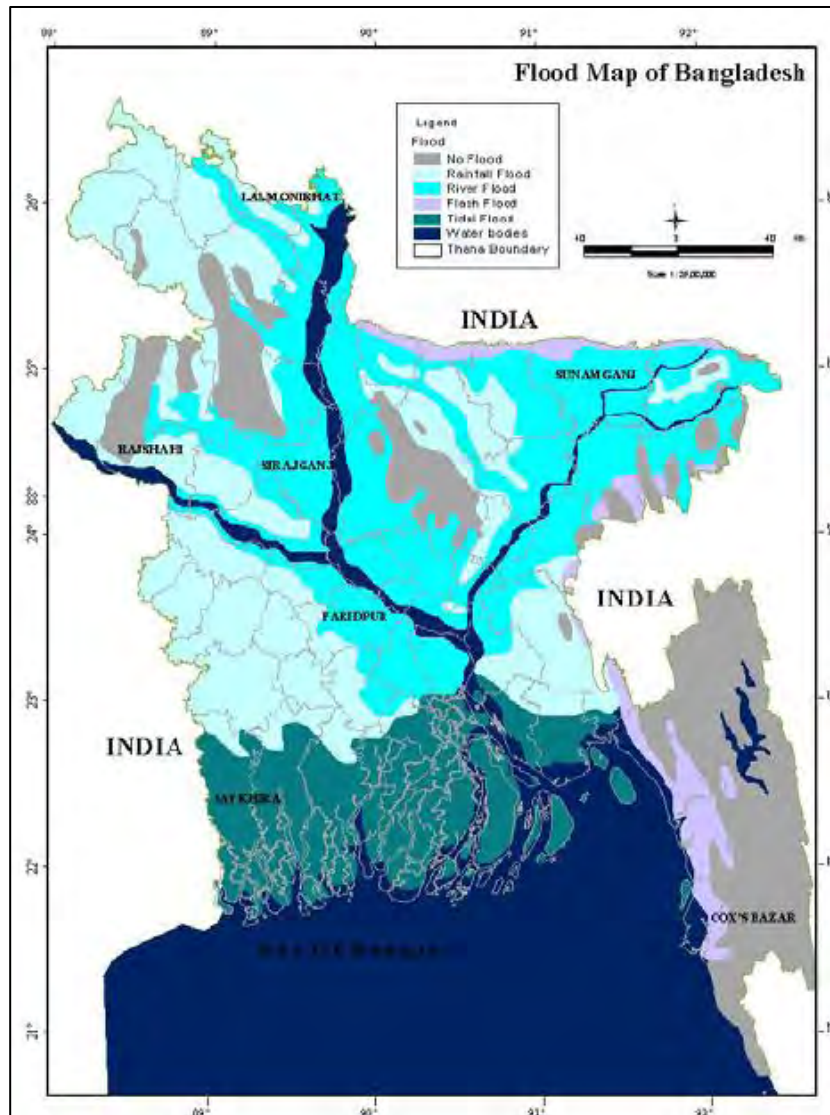
Figure 2.1 Map of Types of Floods in Bangladesh (Source: WARPO)

## 2.1.2 Causes of Flooding

In the monsoon months, the principal sources of floods are the river floods from the overbank flows of the major river systems, the Brahmaputra, the Ganges, and the Meghna. Local rainfall floods often accompany river floods, resulting from high-intensity runoff and long-duration rainfalls over Bangladesh that cannot be drained because of high outfall water levels. The northern and north-eastern transboundary hill streams are susceptible to flash floods from the adjacent hills in India in the pre-monsoon months of April and May (Mozumder, 2005). The areas adjacent to estuaries and tidal rivers in the southwest and southcentral parts of the country experience tidal floods twice

a day due to astronomical tide from the Bay of Bengal. Tide is experienced up to 225 km inland in the wet season and 325 km inland during the dry season (Gallien et al., 2011). Approximately 12,000 km2 of coastal land is prone to occasional cyclonic storm-surge floods due to tropical cyclones in the Bay of Bengal from April to June and September to November (Sumaiya, (2017).

There are few geographical, physiographic, and hydro-meteorological factors responsible for floods in Bangladesh. Hills surround the country on its three sides, Rajmahal hills in the west, the Himalayas and the Meghalaya Plateau in the north, and Tripura–Chittagong hills in the east. The rainfall-runoff from this vast hilly area coupled with snowmelt in the Himalayas brings a massive inflow of water to Bangladesh during the wet monsoon season, and about 80 % of the rainfall occurs during the months from May to September (Biswas, 2008). The country is located at the lower parts of the basins of the Ganges, the Brahmaputra, and the Meghna, but only 7 % floodplain lies within Bangladesh, which drains about 91% of runoff of the basin (Akter et al., 2016). In this process, the country's land consisting of 80% of the floodplain gets inundated by floodwater (Akter et al., 2016). The impacts of this type of flood are on the rise because of a change in hydrological regime in the floodplains due to unplanned construction of different types of infrastructures, such as roads, bridges, culverts. Also, the siltation of riverbeds and encroachment of wetlands in the floodplain are the major reasons for unexpected flooding.

Anthropogenic activities in the form of construction of infrastructure (mainly road) without sufficient drainage capacity through them, road alignments transverse to the main drainage paths, blocked drainage channels due to siltation, cross-dams or fishing activities, and inadequately sized drainage sluices are increasing urban floods (WARPO, 2001). Another cause of concern is the damage caused by sudden floods due to the failure of flood control embankments (Biswas, 2020).

The essential elements that determine the extent of flooding are the magnitude, synchronization of peaks, and duration of floods (Rahman and Salehin, 2013). More minor differences in peaks of major floods can make a big difference in flood-affected areas since it is the spreading of floodwater evenly over a wide and flat floodplain that slows down the rate of rising water levels. As all the flows are drained in the Bay of Bengal only by the Lower Meghna River, it takes time and lengthens the duration of the

flood. Also, the synchronization of peak flows in the Brahmaputra, and the Ganges is a major determinant of the extent of flooding in the country (Islam et al., 2010). When the peaks of the two rivers coincide, severe flooding occurs as it was the case in 1988, 1998 and 2004 (Islam et al., 2010). The country has experienced floods since ancient times. There is an increasing trend in year-to-year variability in the annually flooded area from the mid-1970s. Some severe floods were experienced in 1987, 1988, 1998 and 2004, and some medium floods in 1991, 1993 and 1995 (Hofer and Messerli, 2006).

With the increase of population, more and more people are settling in flood-prone areas, making them more vulnerable to floods. An analysis conducted with 2001 population census data revealed that some 45.5 million people were exposed to severe and moderate floods (Shaibur et al., 2017). Flood-prone zones are the worst off among different disaster-prone areas in terms of food shortages, the incidence of extremely poor, insufficient income, illiteracy, and a high concentration of wage laborers.

### 2.1.3   Historical Floods of Bangladesh

Bangladesh is one of the most flood-prone countries in the world. The country consists of an extensive low-lying flat flood plain of the three principal rivers (Ganges, Brahmaputra and Meghna) and their numerous tributaries and distributaries. As a result of the flat topography of the floodplain, about 20.5 percent of Bangladesh is flooded annually by floods (Akter et al., 2016). Major floods recorded in the 19th century were in 1842, 1852, 1871, 1875, 1885 and 1892. Catastrophic floods that occurred in the 20th century were in 1951, 1987, 1988 and 1998 (Ninno et al., 2001). Recent Major floods include 2004, 2007, 2015 and 2017 floods (FFWC, 2018).  Figure 2.2 shows the historical flood affected areas in Bangladesh.
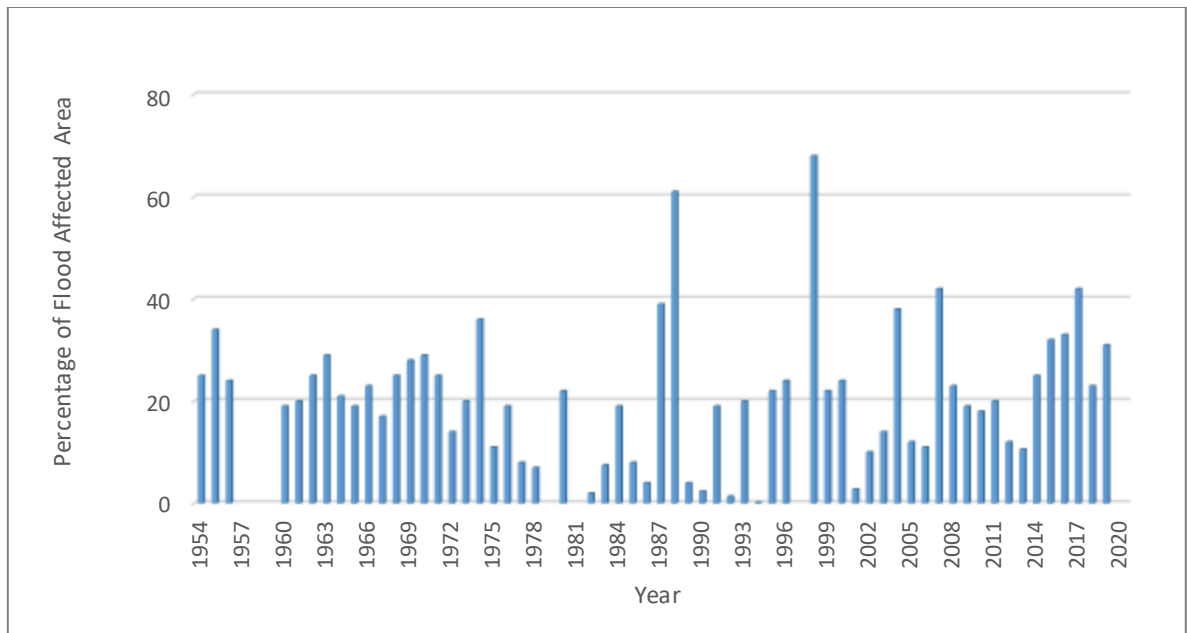
Figure 2.2 Year-wise Flood Affected Area in Bangladesh

The flood of 1987 occurred throughout July and August and affected 57,300 km$^2$ of land (about 40% of the country's total area) (Hofer and Messerli, 2006). The flood affected the western side of the Brahmaputra, the area below the confluence of the Ganges and the Brahmaputra, and areas north of Khulna (Rahman and Salehin, 2013).

The flood of 1988 occurred throughout August and September. This flood inundated about 82,000 km$^2$ of land (57% of the country), surpassing previous records of the extent of flooding (UNDRO, 1988). The catastrophic flood was initiated by heavy rainfall in the Himalayan foothills regions of India, Nepal, Bhutan, and the northern and northeastern districts of Bangladesh. (Rasid and Pramanik, 1993). Rainfall and the synchronization of very high flows of the country's three major rivers in only a few days aggravated the flood.

The flood of 1998 occurred through July–October. The flood inundated over two-thirds of the total area of the country (Hossain and Kolsteren, 2003). It compares with the catastrophic flood of 1988 concerning the extent of flooding. A combination of heavy rainfall within and outside the country, synchronization of peak flows of the major rivers and a powerful backwater effect coalesced into a mix that resulted in one of the country's worst flooding.

The flood of 2004 was very similar to the 1988 and 1998 floods, with two-thirds of the country underwater. The flood of 2007 occurred first in July to August and then again in 1st week of September to mid-September that affected 39 districts of Bangladesh (NIRAPAD, 2007). The flood of 2010 affected 49 districts of Bangladesh and affected millions of people (IFRC, 2014). The flood of 2015 occurred in the monsoon season and flooded 32% of the country. The flood of 2017 was a moderate to severe one which stayed up to medium duration in the Brahmaputra and Ganges basins, but for an extensively long period in the Meghna basin. In the flooding, 42% of the country got flood-affected, corresponding to 35 nos. of flood-affected districts (Ali et al., 2018).

Based on the historical records, it is observed that the frequency, magnitude, and duration of floods have increased substantially during the last few decades. Flooding primarily occurs during the monsoon season as the GBM Rivers dispel enormous discharge that converges in an area with low gradient and flat terrain (Nandargi, 2010).

Mirza (2002) evaluated the relationship between monsoon timing and three extreme historical floods in Bangladesh in 1987, 1988 and 1998, and suggested that the extreme floods of 1988 and 1998 were attributable to the concurrence of peak flows in the Ganges and the Brahmaputra. The author conducted an analysis for the floods of the Ganges, Brahmaputra, and Meghna rivers and concluded that the probability of flooding in this basin would increase.

Studies of the Brahmaputra River in India have found that floods on this river in recent years have already become more severe due to an increased frequency of extreme weather events and a variety of newly emerged manmade interventions: the occupation of the flood plain, destruction of wetlands, and poor management of flood control measures (NIRAPAD, 2010; Jamil et al., 2008)

## 2.2   Flood Management and Mitigation

Flood management and mitigation involve prevention, preparedness plans and related warning systems, emergency response measures, and post-flood reconstruction and rehabilitation. The main aims for flood management are to provide how, through a combination of structural and non-structural measures and to the extent feasible and

affordable, people are adequately warned of an approaching disaster and are adequately supported in rebuilding their lives thereafter (Khan, 2008).

Following severe floods in 1954 and 1955, the Bangladesh Government adopted a policy of protecting agricultural land from river floods. Most of the initiatives were structural measures. The completed flood-related projects are the construction of 12,850 km of embankments, 25,580 km of drainage channels, and 4,190 sluices and regulators (Rahman and Salehin, 2013).

The severity of the floods of 1987 and 1988 led the government to look for a plan, which would provide a comprehensive and permanent solution to the recurrent flood problem in the long term. Several significant studies were taken up in 1989, which led to the formulation of the Flood Action Plan (FAP) in 1989 (Brammer, 2010).

### 2.2.1    Structural Measures

The types of implemented flood control projects include flood control (FC), flood control and drainage (FCD), flood control, drainage and irrigation (FCDI), and drainage (D) projects. Heavy dependence on structural means to manage floods, together with the effects of such other structures as roads, highways and railroads that obstruct the flow of water in some cases, aggravate the flood situation (Brammer, 2010).

The main approaches that have been exercised are (1) complete protection of agricultural lands and urban areas against river flooding by constructing embankments, (2) partial protection against river flooding by constructing low height submersible embankments, (3) evacuating unwanted rainwater through drainage regulators and sluices, 4) providing drainage by pumps (WARPO, 2001). Other structural measures included dredging of rivers and canals, and hard and soft recurrent measures for bank protection and river training works. National and regional highways and railways, to the extent feasible, have been raised above flood level. Raising feeder and rural roads will be determined in the context of disaster management plans.

The flood control structural measures generally used in Bangladesh are (a) Dykes, embankments, polders, levees, bunds, or floodwalls along the major rivers and estuaries, (b) Dredging of major drainage channels which do not have sufficient cross-sectional areas, (c) Diversion of flood flows through the distributaries, (d) Shortening the length

of meander rivers by cut-offs where possible, (e) Closing down the tidal estuaries by cross-dams to stop tidal flooding, (f) Watershed management and afforestation, and (g) Rubber dams as a possibility to flood fighting. Embankments, dykes, polders, levees, bunds, or floodwalls are the most preferred options in Bangladesh (Brammer, 2010).

To reduce the losses from floods as well as to use the surplus water for irrigation, the Bangladesh Development Board, as part of structural measures for flood control, constructed several embankments, barrage and canals. Some major projects are Ganges-Kobadak Irrigation Project (G-K Project), Dhaka-Narayanganj-Demra (DND) Project, Karnafuli Multipurpose Project, Coastal Embankment Project, Tubewell Project in northern Bangladesh, Brahmaputra Right Embankment Project, Chandpur Irrigation Project, Meghna-Dhonagoda Project, Manu River Project, Khowai River Project, Pabna Irrigation Project, Gumti Project, Muhuri Irrigation Project, Teesta Barrage Project (Phase-I), Dhaka Integrated Flood Protection Project, System Rehabilitation Project, and Early Implementation Project (Brammer, 2010).

### 2.2.2   Local Mitigation Technology

The local people of Bangladesh have taken measured on their own to cope and keep themselves safe. These indigenous measures include raising the house's plinth level, making raised platforms for animals, storing valuable items on a platform in the living room, planting water-resistant plants to protect the house from soil erosion (Mozumder, 2005; Ali et al., 2018). Raising plinth levels of the house is done by the extended platform of soil/cement concrete wall. The height of the raised plinth level varies on local experience of previous flooding in the area. The height of the raised plinth level also depends on the economic condition of the individual household. Ponds are dug in the homestead area, and banks are raised to prevent intrusion of floodwater (Rahman and Salehin, 2013).

Moreover, the floating agriculture technique is being practiced in southern floodplains of Bangladesh (Barisal, Gopalganj, and Pirojpur districts) as a traditional/indigenous agriculture system for the waterlogged areas to cultivate in flooded land during monsoons (FAO, 2017). Farmers use boats to manage floating agricultural land cultivation. Aquatic

plant, water hyacinth is usually used as construction material for constructing floating platforms (Irfanullah et al., 2011).

### 2.2.3 Non-structural Measures

Non-structural measures for flood control are human activities and awareness, development of disaster information distributing system at the time of emergency, legal regulations, and so on (Kundzewicz, 2002). Non-structural measures were considered as a means for mitigating flood damages. Understanding disaster risk, strengthening disaster risk governance to manage disaster risk, investing in disaster risk reduction for resilience, enhancing disaster preparedness for effective response, and "Build Back Better" in recovery, rehabilitation and reconstruction are considered as major tools of the non-structural measures (Kundzewicz, 2002).

Non-structural measures include (a) Dissemination of flood forecasts, short- and long-range warning systems, including the height to which the floodwater is likely to rise in the next few hours or so, and a program of speedy evacuation. (b) Land management for reduction of runoff water. In this case, a program of afforestation and reforestation to increase absorption and reduction of runoff water could be undertaken. (c) Land-use change and enactment of building codes, diversification of agricultural production, identification and planting of flood-resistant crops, and adjustment of planting season. (d) Floodplain zoning, involving land-use zoning to control development and restrictive development regulations, should ensure that any development meets specific standards and that they take into consideration the threat to a site (Rahman and Salehin, 2013; Grasso and Singh, 2011)

Non-structural measures can be implemented at nominal costs and in a concise time resulting in a positive benefit to the floodplain users.

### 2.2.3.1 Flood Forecasting

Flood forecasting and warning is one of the major non-structural measures for flood management and mitigation. This is an extensive system and a key tool within the flood risk reduction to provide a timely warning ((UNISDR, 2006; Basher, 2006). Flood forecasting and early warning can reduce the hazardous effect of floods and protect lives

and livelihoods (Garcia and Fearnley, 2012; Osanai et al., 2010; Kelman and Glantz, 2014).

Various sources of uncertainty in operational flood forecasts lead to the discrepancy between simulated and real-time data for the forecast recipients to understand and use forecasting information (Saddagh and Abedini, 2011; Demeritt et al., 2010; Liu et al., 2017). A fit-for-purpose and location-specific forecast system can eliminate the uncertainty and discrepancy in flood forecasting systems.

### 2.2.3.2 Flood Forecasting and Warning Centre of Bangladesh

The Flood Forecasting and Warning Centre (FFWC), under the Processing and Flood Forecasting Circle, Hydrology, BWDB takes hydrological monitoring data of 94 representative water level stations and 70 rainfall stations throughout the country. The main outputs are the daily statistical bulletin of floods, river situation, a descriptive flood bulletin, forecast for 24, 48, 72, 96 and 120 hours at 54 monitoring points on the major rivers during the monsoon season (Rahman et al., 2012; FFWC, 2018). FFWC provides flood warnings with a 3-day lead time (24, 48, and 72 hours) and for some locations with a 5-day lead time (Rahman et al., 2012; FFWC, 2018).

The FFWC of BWDB established in 1972, is making flood forecasts and flood warnings during the flood seasons. The monitoring of floods and issue of flood forecasts are carried out concerning danger levels (FFWC, 2018). The FFWC collects real-time water level data (3 hourly) from 55 observation stations and rainfall from 56 observation stations (FFWC, 2018). As Bangladesh is located downstream of three big river basins, an integrated basin model was needed to increase the forecast lead time for Bangladesh effectively. Fundamental to this was using the advances that have been made in numerical weather modeling and ensemble forecasting (Bhuiyan, 2016). A hydrodynamic mathematical model (MIKE-11) is currently used to forecast the water levels of the rivers.

The forecast is done by running a set of hydrological (NAM) and hydrodynamic (MIKE11) models. Additionally, up to 10 days, probabilistic forecasts are available at 18 designated locations in Bangladesh. The deterministic forecast is generated in collaboration with the Institute of Water Modelling, which uses the MIKE Basin (of DHI) model of the Ganges-Brahmaputra Basin (DEM with SRTM data) with meteorological

input of daily rainfall and rainfall forecast up to 5-days using the WRF model to generate the boundary condition at the border of Bangladesh (Hardinge Bridge for the Ganges and Bahadurabad for the Brahmaputra) (Rahman et al., 2012).

The hydrodynamic module contains an implicit finite-difference computation of unsteady flows in the rivers based on St. Venant equations. The flood forecasting model is customized with the Flood Watch database, which uses a geographic information system. The MIKE GIS module is also integrated with Bangladesh's DEM to generate an inundation model (Hossain and Shah, 2008). The combinations of models generate a forecast of up to 5 days. The probabilistic forecast is generated in collaboration with the Regional Multi-Hazard Early Warning System for Africa and Asia (RIMES), from 1- to 10-day weather forecast from the European Centre for Medium-Range Weather Forecast satellite-based rainfall estimates (with limited gauge data) to produce flood forecasts up to 10 days (Rahman et al., 2012). Although the long forecast horizon of the probabilistic forecast is an advantage, its accuracy is a concern.

Daily forecast bulletin is prepared with forecast up to 5 days and region-wise flood warning messages. FFWC disseminates flood warning information through media and communication outlets using the internet, fax, telephone, mobile SMS, and uploads the forecasted information daily on its user-friendly website (www.ffwc.gov.bd) (Rahman et al., 2012). Moreover, FFWC has also started to disseminate flood warning messages using an interactive voice response system. Anyone in the country can receive a short message regarding current flood information about Bangladesh's major rivers by calling 1090 (Hossain and Shah, 2008; Rahman et al., 2012). This novel system provides timely information to various users, including government departments, agencies, disaster managers, non-governmental organizations, news media, local government institutions, and individuals. The bulletins are disseminated daily to more than 600 recipients, including different ministries, offices (central and district level), individuals, press, development partners, research organizations, and non-governmental organizations (NGOs), including the Presidents and Prime Minister's Secretariat through email, website, fax, hard copy, SMS, and interactive voice response (Hossain and Shah., 2008). The key officials are informed through Short Messaging Service (SMS) whenever the forecasted river stage crosses the danger level (Rahman et al., 2012).

### 2.2.3.3   Flood Forecasting in Floodplain for the Community Level

Basic flood forecasts only provide information about the water level at designated gauging stations on the main rivers. The warning messages need to be understandable to the people. There are some weaknesses of the present flood forecasting system of FFWC. The low-resolution DEMs used for flood modeling are insufficient to produce good local level inundation maps. Flood plain interventions and embankment breach information are very qualitative and cannot provide any location-specific forecasting for the locality. Rahman et al. (2012) assessed the existing early flood warning dissemination system in Bangladesh and suggested suitable improvements in the same system.

Hassan and Shah (2008) developed a participatory model for flood early warning dissemination up to the community level in the Sirajganj district of Bangladesh. Sai et al. (2018) developed impact-based forecasting and warnings in Bangladesh that can connect water levels, through the color code, to localized guidance information tailored to the community. Silvestro et al. (2019) and Smith et al. (2017) worked on a community-based flood forecasting methodology in Nepal.

The TamTam alert project by Akvo, Cordaid worked for better flood early warning in the floodplain of Bangladesh. They have worked for connecting modern technologies with existing local knowledge to have better Flood Early Warning systems and for better up-to-date information from local people in case a disaster happens so that aid can better match with local demands.

In the PROVATi3 Project (Promoting Resilience of Vulnerable through Access to Infrastructure, Improved Skills and Information) of LGED, one component is to build resilience of communities through access to flood information. In this 2.3 sub-component, RIMES is developing an accurate local inundation and flood warning system.

The SUFAL project (Supporting flood Forecast-based Action and Learning) of CARE Bangladesh, with Concern Worldwide, and RIMES is working to contribute to reducing the adverse impacts of the increasing frequency of catastrophic flooding on the vulnerable and poor communities through Forecast-based Action.

## 2.3 Flood Modeling and Mapping

Flood assessments are carried out to identify the source of potential flooding, the possibility of the flooding, the extent of flooding, and the proposed mitigation and protection measures. The statistical model, hydrological and hydrodynamic modeling, and remote sensing and GIS-based mapping of flooded area are widely used to assess flooding. Hydrodynamic models can also be used to assess overtopping or breach scenarios and to undertake blocked culvert analysis. These hydrodynamic models illustrate the flood propagation scenario that information can be used for further assessment like flood forecasting, flood impact, and risk assessment.

Wesemael et al. (2019) assess the potential of sparsely distributed, *in situ* floodplain water level sensors in the Snowdonia region of North Wales to provide accurate, near-real-time flood information as a means to enhance flood predictions.

Yang and Tsai (2000) developed a GIS-based Flood Information System for floodplain modeling, flood damages calculation, and flood information support in the field of China. Liu and Smedt (2005) also used RS-GIS information for flood modeling in the floodplain of Belgium. Salvia et al. (2011) estimated both the flooded area and the mean water level in vegetated river floodplains using a synergy of active and passive microwave signatures. Huang and Jin (2020) generated a flood map of Shouguang City of China using Sentinel-1 SAR and Sentinel 1 Optical Data.

Pinel et al. (2019) have studied flooding dynamics across a medium-size floodplain system along the Amazon/Solimoes River through the integration of remote sensing and limited in situ data in hydrologic-hydrodynamic modeling based on the Telemac-2D model. Mosquera-Machado and Ahmad (2006) assessed floods using statistical techniques of Gumbel and GRADEX, hydraulic modeling (using HEC-RAS), and the Geographic Information Systems (GIS).

Hydrodynamic modeling is the most useful tool for accurate flood modeling and inundation. Jacob et al. (2019), Merwade et al. (2008), and Giustarini et al. (2015) used hydrodynamic modeling for flood assessment in the lower Bharathapuzha basin in Kerala (India), Brahmani-Baitarani River basin (India), and Severn River basin (UK),

respectively. Moftakhari et al. (2019) linked statistical and hydrodynamic modeling for flood assessment, more useful in representing compound flood propagation scenarios.

### 2.3.1 Hydrodynamic Modeling

Based on the modeling approach, flood models are classified as 1D and 2D. In 1D flood models, such as the HEC-RAS 1D, SOBEK 1D, and MIKE 11, a given terrain is represented as a sequence of the river and floodplain cross-sections perpendicular to flow direction (Ullah et al., 2016; Brunner, 2016). Moreover, 1D flood models assume that water remains inside the floodplain and does not consider any lateral flow, often not occurring in the real world. Because of this major limitation, 1D flood models cannot be applied to urban flooding (Rahman, 2006). However, 2D hydrodynamic models consider a variation in the flow in both the longitudinal and transverse directions of the river channel (Tarekegn et al., 2010). Frequently applied 2D flood models include the SOBEK, FLS, LISFLOOD-FP, Telemac 2D, Flow2D Pro, RRI, Flow-2D, HEC-RAS 2D, and MIKE Flood (Horritt and Bates, 2002; Yin et al., 2012; Jakob et al., 2014). Rahman (2006) concluded that 2D hydraulic flood propagation models are crucial for flood hazard assessment. Yarrakula et al. (2010), and Yalcin (2020) developed flood modeling with HEC-RAS.

Many 1D hydrodynamic river models have been conducted throughout the years. However, Andres et al. (2008) stated that a helpful flood model should have the integration approach linking rivers and their floodplains with surface water and full drainage systems. Andres et al. (2008) also validated the robustness of the new 2D hydrodynamic modeling engine, results of its application to a real case study at Brechin, UK. Wing et al. (2019) used a 2D hydrodynamic model for flood forecasting. Recently, 2D hydrodynamic modeling is becoming more popular for flood modeling.

## 2.4  HEC-RAS

HEC-RAS (Hydrologic Engineering Centre's River Analysis System) was first released in 1995 by the United States Army Corps of Engineers (USACE). This is an open-source software which is designed by the USACE. HEC-RAS can calculate water surface

profiles for steady, unsteady, uniform flow and gradually varied flow as well as for subcritical, supercritical, and mixed flow regimes (HEC, 2018). HEC-RAS model can perform 1D, 2D, and combined 1D/2D unsteady flow routing (HEC, 2018), while 2D flow modeling is achieved by including a 2D flow area component in the flood model. HEC-RAS software (USACE Institute for Water Resources Hydraulic Engineering Center, Davis, California) is selected for this assessment due to the popularity of its 1D version and foreseeing the preference potential of this new 2D version, released as public domain in 2016, for future flood studies (e.g., Farooq et al., 2019; Mihu-Pintilie et al., 2019; Rangari et al., 2019). Rahman and Ali (2016), Chowdhury et al. (2020), Islam and Rahman (2020), Subir (2020), and Sheonty (2021) used HEC-RAS for flood inundation modeling in the field of Bangladesh.

Begum (2009) studied on the siltation of Mongla port and developed a hydrodynamic and a sediment model of Passur River system using HEC-RAS. From the model it was found that both siltation and erosion occurred in the Mongla port area and erosion was prominent at the downstream of Mongla port (near downstream of Danger Khal).

Lamia (2014) studied on morphological analysis of the Ganges River using HEC-RAS. This study was based on the assessment of hydrodynamic and morphological characteristics of Ganges River using HEC-RAS from downstream of Hardinge Bridge to Aricha.

Rouf (2015) studied flood inundation map of Sirajgonj district using mathematical model. In this study, a weather forecast model was coupled with a hydrologic model and a hydrodynamic model for predicting floods in Jamuna River at Sirajgonj district with WRF, HEC-HMS and HEC-RAS software.

Mahmud (2017) studied seasonal variation of hydrodynamic parameters of Padma River. He focused on identifying proper behavior and seasonal hydrodynamic variation of the Padma River, different hydro parameters have been studied. In this study, the hydro change of Padma River has been investigated by using HEC-RAS 1D model.

There were many studies in HEC-RAS 1D modeling throughout the world. Nevertheless, recently HEC-RAS 2D is also getting popular for its detailed output features. Costabile et al. (2020), and Quirogaa et al. (2016) concluded the excellent working performance of the 2D HEC-RAS modeling with HEC-RAS version 5.

### 2.4.1 HEC-RAS 2D Model

The HEC-RAS flood model uses the 2D Saint–Venant and the 2D diffusive wave equations for flood simulation (HEC, 2018). Generally, the diffusive wave equation, obtained by ignoring the acceleration terms in the Saint–Venant equations, is used for river flood routing. Moreover, 2D diffusive wave equations can accurately model many modeling situations and have more excellent stability and allow the model to run faster (HEC, 2018; Mehta et al., 2020). Likewise, the 2D Saint–Venant equations can be used for a wide range of problems and are the more accurate option for situations including mixed flow regime, highly dynamic flood waves, abrupt contraction and expansion, tidally influenced conditions, general wave propagation modeling, and superelevation around bends (HEC, 2018). The finite volume method with enhanced stability and robustness has the edge over standard finite difference and finite element methods. The implicit finite volume algorithm used by the 2D unsteady flow equations solver allows larger computational time steps than explicit methods (HEC, 2018). The wetting and drying of 2D flow area cells are very robust, due to which 2D flow areas can handle the abrupt change from totally dry to wet.

Furthermore, the algorithm can solve different flow regimes like subcritical, supercritical, and mixed flow (Mehta et al., 2020). The HEC-RAS 2D uses flow and stage hydrograph, normal depth, and rating curve as a boundary condition and can be calibrated through parameters including Manning's n, and contraction and expansion coefficients (Mehta et al., 2020). HEC-RAS 2D-simulated outputs can be viewed in the RAS Mapper and includes water surface elevation, depth, velocity, arrival and recession time, and duration.

DTM induces most of the topographic features of the study into the HEC-RAS 2D model. HEC-RAS uses the data stored in DTM to visualize the floodplain geometry. The accuracy of the 2D model output boosts with the precision in DTM. HEC-RAS 2D can develop DTM within it with the help of DEM as an input file (Yalcin, 2020).

HEC-RAS-v5 can be used either as a fully 2D model or as a hybrid 1D- 2D model. Kumar et al. (2019) proved the applicability of HEC-RAS 2D in Prayagraj, India. Very few works in Bangladesh have focused on the two-dimensional flood modeling approach. Roy et al. (2021) mapped flood inundation in the Arial Khan River floodplain in

Bangladesh. Rahman (2015) developed the flood inundation model of the Jamuna River. Biswas (2020) used the HEC-RAS 2D for flood modeling in the Padma River floodplain in Bangladesh. Langhammer et al. (2017) built a high-precision 2D hydrodynamic flood model using UAV photogrammetry for the Upper Vydra basin in the Czech Republic, which is very much valuable for developing a fit-for-purpose flood model.

### 2.4.1.1  2D Mesh Area and Cell Size

2D flow area is defined to generate 2D mesh by drawing a polygon within the boundary of the underlying terrain. A uniform hexagonal mesh is developed over the underlying terrain by specifying cell center spacing. The mesh cell size and the model simulation time step dictate the simulation run time and accuracy in mapping the outputs. The run time increases with the number of cells. Goodell and Warren (2006) recommend the mesh size be limited to one million cells, as exceeding this size in the small unit may introduce significant runtime errors due to surpassing the memory allocation.

### 2.4.1.2  Manning's Roughness Coefficient

When water flows through river channels and floodplains, it faces resistance. In HEC-RAS, this resistance to flow is represented as Manning's roughness coefficient (n). The higher the resistance to flow, the higher the Manning's 'n' value. As friction increases with the surface roughness, obstructions, irregularities, or vegetation, it requires a higher 'n' value. So, the n value is site-specific and will be more at floodplain than within a river channel. Also, the n value decreases with the increase in stage and discharge (Brunner, 2016).

### 2.4.1.3  Boundary Conditions

Unsteady flow data are required to perform unsteady flow analysis which consist of boundary conditions and initial conditions. Boundary conditions must be established at all open ends of the modeled river system. In upstream ends, stage hydrograph, flow hydrograph, flow and stage hydrograph can be established as boundary condition. On the other hand, for downstream ends, rating curve, normal depth, stage hydrograph, flow hydrograph, flow and stage hydrograph can work as boundary condition. Besides the boundary condition, initial condition consist of flow and stage information is also

required to be established at each of cross section of the system at the beginning of the simulation.

### 2.4.1.4 Time Step Selection

The time step used in the model run must be sufficient to produce stable results. Generally, the time step or computation interval for model simulation run should be small enough to allow water movement through computational cells (HEC, 2018).

Stability of an unsteady model and the numerical accuracy can be improved by selecting a suitable computational time step. If the time step is too large, it will cause numerical diffusion (the peak becomes lessened) and makes the model instable. On the other hand, if the time step is too small, the model takes a long time for simulation, causes the leading edge of the flood wave to steepen and oscillation and there is also the possibility of instability.

HEC-RAS (2018) manual suggests 30 s as a reasonable time step for a 60 m cell spacing in 2D model, though it may vary as long as good results are produced without sacrificing much accuracy. A rough initial run with a coarser time step (1-5 min) should be performed to balance the model stability and output accuracy.

### 2.4.1.5 Terrain

Flood model requires an accurate representation of floodplains in the form of hydro-enforced terrain data and often uses a DTM for model parameterizations, including terrain slope, cross-sections, and flow pattern. Topography representation in a DTM is essential for 2D food model accuracy (Callow et al., 2007; Skakun et al., 2013). In addition, Saksena and Merwade (2015), and Yalcin (2020) proved the sensitivity of flood models to the resolution and accuracy of the utilized DEM.

DTM is a vector dataset containing enhanced terrain data and natural topographic features such as break-lines and ridges (Hirt, 2014). Thus, DTM enhances DEM by including linear features of the bare earth surface. A pre-developed DTM can be imported from external sources or DEM can be used as an input raster to generate its DTM file. For an inundation map, the developed DTM must be linked to model geometry. As a

precaution, the cell size used to develop DTM must be significantly small, so all the terrain features are captured.

## 2.5   Accuracy of 2D Flood Inundation Model

2D hydraulic modeling technology has advanced significantly in recent years, providing robust and flexible tools that are now routinely used for a wide variety of flood risk assessments. However, the accuracy of the results can be influenced by several factors, including topography (DEM), rainfall data accuracy, catchment area characteristics such as Manning factor, infiltration, and so on (Yalcin, 2020). One of the major benefits of 2D hydraulic modeling is that fewer modeling assumptions and less user judgment yield results that represent actual conditions. For example, the effect of depression areas within the catchment is considered because the model deals with DEM, so there is no need to calculate the depression factor for catchment areas. Another benefit is an accurate representation for complex conditions, including wide floodplains, sinuous channels, multiple channels, bends and confluences, bridge/roadway crossings, roadway overtopping, skewed roadway, tidal waterways, and bridge scour. Langhammer et al. (2017) built a high-precision 2D hydrodynamic flood model using UAV photogrammetry in the Upper Vydra basin in the Czech Republic. Langhammer et al. (2017) explored the potential of the joint application of UAV-based photogrammetry and an automated sensor network for building a hydrodynamic flood model. With this methodology, a substantial increase in the resolution and accuracy of flood information can be achieved with a detailed output of the dynamic processes in the floodplain of Bangladesh.

## 2.6   Digital Terrain Model (DTM)

The digital elevation model (DEM) refers to the digital representation of the earth's topographic surface. DEM represents the spatial and corresponding vertical elevation of the earth's surface, slope, and respective aspects. Typically, different remote sensing generated DEMs from satellite images are widely used. Many global or quasi-global DEMs, Advanced Land Observing Satellite (ALOS), World 3 Dimensions (3D) 30 m DEM (AW3D30 DEM), Shuttle Radar Topography Mission DEM (SRTM DEM),

Multiple-Error-Removed-Improved-Terrain DEM (MERIT DEM), Advanced Spaceborne Thermal Emission and Reflection Radiometer DEM (ASTER DEM), and TanDEM-X 90 m DEM are freely available (Guan et al., 2020; Yamazaki et al., 2017; Wessel et al., 2018)

However, Kundu et al. (2014), Yulianto et al. (2015), Franci et al. (2016), and Munir and Iqbal (2016) showed that those DEMs have issues with accuracy in resolution and vertical elevation. Current global DEMs have issues with the detail of terrain features and micro-topographic variations in relatively flat terrain (Gallien et al., 2011; Chu and Lindenschmidt, 2017). SRTM-90 m, SRTM-30 m, and ASTER-30 m have the vertical accuracy issue with the highest RMS error from 12.62 m to 17.76 m (Rabus et al., 2003; Mukherjee et al., 2013; Azizian and Brocca, 2019). Consequently, with current coarse-resolution global DEMs, it becomes challenging to model floods accurately at local levels in the floodplain. The higher resolution and accuracy in digital terrain data are essential. Schumann and Bates (2018), and Saksena (2015) stated that the importance of the spatial resolution, accuracy in the vertical elevation, and relative gradient (slope) need to be established appropriately to meet the accuracy requirements for flood assessment in inundation predictions and quantifications.

For an accurate high-resolution DEM, the UAV technique is very much popular. It generates DEM from the images with close sensing, providing a platform for different sensors such as visible and infrared sensors, spectrum analyzers, and LiDAR reflectors that can capture various data, so the resolution and accuracy are much (Jakovljevic et al., 2019). When coupled with surveyed ground control, UAV-based photogrammetry can capture spatial data with a richness of detail that can meet high standards (Hashemi-Beni, 2018; Serban et al., 2016). The surveying and mapping method of photogrammetry has several advantages over conventional surveying. Coveney and Roberts (2017) showed that it provides a broad view of the project area and can be used in locations that are unsafe to access. Thus, photogrammetry has its applications where its level of accuracy would be sufficient. Typically, ground control points are taken depending on the area, along with the images to validate the UAV DEM's elevation. Coveney and Roberts (2017) have also shown that the UAV gives a model even more accurate with total station surveys in low grass vegetation. Gafurov (2021) found that the root-mean-square error (RMSE) was 5 cm for the UAV results on low vegetation.

The exponential development of technologies has made the drone and drone equipment smaller, lighter, and more powerful. Kumar et al. (2012) and Kardasz et al. (2016) conclude that the improving stability of drones is helping photogrammetry. Westerveld (2020) stated that because of the data acquisition speed, automation of data processing, and getting more accurate geo-information, photogrammetry from aerial images collected by the drone combined with post-processing has become a very promising methodology. This technique has shown its effectiveness in many studies like archaeological site surveying, river and vegetation changes monitoring, and flood modeling (Bazzoffi, 2015; Chiabrando et al., 2016; Yutaka and Yoshihisa, 2016)

The quickly produced high-quality and high-frequency data is the most significant advantage of UAVs. Besides, UAVs bring a substantial improvement in the flexibility of the data acquisition and the design of fully controlled campaigns. However, it also has some disadvantages. UAV cannot map areas blocked by trees. Westerveld (2020) proved that the photogrammetry images could not penetrate the trees to reach the terrain at the trees' ground and provide surface elevation at the top of the tree. Thus, it cannot measure the terrain in the tree canopy area correctly, which may occur some vertical error in the canopy area. A manual survey needs in the canopy areas for accurate elevation data.

## CHAPTER THREE
## STUDY AREA

### 3.1    Location of the Study Area

Sirajganj is one of the most flood-prone areas of Bangladesh. Sirajganj is located along the Jamuna River and is flooded primarily by riverine floods with associated high-intensity rainfall during the monsoon. It lies between 24°00' and 24°40' north latitudes and between 89°20' and 89°50' east longitudes (GoB, 2021). Figure 3.1 shows the location of the study area. Out of 320 km$^2$ of area, about 259 km$^2$ of the Sirajganj region is designated as land area, while 61 km$^2$ is riverine area (Islam, 2012). The Sirajganj district experiences an average annual rainfall of 1610 mm (BBS, 2016). The danger level at Sirajganj station on the Jamuna River is set at 13.35m PWD, which specifies that if this water level is crossed, it will cause damage in the adjacent area.
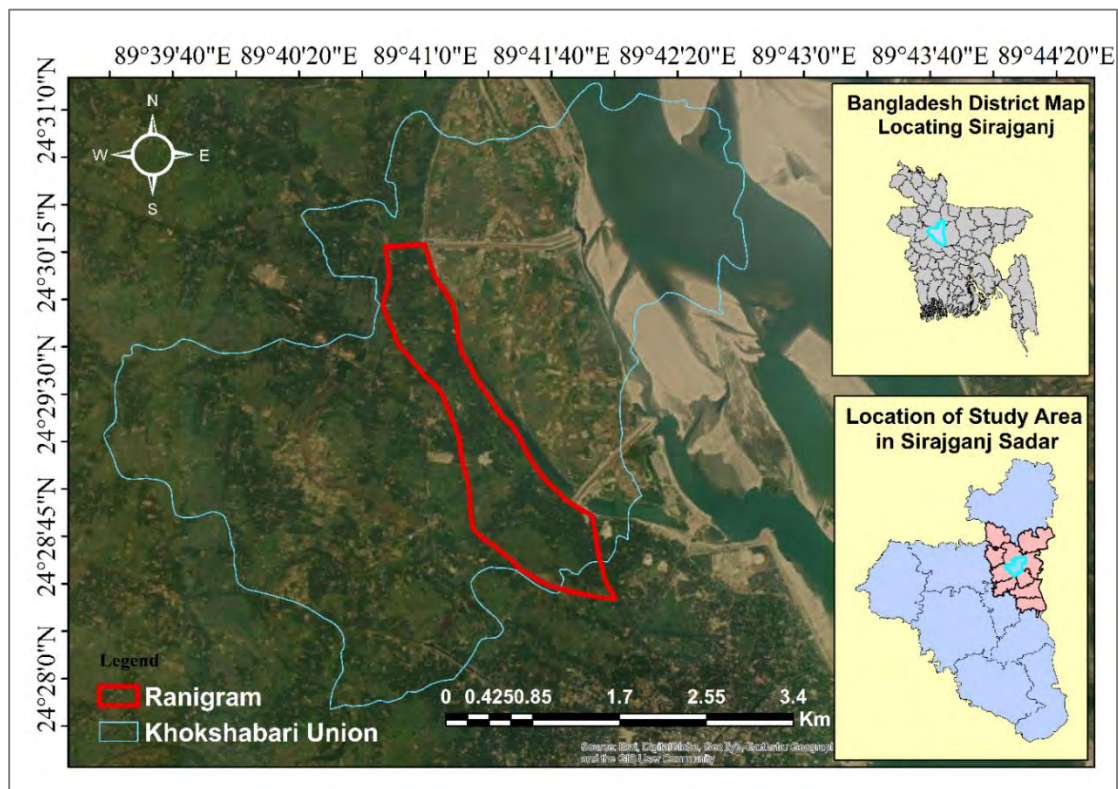


Figure 3.1 Location Map of the Study Area in Sirajganj

Sirajganj district experiences the sub-tropical monsoon climate typical of Bangladesh, with sweltering summer commences in April and lasts up to early June. The monsoon

usually sets in early July and continues till the end of September. The winter season starts in early November and lasts up to the end of February, and in December and January, severe cold is experienced in the Sirajganj district (BBS, 2016). The annual average temperature of the district varies from a maximum of 34.6°C to a minimum of 11.9°C. The average annual rainfall in the Sirajganj district is 1610 mm.

The monsoon discharge of the Jamuna is so high that it regularly overflows the banks and creates flooding in most of the Upazilas of the Sirajganj district. Sirajganj is flooded every year, with the severe floods occurring in 1949, 1956, 1961, 1962, 1966, 1968, 1974, 1979, 1987, 1988, 1996, 1998, 2002, 2004, 2007, 2008, 2014, and 2016. Sirajganj Sadar Upazila is one of the Upazilas of Sirajganj District with a total area of 325.77 km2 (Ali et al., 2018). With such a large area of the country flooded in 1998, the impact was severe for many people. The flood suddenly inundated major parts of all the 9 Upazilas of the district in mid-July, 2007. People took shelter at different shelter places. The total number of flood-affected households of the district was 85015, and the number of affected people was 425075 (Khan, 2008). There is much evidence of embankment breaching during most severe flood years of 1988, 1998, 2004, and 2007. In 2010 floodwater entered Gunergati, Shailabari, Ranigram, Khokshabari, and Khalishakura villages as the Jamuna River swelled and flowed 47 cm above the danger mark (Ali et al., 2018). On September 21, 2010, the Jamuna was flowing 39 cm above the danger level at Sirajganj point (Ali et al., 2018). The Sirajganj district was also inundated for about 15 days in 2014.

Bangladesh was severely hit by flooding during the monsoon season with unremitting rain for mid-July to mid-August, 2016. During the 2016 flood, about 500 villages in 'char' areas in five Upazilas of the Sirajganj district had gone underwater. More than 40 ha of cropland were inundated. The highest river water level above danger level at Sirajganj station was 89 cm (NIRAPAD, 2016).


Sirajganj is one of the most vulnerable flood-prone areas of Bangladesh. Sirajganj Sadar Upazila, which occupies an area of 320km2, is bounded on the north by Kazipur Upazila, east by Bhuapur Upazila and Kalihati Upazila of Tangail district and Sharishabari Upazila of Jamalpur district, south by Kamarkhanda Upazila and Belkuchi Upazila and west by Dhunat Upazila of Bogura district and Royganj Upazila. The Sirajganj Sadar

Upazila consists of 1 paurashava, 15 wards, 50 mahallas, 10 unions, and 294 villages. Out of the total 80,640 acres, 53,445 acres are arable, and the remaining 27,196 acres are farrowed. Moreover, out of the total 320km2 of area, 259km2 are land areas, and 61km2 are riverine areas (BBS, 2016).

The most vulnerable areas in Sirajganj are the low flat areas made up of deposited silt in the river locally called the "char" (island) areas (Ali et al., 2018). These areas are inhabited by destitute people who struggle to survive even in average years. As the floodwater rises in the district, most families try to stay in their homes by simply raising their beds and furniture to live above the water level. When the water reaches the roof level, they move to higher ground within easy reach of their homes (Ali et al., 2018). In many cases, their animals drown as these areas of high ground are barely large enough to accommodate even the people. The flood removes complete villages in the worst-hit areas, and large farmland areas are swept out to the river. The roads are flooded, and this makes it exceedingly difficult to bring relief to the rural areas (Ali et al., 2018). In such severe floods, the deposits tend to be infertile sand rather than silt, and when the water level goes down, large areas become infertile. The central city area (Sirajganj town) is protected by a flood embankment (known as Sirajganj Hard Point) along the right banks of the Jamuna River.

## 3.2 Description of the Study Area

A small village beside the Jamuna River in Sirajganj Sadar that has hydrological interaction with the river is selected for the study. The Ranigram village in the Khokshabari union is a peri-urban area of the Sirajganj district. The village is adjacent to the Jamuna River and is located on the western side of the river (Figure 3.1). The area is 2.4 km$^2$ and is located outside the new 15.351m PWD flood-control embankment of Sirajganj town. It is surrounded on three sides by roads. Two crossbars exist in the north and south of the village. Ranigram is not considered for flood protection by the government projects, and so the area faces an extremely high flood during the monsoon. Widespread flooding, shifting river channels, constantly eroding cultivated land and settlement, and displacement of people are the main problems in this area. Embankment breach is the most common phenomenon for the Jamuna River, especially on the

Jamuna's right embankment. The economy of the Ranigram village is agriculture-based. About 43.64% of holdings are farms that produce crops, namely local and HYV rice, wheat, jute, mustard, potato, sugarcane, various kinds of vegetables, and others. High soil fertility, climatic condition, and silt deposition make the study area agricultural dependent. The homestead area is 461 acres, and the cultivated area is 2386 acres, single-crop 12.29%, double-crop 74.29%, and triple-crop land 13.42%, and cultivable land under irrigation is 71.75%. Among the peasants, 56.36% are non-farm holding, 40.49% small, 3.1% intermediate, and 0.087% rich, and cultivable land per head is 0.10 ha (BBS, 2016). Figure 3.2 shows the image of the area taken by a drone.



Figure 3.2 View of Ranigram area Taken by Drone Survey on 20th October 2019

Because of the inflow from upstream catchment and rainfall, the area is flooded every year and gets massive sediment, so the flood condition is unpredictable from year to year. Along with the environmental and hydrological conditions, many physical structures and interventions in the floodplain have worsened the flood condition of the Ranigram area. People of the area built their houses on elevated mounds for many years to eliminate the flood problems. However, flood inundation depth is increasing each year to distinct levels causing enormous distress for people as local people cannot raise house level sufficient as it is costly and troublesome. Even they cannot predict or forecast the floodwater level to take necessary measures, so they have to evacuate their houses and

have nothing to do for their livelihood that are causing a substantial economic loss and complete disruption of their lives.

## 3.3    Flood Occurrence in the Floodplain of Ranigram Area

At first, by the western bank of the Jamuna River, water overflowed from the river enters from north to south-east between two crossbars. There exists a breach in the eastern shallow old embankment (Figure 3.3). The breach in the old embankment occurred in the 2007 flood from which water entered the Ranigram area. The Union Parishad water level gauge installed is just beside the water entry location. The breach profile is 10-30m at the lowest portion of the breach and extends to 110-170 m at the high flood level.
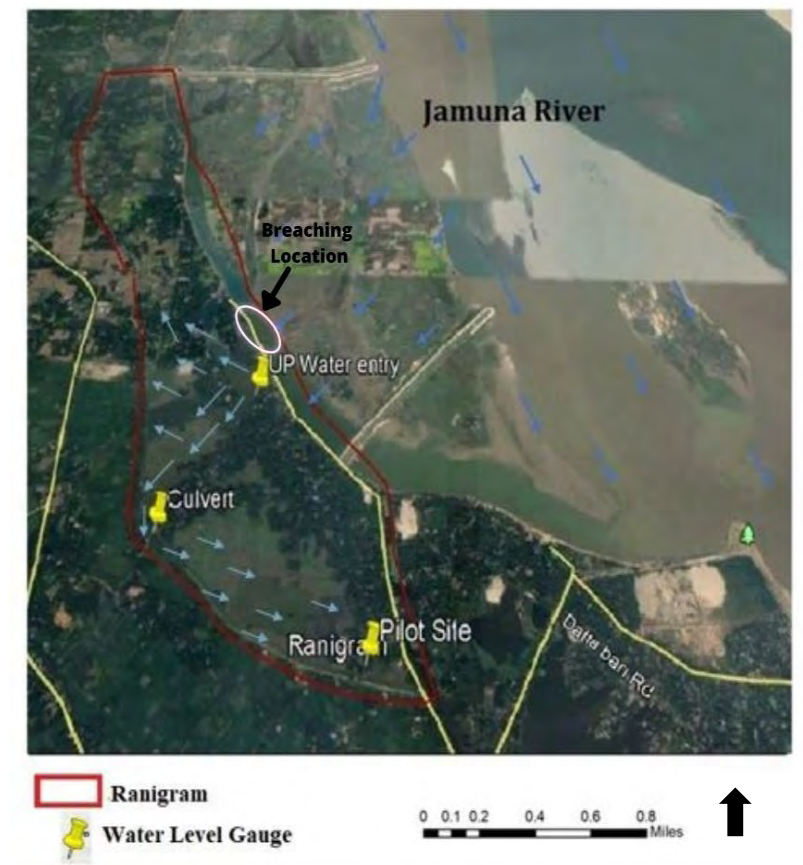


Figure 3.3 Location of Water Level Gauges, Breaching Point and
Flooding Scenario in the Ranigram Area

At first, by bank spilling water from the Jamuna River flows from the north to the southeast side of the area between two crossbars. After that, water enters through the breach, and for high flood levels, the overtopping occurs in the shallow embankment. Then passing the breaching location, the water flows inside the village from south to north and east to west from the Union Parishad. Gradually, water reaches the whole northern part of the village and the culvert area in the middle-western part. From the culvert area, water flows to the southern part of the village and reaches the Pilot Site area. Figure 3.4 shows the floodwater entry location beside Union Parishad where the breaching in the old embankement is.



Figure 3.4 Flood Water Entry Location (Breaching Point) during (a) Dry Season and (b) Flood Season

After entering the village, the water gets stacked because of the embankment roads on all three sides of the village. The water of the Jamuna River stays in connection with the water of the area up to 11.04m PWD water level since it is the lowest entry point. With the decrease of water level in the Jamuna River, the floodwater in the Ranigram village starts going out from the breaching point location. The whole flood water goes out in the same way as it entered. Afterward, a small water volume stays in the ditches and lowlands that disappear through evaporation as well as groundwater recharge.

# CHAPTER FOUR
# MATERIALS AND METHODOLOGY

## 4.1 General

The Ranigram area of the Jamuna riverside in Sirajganj that has interaction with the river is selected for the study. Water level gauges were installed at several important points in the area to monitor the water depths on the floodplain during the floods. From the flood depths, the water levels are calculated with proper benchmarking. Secondary data on the water level of the Jamuna River was collected from BWDB. The floodwater level data of the area is analyzed to understand the relation of the internal flood process with the external river stage of the Jamuna River by analyzing $R^2$, Nash–Sutcliffe Efficiency (NSE), Mean Absolute Error (MAE), and Root Mean Square Error (RMSE) (Mali and Kuiry, 2020).

A 2D hydrodynamic model of the selected area is developed with HEC-RAS using a high-resolution DTM. Water level and normal depth boundary conditions were used for the model. Measured flood water level data of one water level gauge was used for the boundary condition and others for calibrating and validating the model. The model was calibrated and validated with the measured flood levels of 2018 and 2020, respectively. The flood maps of the model were also compared with the collected flood photos of the flood scenario in the Ranigram village. The flood maps of the flood extent and depth, arrival time, and duration were extracted from the simulation results. Figure 4.1 shows the methodological framework of the study.

Then this model is set up and run with different types and resolutions of DEMs. Widely used satellite-based course DEMs (WorldDEM™, ALOS PALSAR, SRTM 30m, and ASTER DEM) and UAV-based high-resolution DTM is used. The UAV imaging technique was used to generate the high-resolution DTM. The results of the simulations, i.e., the Flood Arrival Time, Duration, Percent Time Inundated, and Maximum Extent and Depth from all the models, were compared to find out which DEM provides reliable results. Finally, the model was run with the FFWC forecasted water level of the river, and the result provides forecasted flood information in the Ranigram locality.
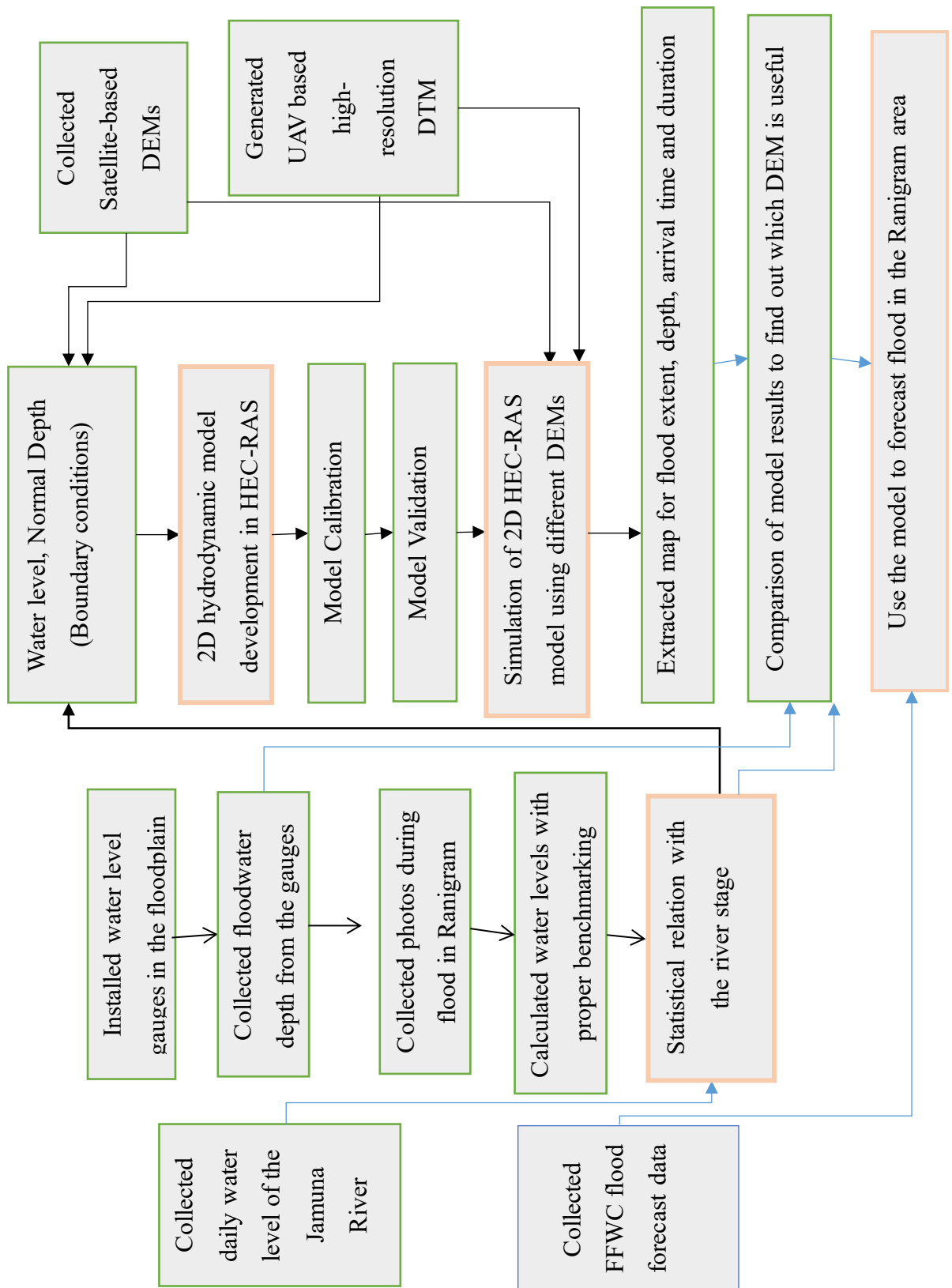
Figure 4.1 Methodological Framework of the Study

## 4.2    Data Collection

The secondary data on rainfall and river water level and primary data on floodplain water level were collected for the study.

### 4.2.1    Secondary Data

The rainfall and river water level data were collected from Bangladesh Meteorological Department (BMD) and Bangladesh Water Development Board (BWDB).  BMD and BWDB have gauges installed in the primary location along Bangladesh to measure the rainfall and river water level, respectively. The rain gauge of BMD is in the floodplain to measure the rainfall, and BWDB gauges are in different locations of the river to measure the associated water level, discharge, and velocity. Hence, the Flood Forecasting and Warning Centre (FFWC) of BWDB provides forecasts of river water levels for the different locations used for flood forecasting-related analyses. The historical time series of rainfall at Bogura (1948- 2015) and daily time-series of the Jamuna water level at Sirajganj (1984 -2020) are used for the study.

### 4.2.2    Primary Data

In Ranigram, to get a clear overview of water level fluctuation in the floodplain, three water level gauges were installed at strategically crucial locations to monitor the floodplain's water depth. For this, 5 m long wooden-plunks were marked in meter scale as shown in Figure 4.2.

The water level readings of the three installed gauges were closely monitored for the whole flood period of the years 2018 and 2020. The distance from the Union Parishad gauge at the breaching location to the gauge at the Culvert is about 0.82km. The distance from the gauge at the Culvert to the Pilot Site gauge is about 1.35km. When the water started overtopping the river, the water depth at each gauge was collected in the morning regularly. From the flood depth, the water levels are calculated with proper benchmarking.

The gauges' reduced level (RL) was measured earlier with reference to the BWDB measured datum. Then the water levels at the three locations were measured by adding the depths with the respective reduced levels. At the same time, the water level at the Sirajganj station on the Jamuna River was recorded daily from the FFWC website of BWDB.



Figure 4.2 Installed Water Level Gauges in the Ranigram Area

## 4.3    Statistical Analysis for the Hydrological Aspects of Floods in Ranigram

### 4.3.1    Frequency Analysis

Frequency analysis is essential to understand future flood occurrences. The estimation of frequencies of the flood is done by using the record of flood events. Frequency analysis has been conducted both for the rainfall and the water level of the Jamuna River at Sirajganj Station. The daily rainfall data at the nearby Bogura station (1948-2015) was collected and used for the Sirajganj region to perform the necessary rainfall analysis. Water level data at Sirajganj station of the Jamuna from 1984-2020 (37 years) has been analyzed for 2-, 5-, 10-, 25-, 50- and 100-year return period floods.

Gumbel's distribution method is used for the frequency analysis. It is a probability distribution function for extreme values in hydrologic and meteorological studies to

predict food peaks and maximum rainfalls. In this method, the variate X is the maximum rainfall or flood peak with a recurrence interval T is given by (Subramanya, 2008):

$$X_T = u + \alpha Y_T \quad \text{----------------} \quad (4.1)$$

Where, $X_T$ is a flood of specified return period T.

$u = X_{avg} - 0.5772\alpha$; Where, $X_{avg}$ is the mean of the flood series, and $\alpha = \frac{\sqrt{6}}{\pi} S$ ; where, S= Standard deviation of the sample.

$$Y_T = -\ln\left[\ln\left(\frac{T}{T-1}\right)\right] \quad \text{----------------} \quad (4.2)$$

### 4.3.2    Contribution of Rainfall and River Water in Flooding of Ranigram

There is no rain gauge of the Bangladesh Meteorological Department at Sirajganj. The nearby rainfall station of Sirajganj is found at Bogura. The daily rainfall data of the Bogura station was used for the Sirajganj region to perform the necessary rainfall analysis.

The discharge (Q) contributed to the Ranigram area by rainfall is calculated using the Rational Method. The equation is (Subramanya, 2008):

$$Q = CIA \quad \text{----------------} \quad (4.3)$$

Here A is the area, I is the rainfall intensity, and C is the run-off co-efficient.

The area (A) of the Ranigram area is 2.4 km2, and the maximum daily intensity of rainfall (I) is found from the frequency analysis of maximum daily rainfall. The run-off coefficient (C) is used to be 0.6 for the rural and agricultural areas.

Water level data at the Sirajganj station of the Jamuna from 1984-2020 (37years) has been used in the frequency analysis to calculate contribution from the Jamuna River. River water enters the Ranigram area through the area of breach beside the Union Parishad. The Length (L) of the breach is 30m and the datum at the breaching location is 10.72 mPWD. The water depth (h) at the breaching point was calculated by subtracting the water level of different return periods from the datum of the location. For Ranigram, the area of water entry is:

$$A = L \times h \quad \text{----------------} \quad (4.4)$$

The area is A, L is the length, and h is the depth.

The area was calculated at the breaching point for water entry for the different return periods. The velocity (V) of water at the breaching point was measured at the field during the flood season of 2018.

The equation for calculating the discharge from the Jamuna River is (Subramanya, 2008):

$$Q = AV \text{ ----------------- } (4.5)$$

Using the above equations (3) and (5), the discharge contributed to the Ranigram area was calculated for the different return periods.

### 4.3.2.1 Statistical Analysis

The floodwater level data of the area has been analyzed to understand the relation of the internal flood process with the external river stage of the Jamuna River. The relation of water level at this gauge location in Ranigram with the Jamuna River water level has been analyzed to establish a statistical relationship between the water level of the Jamuna River and the water level at the location of gauges. The accuracy of the statistical model has been investigated with the coefficient of determination ($R^2$), Nash–Sutcliffe model efficiency coefficient (NSE), Mean Absolute Error (MAE), and Root Mean Square Error (RMSE) analysis (Mali and Kuiry, 2020).

### 4.3.2.1.1 Regression

Regression analysis is a reliable method of identifying which variables have an impact on a topic of interest. The process of performing a regression allows us to determine how these factors influence each other confidently. Regression analysis includes several variations, such as linear, multiple linear, and nonlinear. The most common models are simple linear and multiple linear. Nonlinear regression analysis is commonly used for more complicated data sets in which the dependent and independent variables show a nonlinear relationship.

In order to understand regression analysis fully, it is essential to comprehend the following terms as the dependent and independent variables:

(i) **Dependent Variable:** This is the main factor that is to understand or predict.

(ii)     **Independent Variables:** These are the factors that are hypothesized to have an impact on the dependent variable.

### 4.3.2.1.2  Simple Linear Regression

A relationship between the water level on the floodplain and the river was established using the simple linear regression analysis. The simple linear model is expressed (Freund et al., 2006) using the following equation:

$$Y = aX + b \quad \text{----------------} \quad (4.6)$$

Where Y is the dependent variable (the water level at the gauges in the floodplain), X is the independent variable (the water level on the Jamuna River at Sirajganj station), a is the slope of the regression line, and b is the intercept of the line.

### 4.3.2.1.3  Multiple Linear Regression

Multiple linear regression analysis is essentially similar to the simple linear model, except those multiple independent variables are used in the model. Multiple linear regression follows the same conditions as the simple linear model.

The mathematical representation of multiple linear regression:

$$Y = a + bX_1 + cX_2 + dX_3 + z \quad \text{----------------} \quad (4.7)$$

where Y is the dependent variable (the water level at the gauges in the floodplain), and $X_1, X_2, X_3$ are the independent variables, b, c, d are the respective slopes, and a is the intercept of the line.

### 4.3.2.1.4  Coefficient of Determination ($R^2$)

The $R^2$ is the quantification of the predictive extent of a regression model. It is also known as the coefficient of determination. It explains the strength of the relationship between the independent and dependent variables and quantifies the goodness of fit. For example, if the $R^2$ of a model is 0.50, half of the observed variations are explained by the model's inputs. The $R^2$ values range from 0 to 1 and are commonly stated as percentages from 0% to 100%. A higher $R^2$ value indicates a better model fit to the observed data (Freund et al., 2006).

#### 4.3.2.1.5 Nash–Sutcliffe Efficiency Coefficient (NSE)

The Nash–Sutcliffe model efficiency coefficient (NSE) is used to assess the predictive skill of a model. It represents the robustness of the model. NSE value close to 1 means the model quality is good, and if the value is negative, the model is unacceptable (Zeybek, 2018). The NSE is calculated as one minus the ratio of the error variance of the modeled time-series divided by the variance of the observed time-series data (Zeybek, 2018). It is calculated using the following equation:

$$\text{NSE} = 1 - \frac{\sum_{i=1}^{n}(Y_{obs} - Y_{sim})^2}{\sum_{i=1}^{n}(Y_{obs} - Y_{mean})^2} \quad \text{------------------} \quad (4.8)$$

Where $Y_{obs}$ is the observed data, $Y_{sim}$ is the model data, and $Y_{mean}$ is the mean of the observed data.

In the situation of a perfect model with an estimation error variance equal to zero, the resulting Nash–Sutcliffe Efficiency equals 1 (*NSE = 1*). Conversely, a model that produces an estimation error variance equal to the variance of the observed time series results in a Nash–Sutcliffe Efficiency of 0 (*NSE = 0*). In the case of a modeled time series with an estimation error variance that is significantly larger than the variance of the observations, the NSE becomes negative.

#### 4.3.2.1.6 Mean Absolute Error (MAE)

Mean Absolute Error (MAE) is an error function used for regression models. MAE is the sum of absolute differences between the measured and predicted values. So, MAE measures the average magnitude of errors in a set of predictions without considering their directions. The formula is :

$$\text{MAE} = \frac{\sum_{i=1}^{n}|Y_{sim} - Y_{obs}|}{n} \quad \text{---------------------} \quad (4.9)$$

Where n is the number of data, $Y_{sim}$ is the model data, $Y_{obs}$ is the measured data, and $|Y_{sim} - Y_{obs}|$ is the absolute error.

#### 4.3.2.1.7 Root Mean Square Error (RMSE)

Root mean square error (RMSE) is the standard deviation of the residuals or simply called prediction errors. RMSE is a measure of how spread out these residuals are. Thus, RMSE represents how robust the data is around the line of best fit. The equation is:

$$RMSE = \sqrt{\frac{\sum_{i=1}^{n}(Y_{sim} - Y_{obs})^2}{n}} \quad \text{------------------} \quad (4.10)$$

If the RMSE value is smaller, the predicted values are close to observed values and vice versa.

## 4.4 Different Digital Elevation Models (DEMs) Used in the Study

### 4.4.1 UAV-based High-resolution DTM

A high-resolution DTM has been generated with UAV incorporated with measured bathymetry data of the Ranigram area (Langhammer et al., 2017). The Agisoft Metashape 1.5.2 photogrammetry software and ArcGIS 10.5 software was used to generate the DTM (Yamazaki et al., 2017; Serban et al., 2016)). The UAV data was used for the non-canopy areas, and the measured topographic and bathymetric data was used for the canopy areas, which are covered by dense trees and water where UAV cannot penetrate to take the land elevation data (Hashemi-Beni et al., 2018). Combining UAV and field-measured data with this hybrid approach, a more accurate and high-resolution DEM has been generated. Figure 4.3 shows the methodological framework used for the UAV-based high-resolution DEM generation.

#### 4.4.1.1 Unmanned Aerial Vehicle Technique with Drone

For creating the DEM, firstly, the UAV technique was followed using a drone (Langhammer et al., 2017). The drone survey farm cost 5000taka per square feet of survey. Instead a DJI Mavic 2 Pro drone was bought with 1,80,000 taka. The drone was taken, calibrated, and flown over the area. Forty-Six Ground Control Points were taken, and marks were drawn on the land. The images from the UAV were processed with Agisoft Metashape 1.5.2 photogrammetry software. The camera was calibrated before flying over the Ranigram area. Before flying drone in Ranigram, permission was taken from the local Thana (Police Station).

```
                    ┌─────────────────────────┐
                    │   Selection of Study Area │
                    └─────────────────────────┘
                                 │
                                 ▼
┌──────────────────────┐  ┌─────────────────────────┐
│ Draw mark on land for │  │ Drone selection, Calibration, and │
│ the Ground Control    │  │     flight over the area          │
│ Point                 │  └─────────────────────────┘
└──────────────────────┘               │
           │                            ▼
           │              ┌─────────────────────────┐   ┌──────────────────────┐
           ▼              │ Processing the UAV images into │   │ Collect some measured │
┌──────────────────────┐ │   digital elevation data       │   │ topography and        │
│  Measure RL of the    │ └─────────────────────────┘   │ bathymetry of the     │
│  Ground Control Point  │              │                   │ Ranigram from LGED    │
└──────────────────────┘              ▼                   └──────────────────────┘
           │              ┌─────────────────────────┐              │
           │              │ Identifying artifacts in the DEM │     ▼
           │              └─────────────────────────┘   ┌──────────────────────┐
           │                            │                │ Generate more point   │
           │                            ▼                │ elevations from relative │
           │              ┌─────────────────────────┐   │ measurement in the field │
           │              │ Classified into tree-canopy and non- │ └──────────────────────┘
           │              │   canopy and water area    │              │
           │              └─────────────────────────┘              ▼
           ▼                            │
┌──────────────────────┐              │                ┌──────────────────────┐
│ Use Ground Control     │◄────────────┘                │ Use measured topography and │
│ Point with the UAV-    │                              │ bathymetry data for the tree-canopy │
│ generated data         │                              └──────────────────────┘
└──────────────────────┘                                           │
           │                                                       ▼
           ▼                                         ┌──────────────────────┐
┌──────────────────────┐                             │ By Triangulated Irregular Network (TIN) │
│ Create Digital Elevation Model for the non- │      │ process, create Digital Elevation Model │
│   canopy area          │                             │  for the tree-canopy area │
└──────────────────────┘                             └──────────────────────┘
           │                                                       │
           ▼                                                       │
┌──────────────────────┐                                          │
│ Error correction for artifacts and manual │                     │
│ correction for hydraulic structures like culvert │               │
└──────────────────────┘                                          │
           │                                                       │
           ▼               ┌─────────────────────────┐            │
           └──────────────►│   Merge the two DEM data  │◄──────────┘
                           └─────────────────────────┘
                                        │
                                        ▼
                           ┌─────────────────────────┐
                           │ Generate final DTM for the whole Ranigram area │
                           └─────────────────────────┘
```
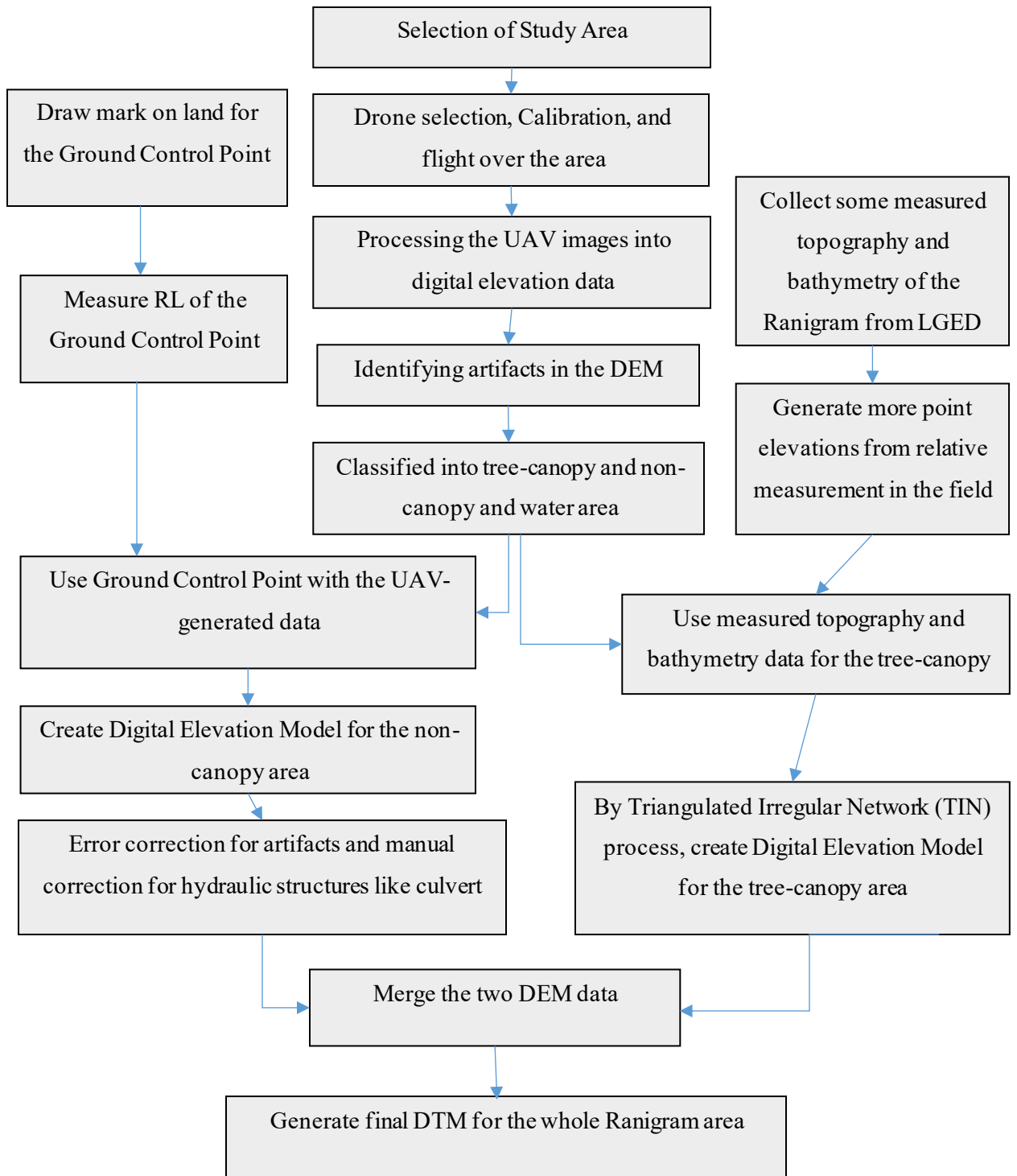
.

Figure 4.3 Methodological Framework for Generating UAV-based Hybrid High-resolution DTM of Ranigram

The processed digital data from UAV was classified into two categories into (i) tree-canopy and (ii) non-canopy and water area. For the non-canopy area, the UAV-generated

data was used with the ground control points. Some error in water areas was corrected, and for hydraulic structures, i.e., culvert, a manual correction was done in the location (Hashemi-Beni et al., 2018). For the tree-canopy area, measured bathymetry data was used. DEM for the canopy area was created with this measured data by Triangulated Irregular Network (TIN) process in ArcGIS 10.5 software. Then the two DEM data of the tree-canopy and the non-canopy areas were merged into one to get the final DEM of the Ranigram area.

#### 4.4.1.1.1 Drone Flight

DJI Mavic 2 Pro drone was used for the UAV photogrammetry. The flying direction was set to cover a 3.3 km² area, and the vertical imaging technique was followed for taking the photos. Three days of field data collection including drone survey and ground control points survey was done in the end of October 2019. As the battery support three hours support only, the drone was set to fly for three hours and then the battery was changed for the next flight. Flying altitude was 138m from the ground level, and the ground resolution was 2.16 cm/pix. Focal Length Pixel Size was 2.41 x 2.41 μm. A total number of 3981 images were taken by the drone, having 3,347,840 Tie points.

#### 4.4.1.1.2 Post-Processing of Drone Images in Photogrammetry Software

The main aim of the post-processing is to produce a georeferenced 3D point cloud by handling with irregular and overlapping aerial image data. In scientific literature, the image-based point cloud is obtained with structure from motion (SfM) approach. Briefly, it uses matched pixels of overlapping images to reach 3d structure of concerned object. This method has reached a sufficient maturity and become commercial software such as Agisoft Metashape software. The software is advanced in UAV applications and allows to generate DEM and ortho-photo in a willed coordinate system. For a full performance of software, it's recommended to use a powerful computer due to the huge amount of data.

The data processing starts with uploading photos from camera to computer and eliminating distorted or blurred ones. The interior orientation of photos was determined. The process proceeds with aligning photos, building geometry, and texture building for realistic appearance. For a geomatic application, it is necessary to geo-reference the data. The Ground Control Points (GCP) that were measured at Ranigram before the flight are

used to geo-reference the drone image data. The color and size of GCPs was made suitable to distinguish at the natural color of study area by marking them with color spray during the process.  At the end of the image processing, a dense 3D point cloud is generated. Finally, DEM was generated from the dense point cloud at a resolution of 17.2cm per pixel.

### 4.4.1.1.3  Ground Control Points

Forty-Six ground control points were taken for validating the DTM from the UAV data which are shown in Figure 4.5. The coordinates of each ground control point were determined using a kinematic GPS machine.

At first, the datum of the points was measured with proper benchmarking.  The point was marked on the surface by using a spray can, which is shown in Figure 4.5. This can be visible in the UAV images so that these points can be directed with the measured elevations (Langhammer et al., 2017). The process was done for all the GCPs. Then the points were loaded using the corresponding projection (WSG84) in the photogrammetry software. The photos with the spray-painted marks were aligned to the points. Finally, a 3D point could and subsequent DTM was created.
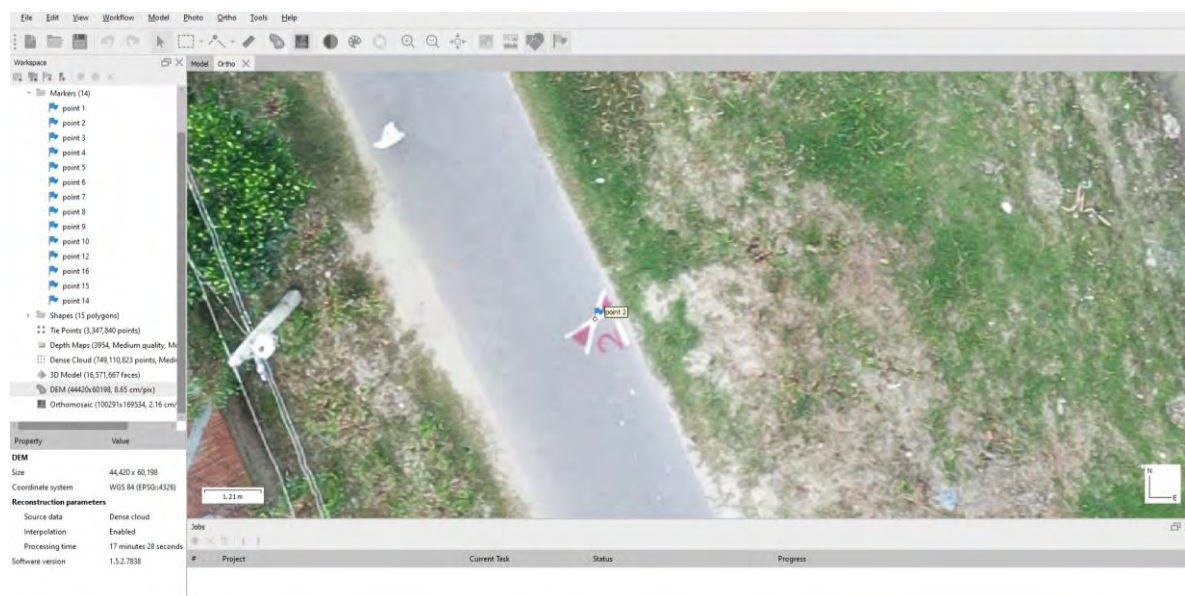


Figure 4.4 Ground Control Point Mark on the Surface of Ranigram before Flying the Drone
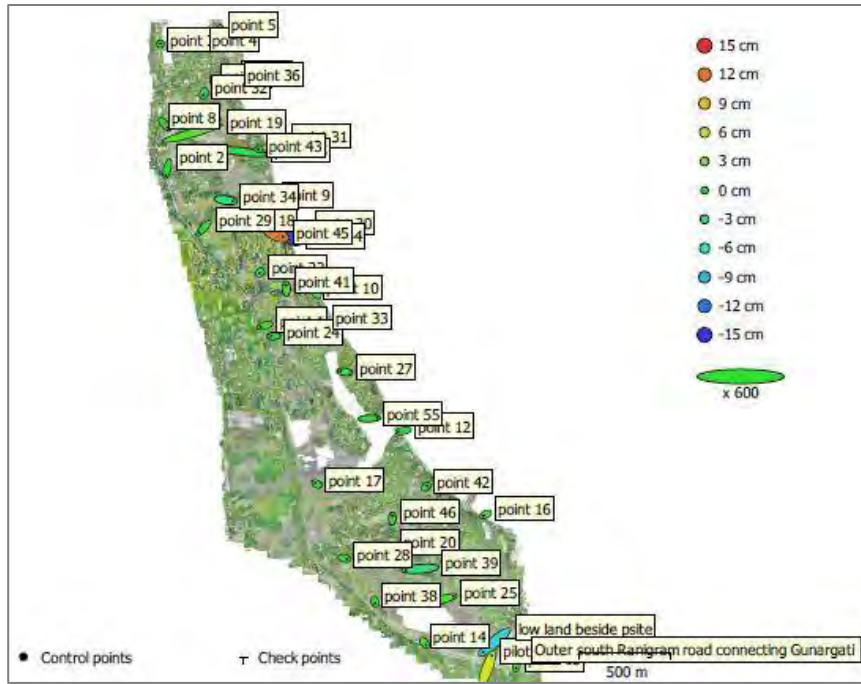
Figure 4.5 Ground Control Points for the UAV Photogrammetry

The error in the DTM with respect to the GCP is very low. Table 4.1 shows the error in the Ground Control Points from the UAV-based DTM, where X - Longitude, Y - Latitude, Z – Altitude.

Table 4.1 RMSE in the Ground Control Points from the UAV-based DTM

| Count | X error (cm) | Y error (cm) | Z error (cm) | XY error (cm) | Total (cm) |
|---|---|---|---|---|---|
| 46 | 10.7878 | 7.93704 | 4.43871 | 13.3931 | 14.1094 |

#### 4.4.1.1.4 Classification of the DTM Area into Tree-canopy and Non-canopy Areas

As the photogrammetry images cannot penetrate the trees to reach the terrain at the trees' ground, it cannot correctly measure the terrain in the tree canopy area. In the area where there is no tree, the terrain of the locations is visible from the close sensing images of UAVs and can be used for DTM data. The whole area is divided into two categories shown in Figure 4.6 for selecting the area for different data (Hashemi-Beni et al., 2018). The tree-canopy and non-canopy areas were drawn using the Google Earth Pro. The kml file was extracted from the Google Earth Pro and was converted into shapefile in ArcGIS

using the kml to layer tool. The non-canopy area was selected for using the UAV data, and with tree canopy was selected for the measured topographic and bathymetric data. For this reason, the topographic and bathymetric data of the canopy area was collected and measured along with the ground control points. From the measured data, a more accurate elevation model of the canopy and water areas was generated.



Figure 4.4 Two-classified Areas of Tree-canopy and Non-canopy

#### 4.4.1.1.5 Artefacts Correction for UAV DTM

Some implausible terrain features were experienced in the UAV-based DTM. In the UAV, some artifacts were caused by the presence of water in the field. In some areas, there was no data value. These issues were identified and corrected by field observation. This editing step comprises the extraction, void filling, and editing of these features, and

the elevation of these areas was fixed with measurement and interpolation (Hashemi-Beni et al., 2018).

Some manual correction was also required to ensure the quality of the DTM results. There was a small culvert in a road below which water passes from north to south of the village. In the drone data, the upper elevation of the culvert was taken as a road. Culvert location was found in the DEM, and it was edited manually as land having the elevation of the lower surface. The UAV-based DTM for non-canopy area is shown in Figure 4.7.
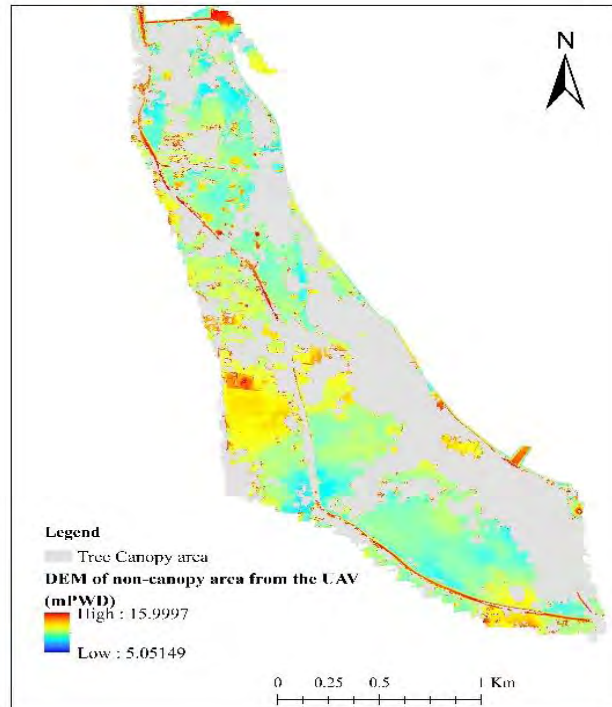


Figure 4.5 The DTM of Non-canopy Area with UAV-based Data

### 4.4.1.1.6  DTM with Measured Point Cloud for Tree-canopy Area

In order to remove the errors in the tree-canopy area in the UAV-based DTM, the measured bathymetry data was used in the water and tree canopy area. Few point elevation data in the Ranigram area was measured, and few bathymetry data of the Ranigram area was collected from the Local Government Engineering Department (LGED) survey, which is shown in Figure 4.8. The spatial resolution of the measured data was not very high. The relative measurement of the area's critical points was taken from the field concerning the measured data.

This data was processed with ArcGIS 10.5 software for creating a DEM of the whole area from the measured points. The measured elevation data were interpolated with the Triangulated Irregular Network (TIN) procedure to create a digital terrain model for the selected area (Yutaka and Yoshihisa, 2016). In ArcGIS 10.5, the excel data sheet was added, and after displaying XY data, it was exported as a layer. The geographic coordinate system was converted to WGS 1984, the same as the UAV data geographic coordinate system. The geographical reference was checked using satellite web imagery. The point elevation data were fitted in the Ranigram area. With this point elevation,
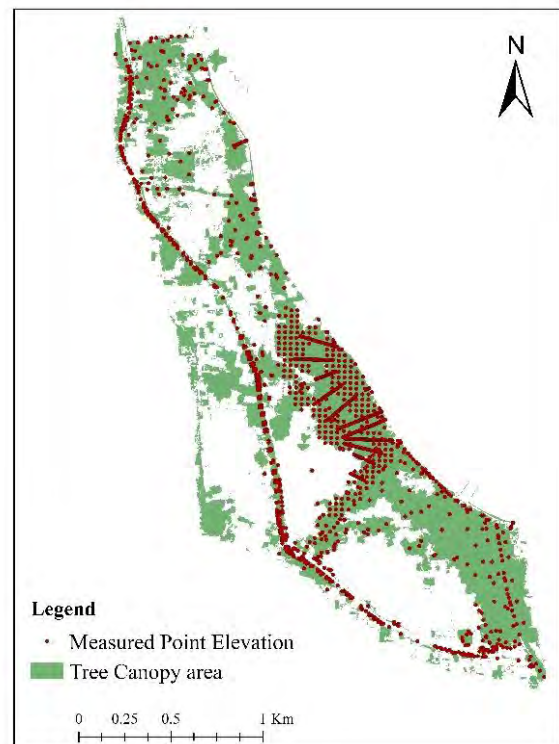


Figure 4.6 Measured Elevation Points in Tree-canopy of Ranigram
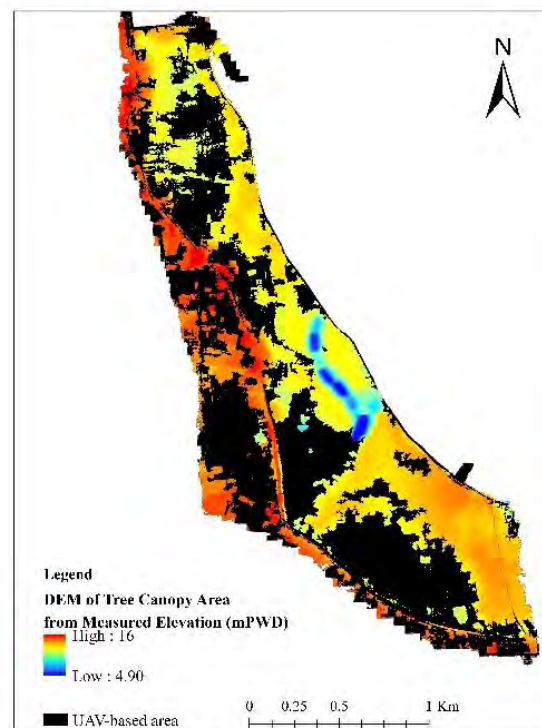


Figure 4.7 DEM of Tree-canopy Area where Measured Elevation Data are Used

using the 3D analyst tool, a TIN was created. SF type was set to Mass points in the analysis, and the Height field was set "z." From the TIN, the DTM was made by raster interpolation. In the 3D analyst, the TIN to Raster tool was used to get the DTM. The data type was set as Float, and the linear method was followed. The cell size was 2m, and the z factor was 1. Thus, the DEM shown in Figure 4.9 for the tree-canopy area of Ranigram was generated.

Finally, the two different digital terrain data from UAV and measured topography and bathymetry were taken to ArcGIS software. These selected two portions of the Ranigram area were merged to a single raster to get the UAV-based high-resolution DTM of the Ranigram area.

Figure 4.10 shows the final high-resolution accurate DTM of the Ranigram area using the hybrid technique with UAV and measured bathymetry data. The resolution of the final UAV-based DTM is 17.5 cm only.
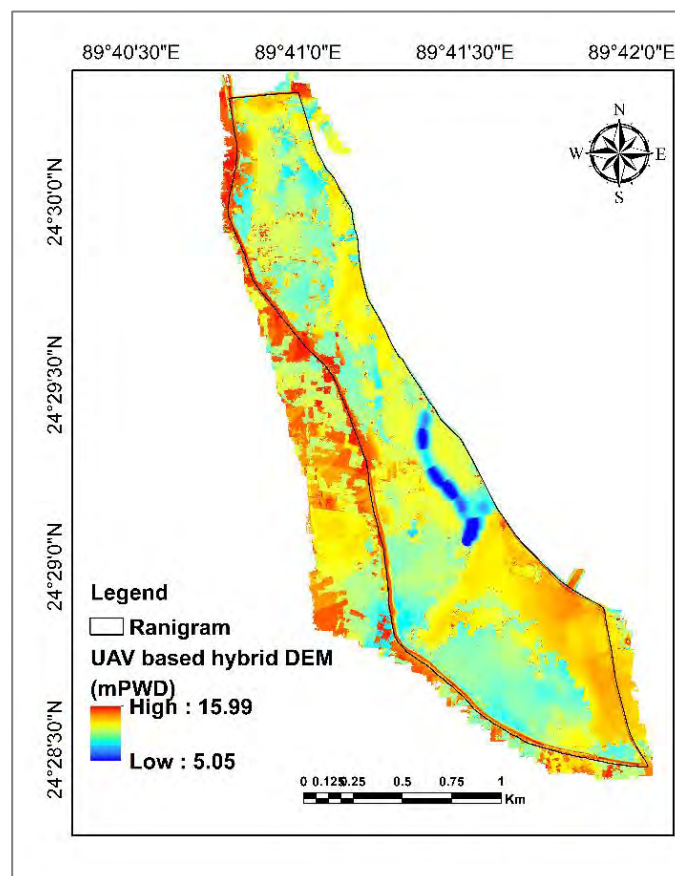


Figure 4.8 Final UAV-based DTM of Ranigram

## 4.4.2 SRTM 30m DEM

The Shuttle Radar Topography Mission (SRTM) DEM was developed based on the images acquired by two synthetic aperture radars aboard Space Shuttle Endeavour (USGS, 2021; Rabus et al., 2003). The shuttle flew and mapped continental areas between 60°N and 60°S for 11 days in February 2000 (USGS, 2021; Cowan and Cooper, 2005). The SRTM DEM that we used, with a spatial resolution of 30 m, was developed based on the C-band radar interferometry data and reported accuracy of ±16 m (Jarvis et al., 2008). The new data was released in September 2014, increasing the detail to 30-m (or 1 arc-second), revealing the full resolution of the world's landforms as measured initially by SRTM in 2000 (JPL, 2014; Jarvis et al., 2008). The geographic projection of SRTM 30m DEM is specified as WGS84 for the horizontal datum and EGM96 (Earth Gravitational Model 1996) for the vertical datum, which is more commonly known as Mean Sea Level (MSL) datum (USGS, 2021). The vertical unit is the meter for the DEM (USGS, 2021). According to its mission objectives, SRTM DEMs are expected to have linear vertical absolute height error of less than 16 m, linear vertical relative height error of less than 10 m, circular absolute geolocation error of less than 20 m, and circular relative geolocation error of less than 15 m (Farr et al., 2007). SRTM 30m accuracy assessments conducted by NIMA, the USGS, and the SRTM project team have shown the absolute vertical error to be much smaller, with the most
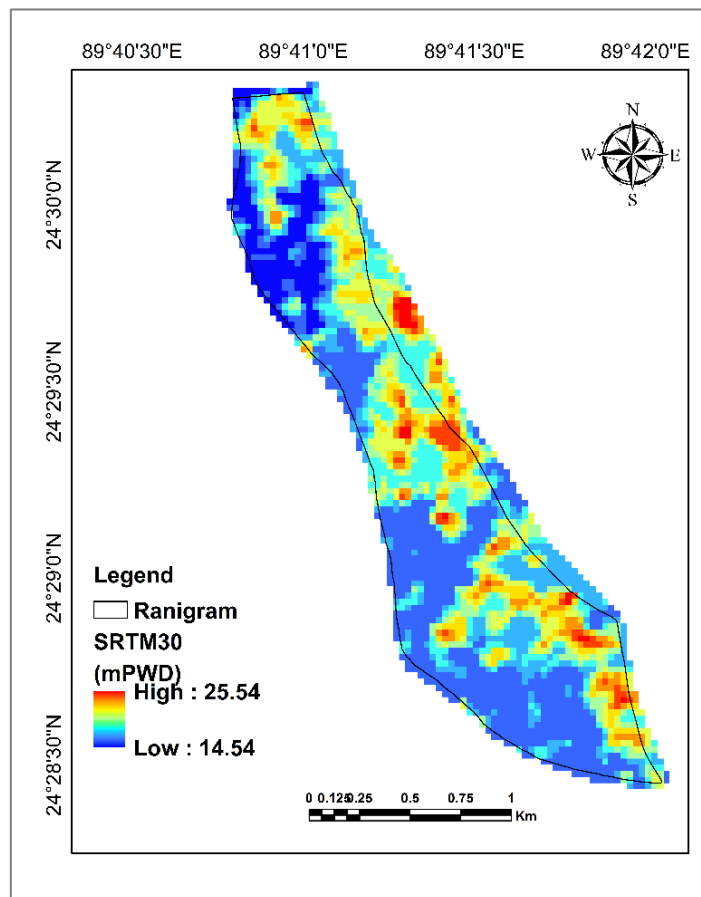
Figure 4.9 SRTM 30m DEM of Ranigram

reliable estimates being approximately 5 m (Kellndorfer et al., 2004).

In order to use in the study, the vertical elevation of the DEM was converted to Public Works Department Datum (m PWD Datum) from MSL datum. The MSL datum is 0.46m higher than the PWD datum.

Vertical Elevation (m PWD) = Vertical Elevation (MSL) + 0.46  ---------------- (4.11)

Using equation (4.11), the vertical elevation of the SRTM 30m DEM was converted to the PWD which is shown in Figure 4.11.

### 4.4.3    WorldDEM™

WorldDEM™ is a DEM offered by Airbus Defense and Space (Airbus, 2018). The WorldDEM™ products are based on the radar satellite data acquired during the TanDEM-X Mission, which is funded by a Public-Private Partnership between the German State, represented by the German Aerospace Centre (DLR) and Airbus Defense and Space (Airbus, 2018).

The WorldDEM™ consists of a DSM representing the Earth's surface, including heights of buildings and other artificial objects, trees, forests and other vegetation, and a DTM representing bare Earth, i.e., vegetation and artificial objects are removed (Farooq et al., 2019). The DSM product, called "WorldDEM," is an edited surface model. Post-processing of the TanDEM-X DEM data is done to reduce the impacts of SAR-specific data
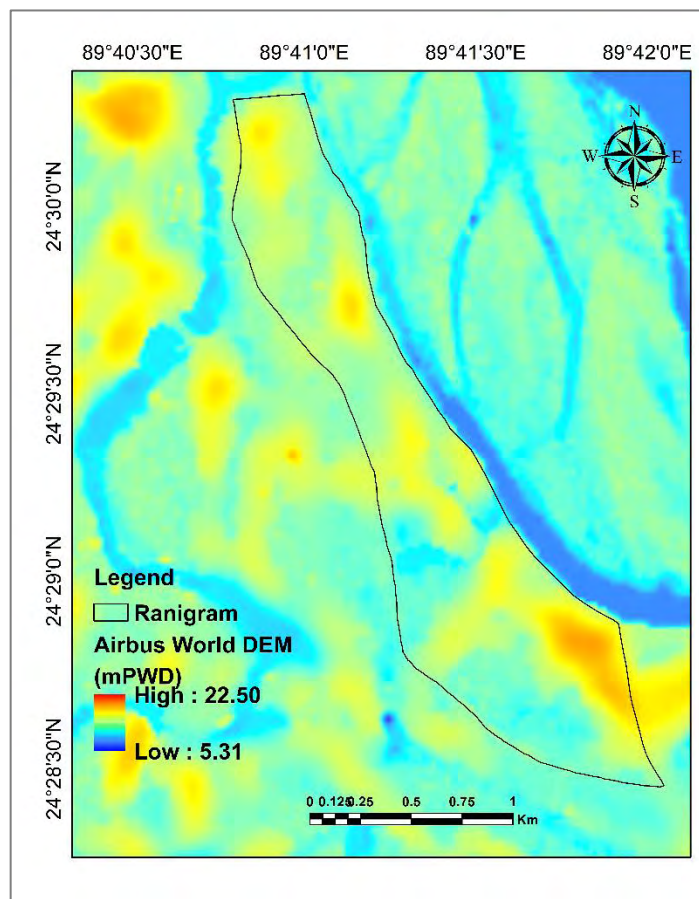


Figure 4.10 WorldDEM™ of Ranigram

features and artefacts in the elevation model to create the terrain model (Airbus, 2018). The WorldDEM™ editing process was done in two significant steps: terrain artifacts correction caused by SAR specific characteristics (e.g., layover and shadow) and the DSM processing. The DTM, called WorldDEM™ dataset, represents elevation information without obstruction features above ground; however, terrain characteristics are preserved. Each editing Quality Control (QC) was checked by a thematic validation and is performed according to ISO 2859 (Airbus, 2018).

The grid spacing of the WorldDEM™ products is 0.4 arc seconds in latitude, which equals approximately 12m (exactly 12.37m at the equator and 12.33m near the poles) (Airbus, 2018). The WorldDEM™ products are available as 32-bit floating data in GeoTIFF format. The vertical unit for measurement of elevation height is meter. The WorldDEM™ products are in Geographic Coordinates; the horizontal reference datum is the World Geodetic System 1984 (WGS84), and the vertical reference datum is the Earth Gravitational Model 2008 (EGM2008). Absolute Vertical Accuracy is less than 4 m, Relative Vertical Accuracy is less than 2 to 4 m, and Absolute Horizontal Accuracy is less than 6 m in WorldDEM™ (Becek et al., 2016). Using equation (4.11), the vertical elevation of the WorldDEM™ was converted to PWD and the DEM for the Ranigram area is shown in Figure 4.12.

### 4.4.4 MERIT DEM

The MERIT (Multi-Error-Removed Improved-Terrain) DEM was developed by removing multiple error components, i.e., the absolute bias, stripe noise, speckle noise, and tree height bias from the existing space-borne DEMs SRTM3 v2.1 and AW3D-30m v1 (MERIT DEM, 2021; Yamazaki et al., 2019). After the error removal, land areas mapped with 2 m or better vertical accuracy were increased from 39% to 58%. Significant improvements were found in flat regions where height errors were more prominent than topography variability, and landscapes such as river networks and hill-valley structures became represented (Yamazaki et al., 2019). The topography slope of previous DEMs was distorted mainly in most of the world's major floodplains, e.g., the Ganges, the Nile, the Niger and the Mekong basins, and swamp forests, e.g., Amazon, Congo and Vasyugan (Yamazaki et al., 2019). The newly developed MERIT DEM enhances many geoscience applications which are terrain dependent (Yamazaki et al., 2019). The horizontal datum of MERIT DEM is referenced to WGS84 and at a 3sec horizontal resolution (~90m at the equator), and vertically referenced to EGM96 geoid having a vertical unit of the meter (MERIT DEM, 2021). Using equation (4.11), the vertical elevation of the MERIT DEM was converted to PWD and the DEM is shown in Figure 4.13.
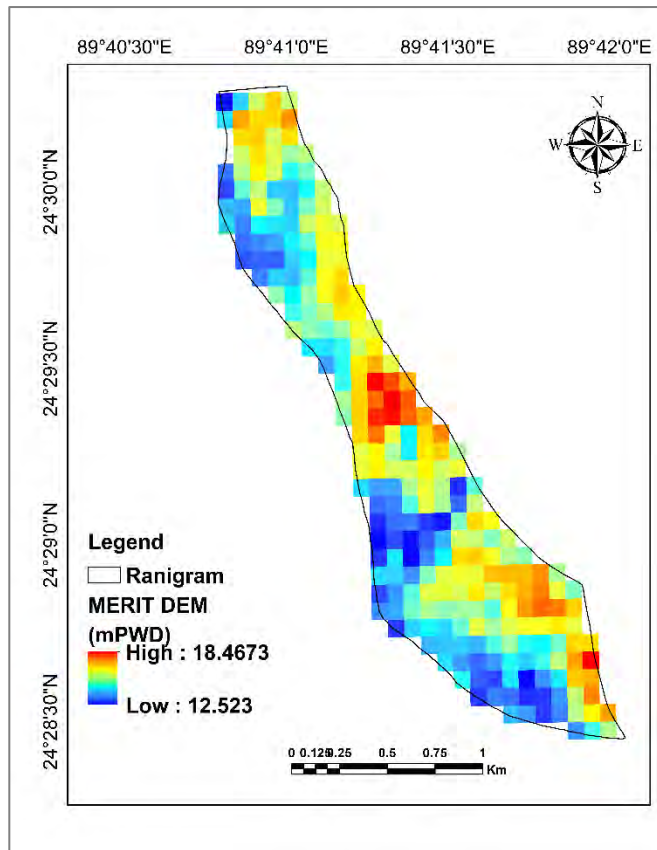


Figure 4.11 MERIT DEM of the Ranigram Area

## 4.4.5   ALOS PALSAR

The ALOS PALSAR DEM with 12.5 m resolution was downloaded from the Alaska Satellite Facility Distributed Active Archive Data Center (ASF DAAC) as a suite of geometrically and radio-metrically terrain corrected data products (ASF, 2021). The DEM is derived from ALOS PALSAR, processed using the Gamma Remote Sensing software package (ASF, 2021; Xiong et al., 2017; Das et al., 2014). Radiometric terrain correction (RTC) addresses two aspects of the effects of side-looking geometry of SAR imagery.  RTC DEMs are distributed at two resolutions. RT1 products with a pixel size of 12.5 m are generated from high-resolution and mid-resolution digital elevation models (DEMs). RT2 products are generated at a 30 m level for all available DEMs. The RT1 as ALOS-PALSAR 12.5 m DEM was downloaded in GIS-ready GeoTIFF format. However, the vertical elevation of the DEM is in ellipsoidal height. The ellipsoidal height was converted to mean sea level height by a geoid undulations model of the region (Takaku et al., 2014).

To obtain an orthometric height or a height above mean sea level (MSL) H, an interpolated geoid height N, was subtracted from the GPS ellipsoidal height *h*.

$$H = h - N \text{ ---------------- } (4.12)$$

An average geoid height (N) of -55.324 m for the Sirajganj area was selected and was subtracted from the original DEM elevation (z) in ArcGIS using the math calculator tool. Then using equation (4.11), the vertical elevation of the DEM was converted from MSL to PWD and the final DEM for Ranigram is shown in Figure 4.14.



Figure 4.12 ALOS PALSAR of Ranigram

56

### 4.4.6 ASTER DEM

The Terra Advanced Spaceborne Thermal Emission and Reflection Radiometer (ASTER) provides a global DEM of land areas on Earth at a spatial resolution of 1 arc-second approximately 30-meter horizontal posting at the equator (JPL, 2021). The development of the ASTER GDEM data is a collaborative effort between the National Aeronautics and Space Administration (NASA) and Japan's Ministry of Economy, Trade, and Industry (METI) (JPL, 2021; DeWitt et al., 2015). The ASTER Global DEM (GDEM) was created photogrammetrically from a compilation of cloud-free ASTER stereo-pair images [DeWitt et al., 2015; Gesch et al., 2012)]. The sensor is carried aboard the Terra satellite, and the images-stereo pairs were acquired by nadir- and after-looking angles in the near-infrared band (Moradas and Viveen, 2020; Hirano et al., 2003). A significant advantage of the along-track mode of data acquisitions, as compared to cross-track acquisition, is that the images that form the stereo-pairs are acquired a few seconds apart rather than days under uniform environmental and lighting conditions (Uuemaa et al., 2020). The geographic projection of ASTER DEM is specified as WGS84 for the horizontal datum and MSL for the vertical datum (Moradas and Viveen, 2020). Using equation (4.11), the vertical elevation of the DEM was converted from MSL to PWD for Ranigram and is shown in Figure 4.15.
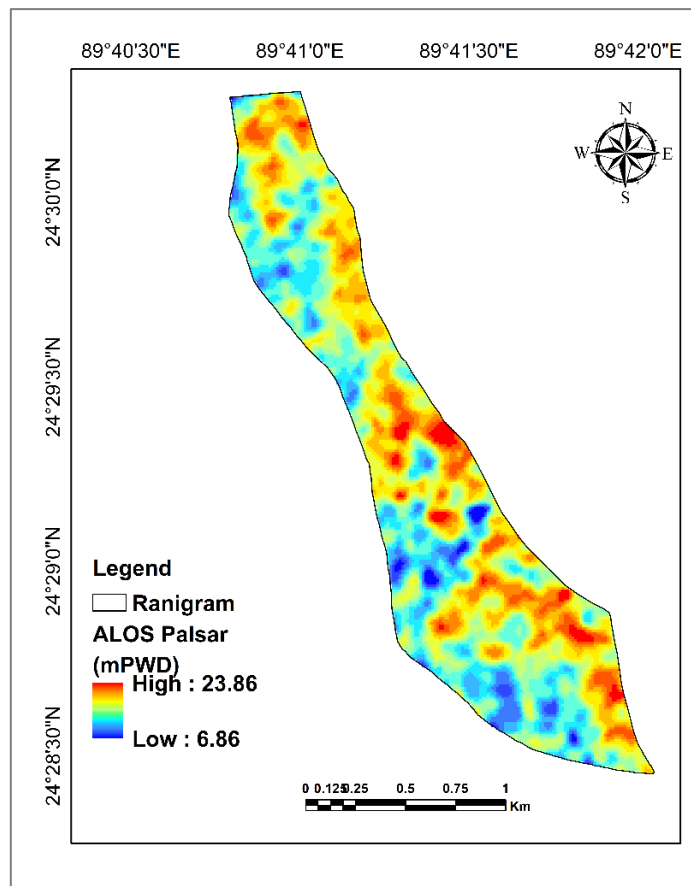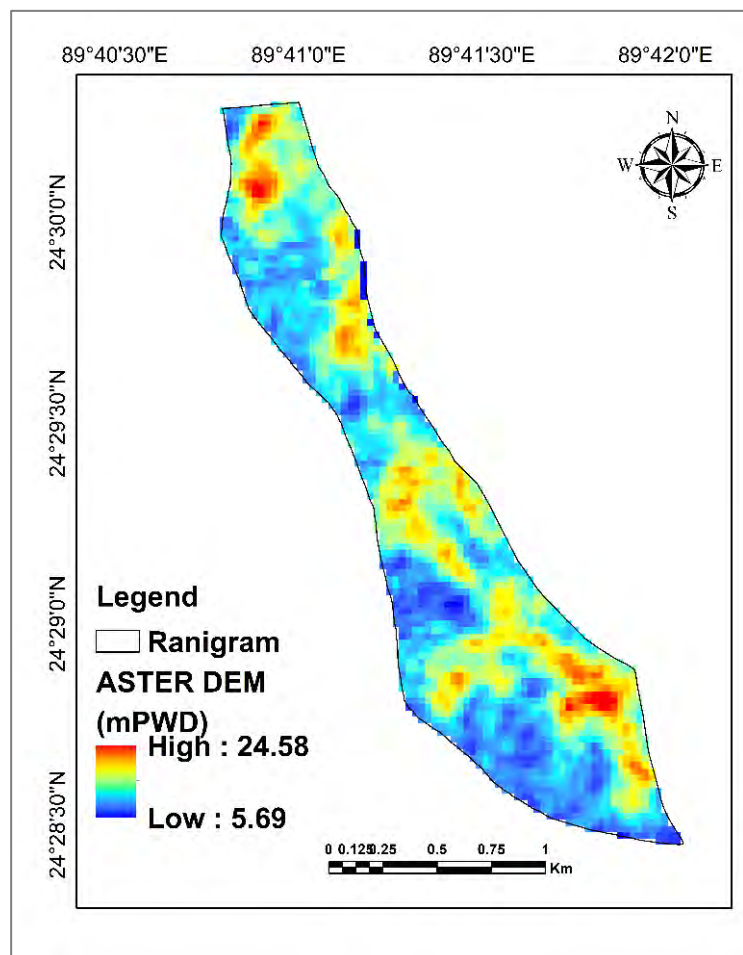


Figure 4.13 ASTER DEM of Ranigram

## 4.5 Flood Inundation from Open Source Satellite Image

For this analysis, the Ground Range Detected (GRD) product of Sentinel 1 data was used for flood mapping. The GRD products are multi-looked amplitude images with no phase information and projected from slant range to ground range using an Earth ellipsoid. Sentinel 1 images from the Google Earth Engine's data catalog of the required dates have been used for the analysis.

Earth Engine has undergone preprocessing steps that include applying orbit files, border noise removal, thermal noise removal, radiometric calibration, and terrain correction. The final terrain-corrected backscatter coefficient values are then converted to decibels via log scaling. Backscattering values in VV polarization have been used to extract flood-affected areas because of the stronger backscattering intensities of the co-polarized VV band compared to the cross-polarization VH band (Anusha and Bharathi, 2019; Liang and Liu, 2020). The methodological framework for the flood inundation mapping from Sentinel 1 image is shown in Figure 4.16.
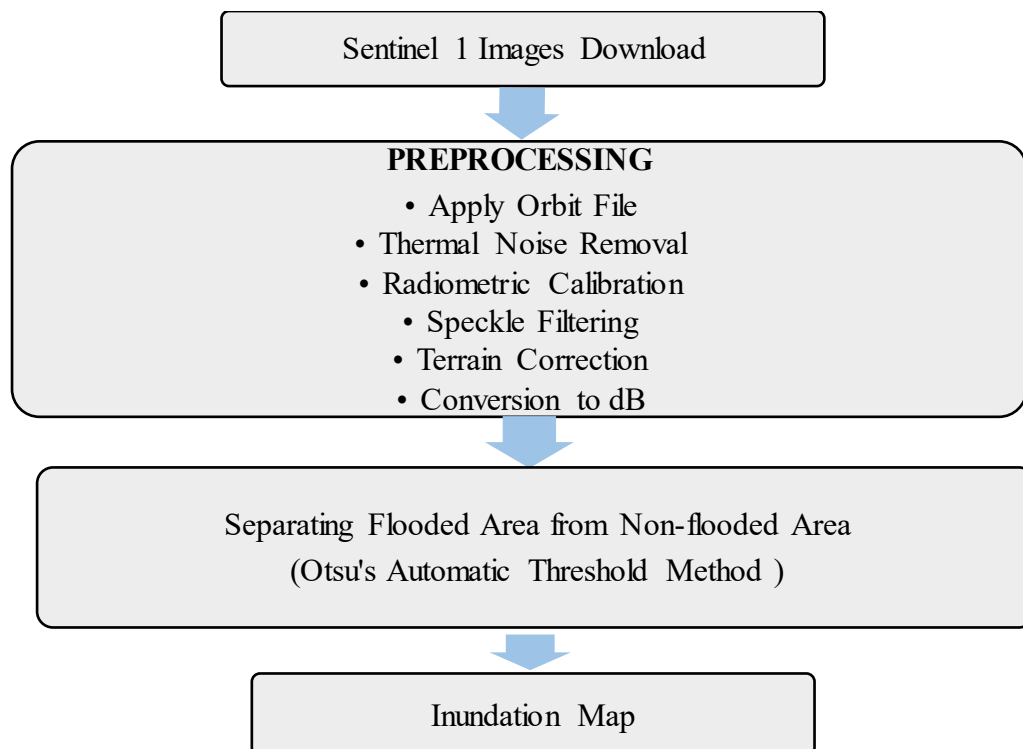


Figure 4.14 Methodology for Flood Map Generation with Sattelite Image

Otsu's (1979) automatic algorithm has been used to separate the flooded and non-flooded areas in a series of Sentinel 1 images via the Google Earth Engine. The image of January, 2020 was taken as the non-flooded image, and then images during the 2020 flood period were compared with this image. The algorithm involves iterating through all the possible threshold values and calculating a measure of spread for the pixel levels on each side of the threshold, i.e., the pixels that fall in the foreground or background.

## 4.6 HEC-RAS 2D Model

Flood simulations of the Ranigram area for 2018, 2019 and 2020 were conducted through a 2D hydrodynamic model developed in HEC-RAS software (version 5.0.7) (Farooq et al., 2019; Jung et al., 2014). The methodological framework for the HEC-RAS 2D model development is shown in Figure 4.17.
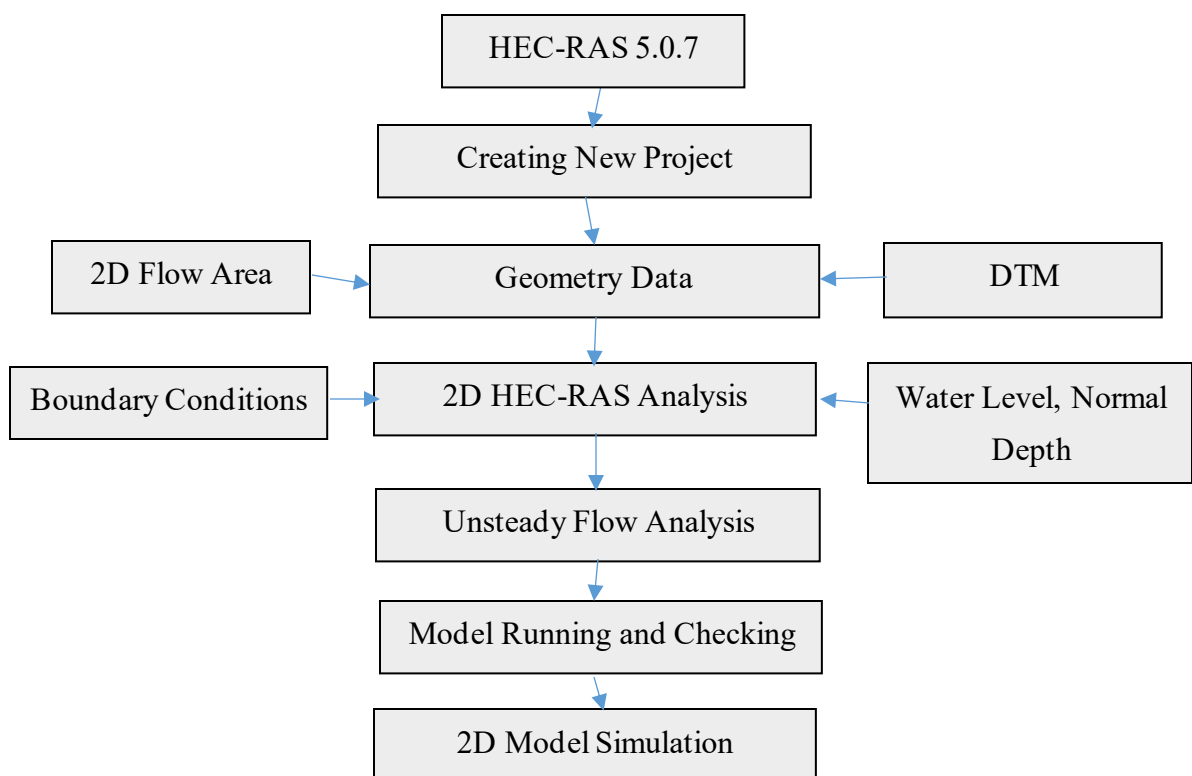


Figure 4.15 Methodological Framework for HEC-RAS 2D Model Development

HEC-RAS can calculate water surface profiles for 2D unsteady flow (Mehta et al., 2013; & Mehta et al., 2020). At first, a new project was created, and then the geometry file for the study was created. The geometry data was edited using the RAS Mapper

### 4.6.1 Digital Terrain Model (DTM)

The RAS Mapper was used for creating the geometry data setup and processing. The high-resolution DTM of the Ranigram area was used in creating the terrain in the RAS Mapper which is shown in Figure 4.19. The projection was taken as WGS 1984 – UTM zone 45N. The extent of the inundated area, inundation depths, duration of the flood, and arrival time, are assessed by using the model outputs.
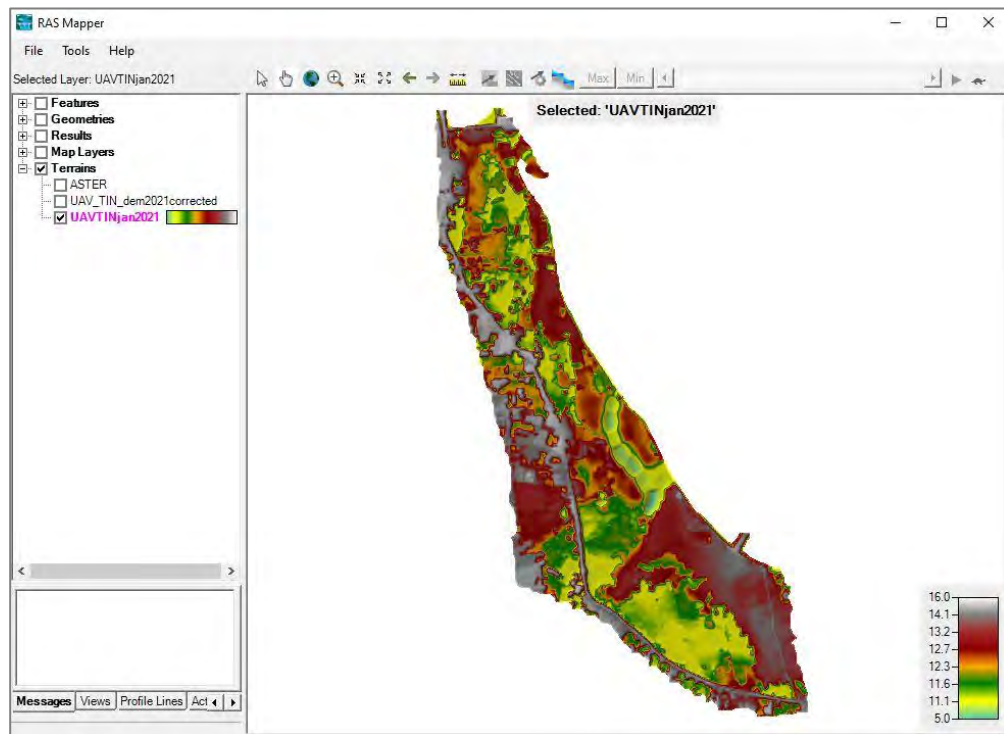


Figure 4.16 Terrain Model in RAS Mapper

In the modeling process, after uploading the produced terrain raster, the horizontal position correctness of the terrain is checked with satellite images which is shown in Figure 4.20.
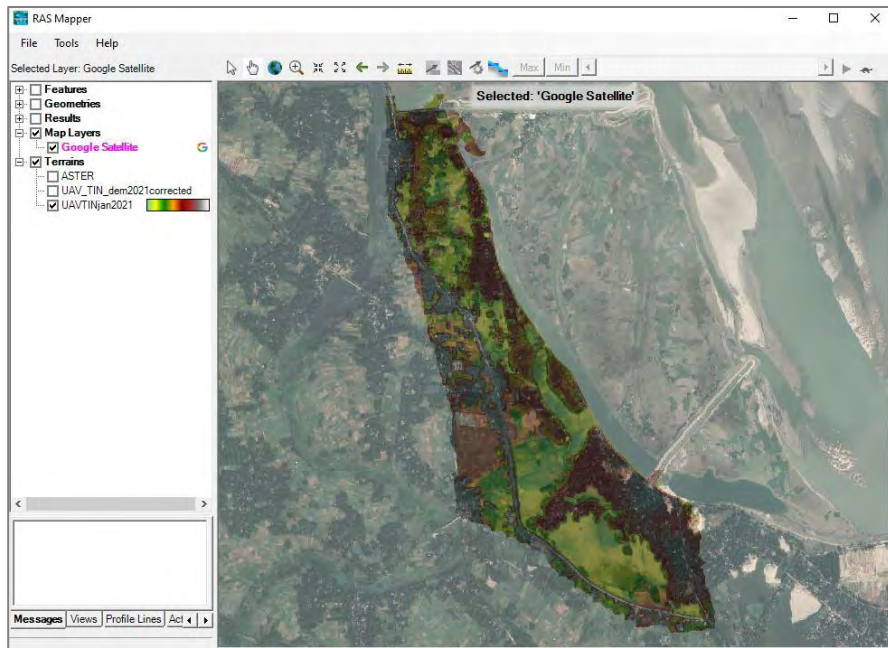
Figure 4.17 Terrain Checked with Satellite Imagery

## 4.6.2　2D Flow Area

At first, the 2D flow perimeter of the study area was set. The shapefile of the Ranigram area was imported for the 2D flow area perimeter. A 2D flow area describing the boundary of the presumed flood domain was added by exporting the Ranigram boundary shapefile in the geometric data editor in the RAS Mapper of the software. Figure 4.21 shows the 2D flow area perimeter used in the Mapper.
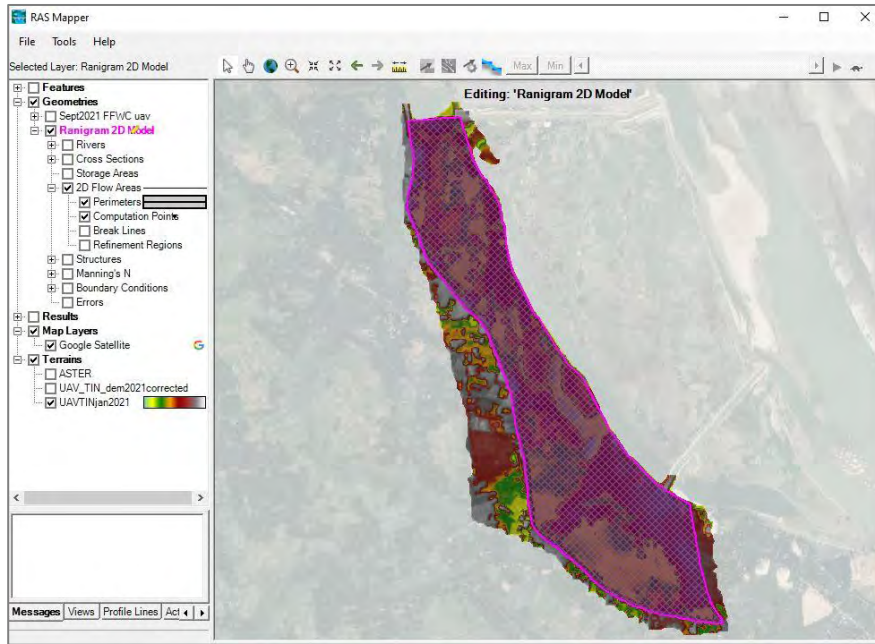
Figure 4.18 2D Flow Area Perimeter

Then, a computational mesh within the boundary layer was developed automatically with 2m×2m computational point spacing (CPS), resulting in a total of 21500 grid cells. Manning's roughness coefficient values of 0.04 and 0.05 were used for the agricultural land and housing land, respectively, in the 2D flow area. Figure 4.22 shows the 2D flow area properties used in the model.
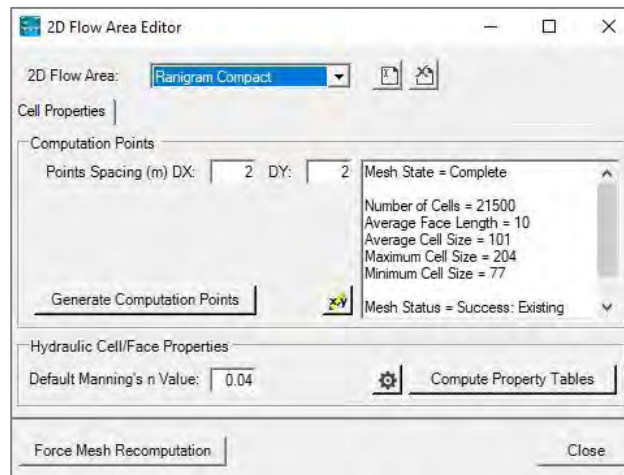


Figure 4.19 2D Flow Area Properties Used in the HEC-RAS Model

### 4.6.3 Boundary Conditions

The upstream and downstream ends of flooding were defined by drawing boundary condition (BC) lines along the outer boundary of the 2D area. The upstream and downstream boundary condition lines were created to replicate the actual input and output locations in the 2D flow model for the unsteady simulation. Two external boundary condition lines were drawn, which are shown in Figure 4.23. First boundary condition is at the breaching location beside the Union Parishad from where the water enters the Ranigram area, and the other is in the south of the Ranigram village beside the pilot site.
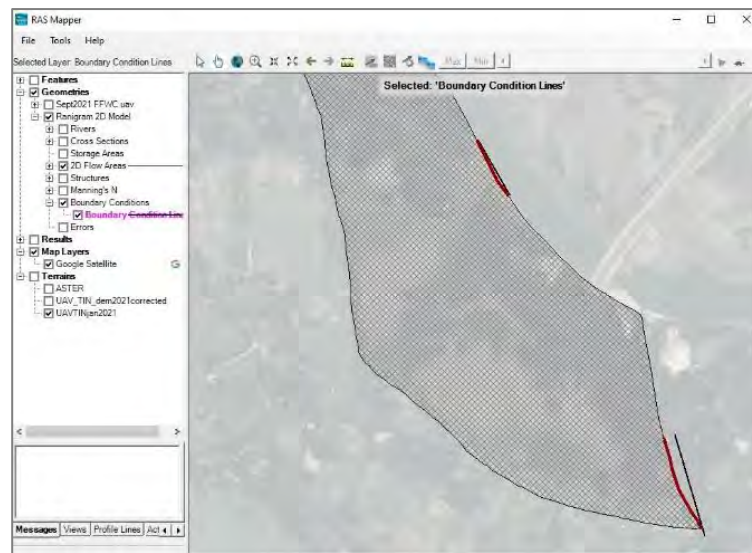


Figure 4.20 Boundary Condition (BC) Lines Used in the Model

The stage hydrograph was taken for the first (upstream) boundary condition, and for the second (downstream) boundary condition, the normal depth was taken. The daily flood water level was used for the stage boundary condition at the water entry location beside the Union Parishad. Normal depth is the depth of flow in a channel when the slope of the water surface and channel bottom is the same and the water depth remains constant. The normal depth boundary requires an energy slope be entered in the HEC-RAS and the software then back-calculates a starting water surface elevation using Manning's equation:

$$Q = \frac{1}{n} A R^{2/3} \sqrt{S_f} \text{ --------------- (4.13)}$$

Where, Q = Flow Rate, A = Flow Area, n = Manning's Roughness Coefficient, R = Hydraulic Radius, and Sf is the friction slope. $S_f$ is the slope of the energy grade line and can be estimated a prior by measuring the slope of the bed. With the friction slope, the flow, the n-value and the cross-section shape specified, HEC-RAS can back-calculate stage from Manning's Equation. To define the normal depth type BC, the average slope was calculated from the measured water level data at the UP and Pilot Site gauges in the Ranigram area. The average slope for the second boundary condition estimated from the measured water level data found to be 0.0001 and was used for the second boundary condition for the 2D area of Ranigram.

### 4.6.4 Unsteady Flow Analysis

Before performing model simulations, calculation options are specified within the unsteady flow analysis editor of the software. 2D flow area in HEC-RAS specifies the extent of the area within which 2D flow calculations are performed. It is marked as a polygon layer for the study area. A computational 2D mesh is established within a defined 2D flow area having computational cells. The unsteady flow component of the HEC-RAS is capable of performing subcritical, supercritical, and mixed flow regime calculations.

The HEC-RAS model has two equation sets that can be used for unsteady flow modeling, namely, the full momentum equations and the diffusion wave equations. The model solves either of these equation sets to determine the flow moving over the computational mesh (Brunner, 2016). These equations are obtained from the continuity and momentum equations by depth averaging technique (Quiroga et al., 2016). The governing equation for surface flow can be expressed as follows:

$$\frac{\partial u}{\partial t} + \left( u \frac{\partial u}{\partial x} + v \frac{\partial u}{\partial y} \right) = v_t \left( \frac{\partial^2 u}{\partial x^2} + \frac{\partial^2 u}{\partial y^2} \right) - g \frac{\partial H}{\partial x} - nu + fv \text{ ------ (4.14)}$$

Where,

| | |
|---|---|
| u | = specific flow in the x directions |
| v | = specific flow in the y directions |
| H | = water depth |
| $g$ | = gravitational acceleration |
| n | = Manning resistance coefficient |

$$f \qquad = \text{Coriolis force}$$

The acceleration terms in the Full Momentum equation can be neglected in most practical applications (Babister and Barton, 2012; Ponce, 1990). Then these become simple parabolic equations known as the diffusion wave equations. The acceleration terms such as the viscosity and Coriolis terms are neglected for this study. For the diffusion wave equation, the bottom friction is equal to the pressure gradient. The water surface slope is balanced by the friction slope. This means the local acceleration, advective acceleration, viscosity (turbulence), and coriolis effect are not considered.

The governing diffusion wave equation is:

$$g \frac{\partial H}{\partial x} + nu = 0 \quad \text{------ (4.15)}$$

In general, the diffusion wave equations are more forgiving numerically than the full momentum equations and still get numerically stable and accurate solutions (Brunner, 2014). In the diffusion wave simplification, all acceleration and turbulence terms are neglected which reduces computation time and numerical instability. Since the diffusive wave equations can yield satisfactory solutions for unsteady flow simulation, it has been used more frequently and so the diffusion wave is selected in the HEC-RAS model (Fan and Li, 2006). One can easily switch between the equations sets and each set of equations can be tried for a given problem.

The model run was performed for the time series similar to the measured data. The model was run with a 1-minute computation interval. The output of the model was taken for a 1-day interval.

### 4.6.5 Calibration and Validation at Cell Location of Ranigram Area

After the simulation in HCE-RAS, the computational cell at the Culvert water level gauge location was selected in the RAS Mapper which is shown in Figure 4.26. The water level reading at the Culvert and Pilot Site was used for calibrating and validating the model. The measured water level data of 2018 and 2020 were used for the calibration and validation of the model, respectively. The cell's daily water surface elevation data for the whole flood period was collected from the model result for both the Culvert and Pilot

Site location cells (Yalcin, 2020). Then this model water level was compared with the measured water level.
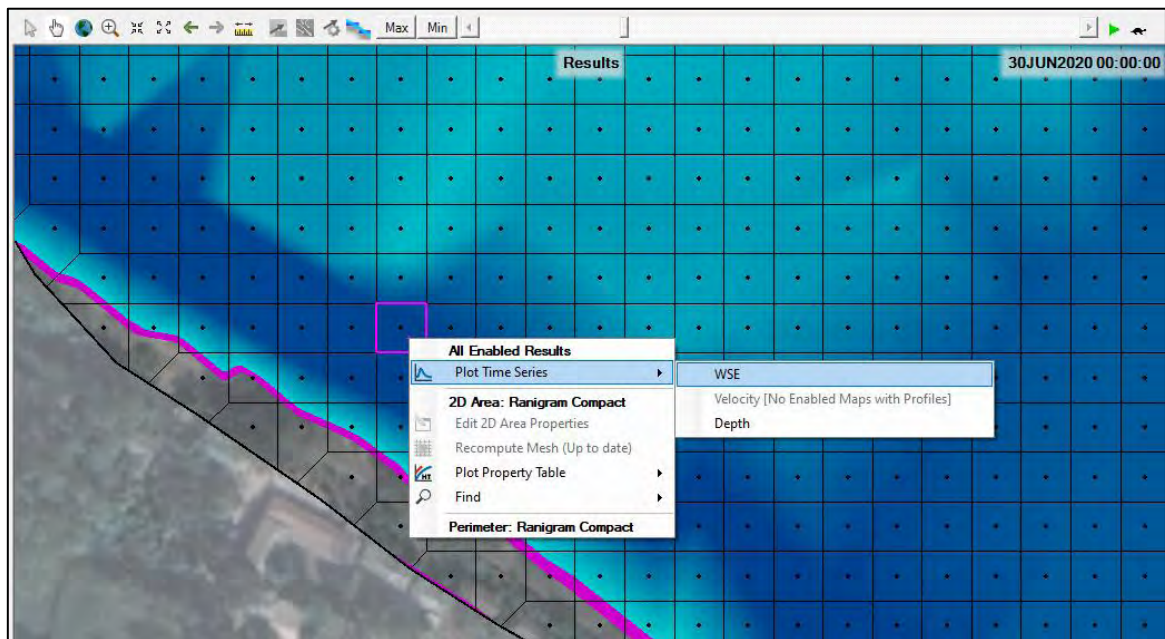


Figure 4.21 Cell Selection in the RAS Mapper

The result of the HEC-RAS model was also compared with an actual flood event. The flood photos were collected from some crucial locations in the Ranigram area for a few days during the flood. Then flood inundation maps were extracted from the HEC-RAS model for the specific dates for which the flood photos were collected from the Ranigram area.

## 4.7    GIS Analysis and Mapping with ArcGIS

Arc-GIS is a group of Geographic Information System (GIS) software products produced by Environmental Systems Research Institute, Inc. (ESRI). ArcGIS 10.5 software was used in the study for working with maps and geographic information analysis (Mehta et al., 2020). It is used to create maps, compile geographic data, analyze mapped information, share and discover geographic information, using maps and geographic information in various applications. First, the HEC-RAS flood results were exported from the RAS Mapper as raster files. Then the raster was taken in ArcGIS in Layout view to create the flood maps. Next, the north arrow, legend, and scale bar were inserted for

the maps correctly. Then the png file of the flood map was exported from ArcGIS in 300 dpi resolution.

## 4.8    Comparing UAV-based DTM with Different Global DEMs

This model was again simulated using different types of DEMs to investigate the influence and performance of other globally available comparatively lower-resolution DEMs. The vertical elevation of each DEM was compared with the measured UAV-based high-resolution DTM. At first, the vertical elevation of the WorldDEM$^{TM}$, ALOS PALSAR, SRTM 30m, and ASTER DEM was converted to 17.5 cm as the resolution of the UAV-based DTM. Then raster calculator of the spatial analysis tool was used to find out the vertical elevation.

## 4.9    Using FFWC Forecast Data for the Model to Forecast Flood

This 2D model was used to forecast floods in the Ranigram area. Therefore, the model's boundary condition was developed from the FFWC's forecasted water level in the Jamuna River. Thus, the result of the model represents the forecasted flood scenario in the Ranigram area for the corresponding FFWC forecast.

# CHAPTER FIVE

# RESULTS AND DISCUSSION

## 5.1    Statistical Analysis for the Hydrological Aspects of Floods in Ranigram

### 5.1.1    Rainfall Statistics for Sirajganj

The daily rainfall data at the nearby Bogura station was collected and used for the Sirajganj region to perform the necessary rainfall analysis. The average annual rainfall is found to be 1736 mm. The 1-day maximum rainfall is found to be 279 mm, and the 2-day maximum rainfall is found to be 335 mm.

Figure 5.1 shows the frequency analysis for the maximum daily rainfall at Sirajganj. The rainfall intensity is found to be 125 mm for a 2-year return period, 190 mm for 10-year, and 279 mm for 100-year rainfall.
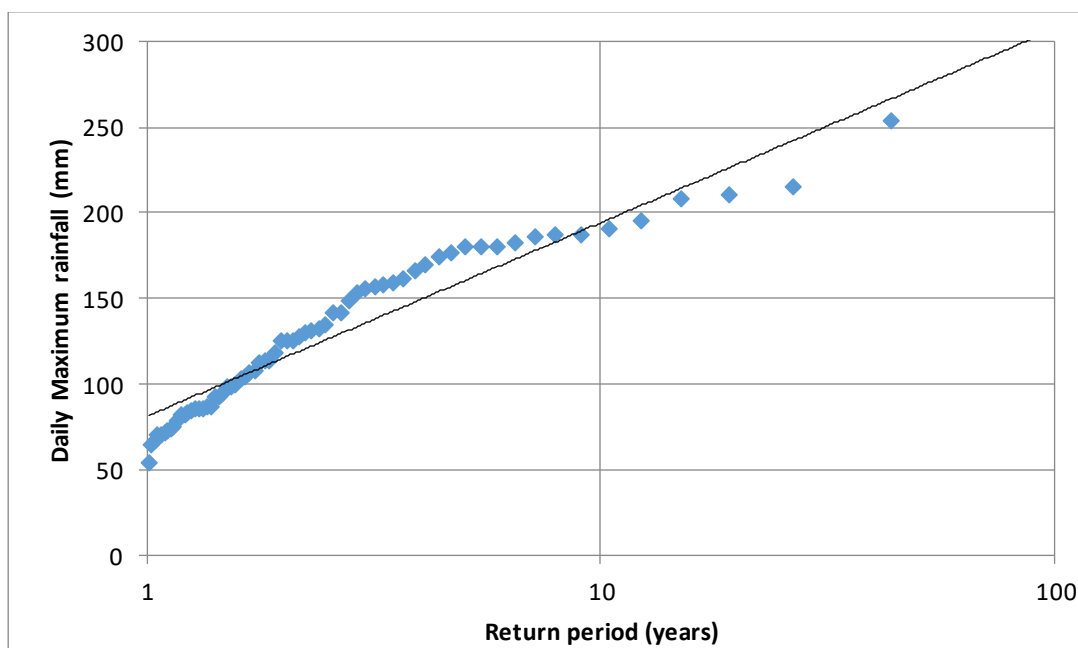


Figure 5.1 Frequency Analysis for Rainfall in the Sirajganj Region

### 5.1.2    Statistics of Highest Water Level of the Jamuna River

The water level data at Sirajganj station of the Jamuna River for 37 years (from 1984 to 2020) has been analyzed to determine the riverine flooding in the Sirajganj area. The

yearly maximum water level at Sirajganj station of the Jamuna River is shown in Figure 5.2. The danger level at the Sirajganj station of the Jamuna River is 13.35 mPWD specifies the water level, which will cause flooding in the surrounding area if the river crosses the level. It is seen from the figure that the Jamuna River crossed the danger level every year except for 5 years in the 37 years of available data at the Sirajganj station.
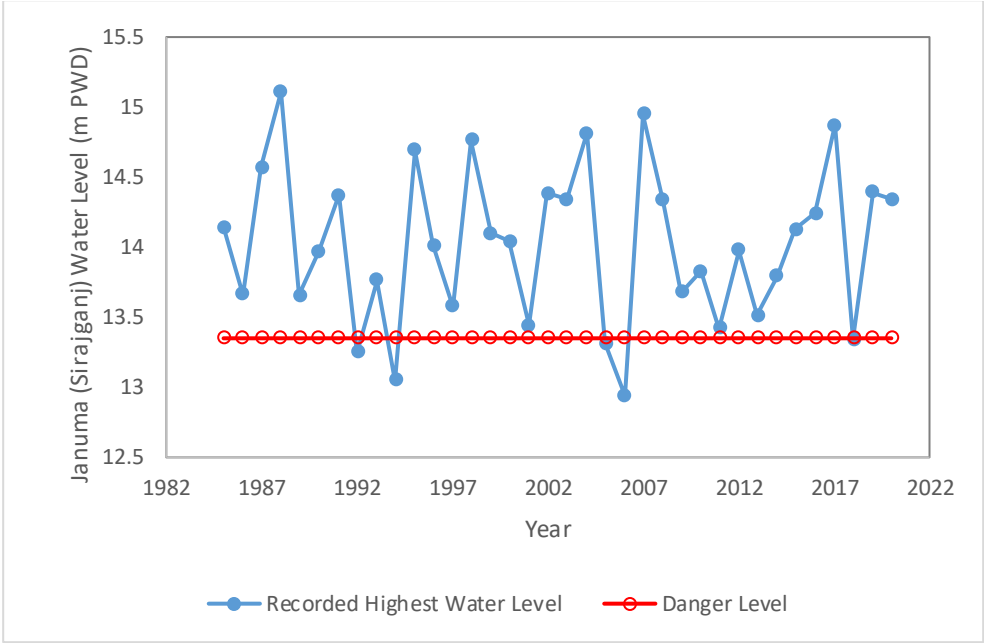


Figure 5.2 Historical Highest Flood Level of the Jamuna River at Sirajganj Station

### 5.1.3 Frequency Analysis of the River Water Level at Sirajganj Station

Figure 5.3 shows the water level for different return periods compared with the danger level of the Jamuna River at Sirajganj station. For the 1-year return period, the water level is found to be 12.94 mPWD and for the 2-, 10-, 20-, 50- and 100-year return periods, the water level is found to be 14.04, 14.81, 14.95, 15.09 and 15.12 mPWD, respectively.
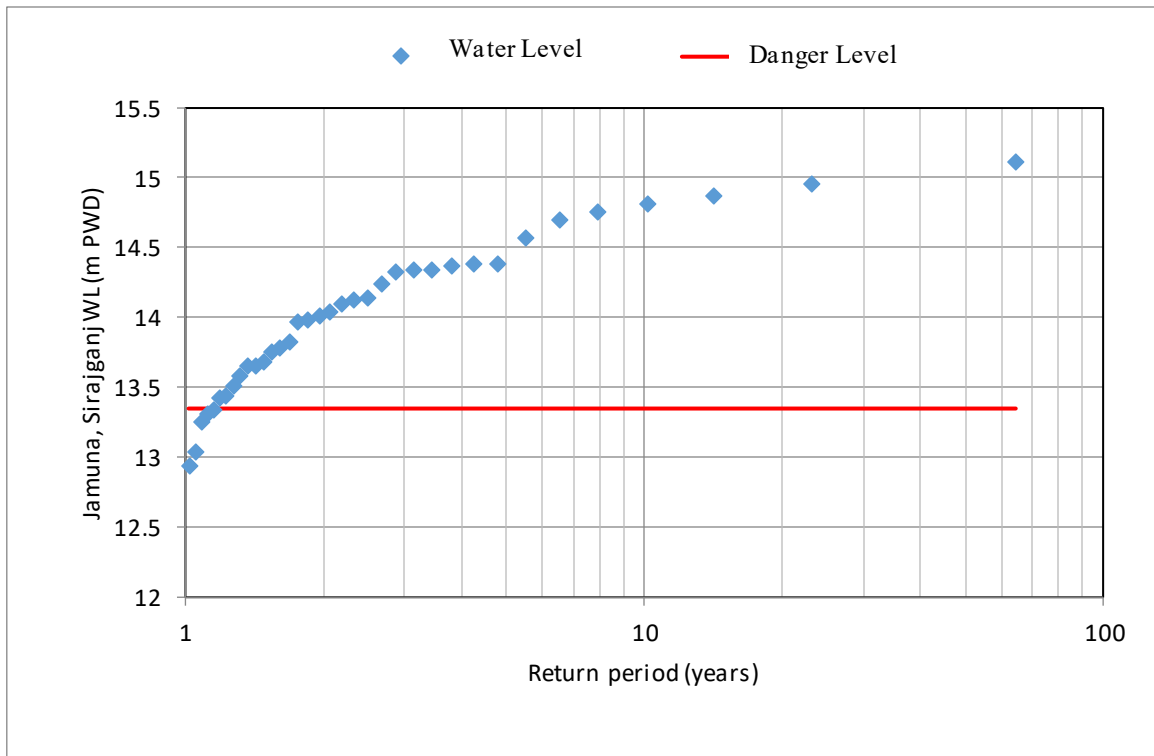
Figure 5.3 Frequency Analysis for the Jamuna River Water Level at Sirajganj Station

It is found that, for only a 1.18-year return period, the water level in the Jamuna River at Sirajganj crosses the danger level, and for a 2-year return period, the water level at the Jamuna River is 0.65m above the danger level.

### 5.1.4 Contribution of Rainfall and Jamuna River Water in Ranigram

The contribution of rainfall and the contribution of the Jamuna River water for different return periods in the Ranigram area are shown in Figure 5.4, 5.5 and 5.6.

For the 2-year return period, the maximum rainfall intensity can contribute to the water of 319680 $m^3$ in one day, 446976 $m^3$ in two days, and 508032 $m^3$ in three days. In contrast, the contribution to the Ranigram area from
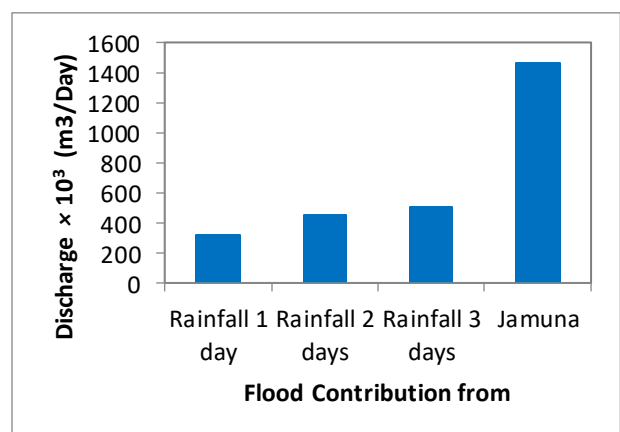


Figure 5.4 Contribution by Rainfall and Jamuna River for 2-year Return Period

the Jamuna River is 1467813 m$^3$ in one day, which is 4.6 times more than the rainfall contribution.

For the 10-year return period, the maximum rainfall intensity can contribute to the water of 470592 m$^3$ in one day, 639360 m$^3$ in two days, and 739584 m$^3$ in three days in the Ranigram area. In contrast, the contribution to the Ranigram area from the Jamuna River is 2950358 m$^3$ in one day, which is 6.2 times more than the rainfall contribution.
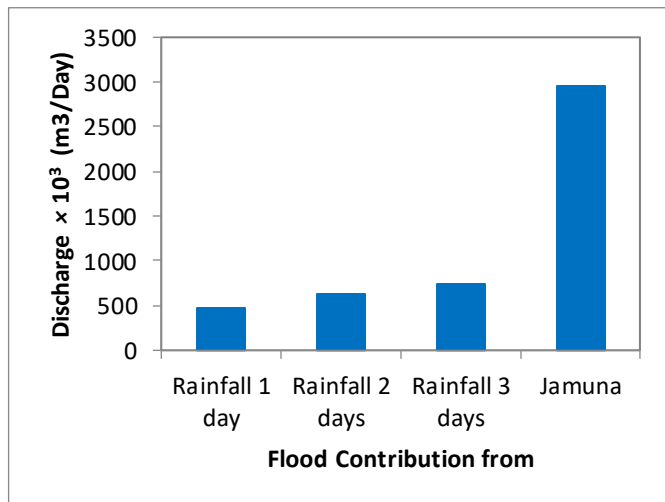


Figure 5.5 Contribution by Rainfall and Jamuna River for 10-year Return Period

For a 100-year return period, the maximum rainfall intensity can contribute to the water of 645120 m$^3$ discharge in one day, 849024 m$^3$ in two days, and 1012608 m$^3$ in three days. In contrast, the contribution to the Ranigram area from the Jamuna River is 3437010 m$^3$ in one day, which is 5.4 times more than the rainfall contribution.
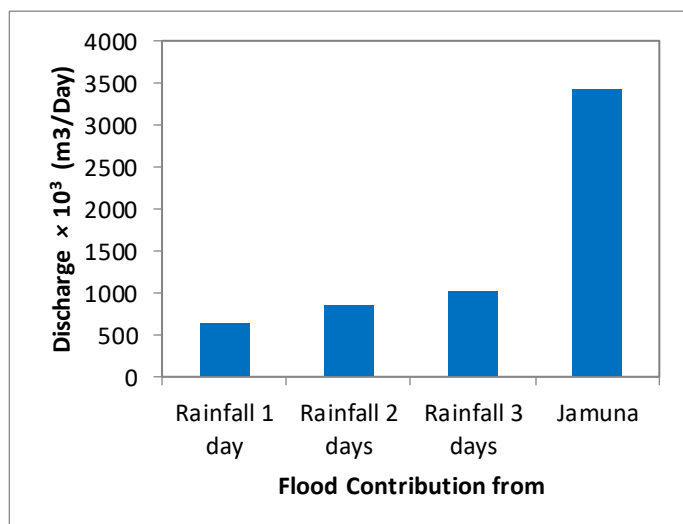


Figure 5.6 Contribution by Rainfall and Jamuna River for 100-year Return Period

Thus, the contribution of the Jamuna River is by far more dominant than the contribution of rainfall. Even the 1-day contribution by the Jamuna River water is far dominant than the 3-day rainfall discharge. As the Ranigram area is just beside the river, the rainfall water finally makes its way to the river, and so it is accumulated and measured as the river water.

Hence, in this study, the contribution of rainfall is not considered. The very small flood upto 0.279 m contributed by rainfall and the water logging in some bounded area is not considered. The flooding in the Ranigram area is analyzed for the effect of the Jamuna River water.

## 5.2 Statistical Relation of the Jamuna River Water with the Flood Water in Ranigram

### 5.2.1 Flood Data Analysis of 2018

The flood depth data at each water level gauge in the Ranigram village was collected during the flood season of 2018. The floodwater level for the corresponding depth was calculated using proper benchmarking for each day at each gauge. The water level at Ranigram is plotted with the water level of the Jamuna at Sirajganj station in Figure 5.7.
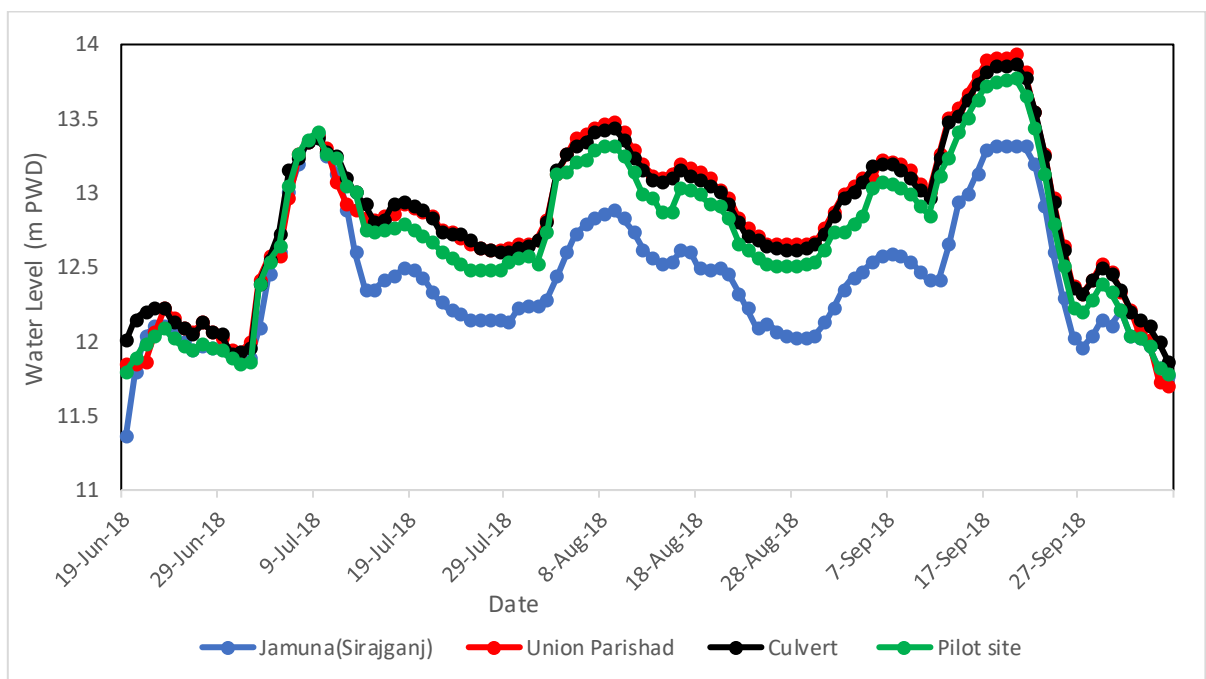


Figure 5.7 Flood Water Level Data at the Gauges in the Ranigram and Sirajganj Station of the Jamuna River in 2018

Flood water levels of the Jamuna and Ranigram reveal that the water level in the floodplain rises with the increase of the Jamuna water level and falls with the decrease of the Jamuna water level. Thus, in the initial period of flooding and during the end of

the flooding period, the river's water level stays higher than the water gauges in the floodplain. It is found that when there was a sudden rise or fall in the water level of the Jamuna River, the water level in the floodplain did not follow that trend. The co-relation with each gauge was found from the flood water level at the gauges in the Ranigram area.

### 5.2.1.1 Relation among Installed Water Level Gauges

The co-relation among each gauge was found from the flood water level at the gauges in the Ranigram area. The scatter plot (Figure 5.8) shows that the $R^2$ value from the relation between Union Parishad with Culvert, Union Parishad with the Pilot site, and Culvert with the Pilot site is more than 0.97. It shows that there is a very good co-relation among each gauge water level. This led us to the decision that the flooding pattern inside the Ranigram area is quite similar to the water level variation in the Jamuna River.
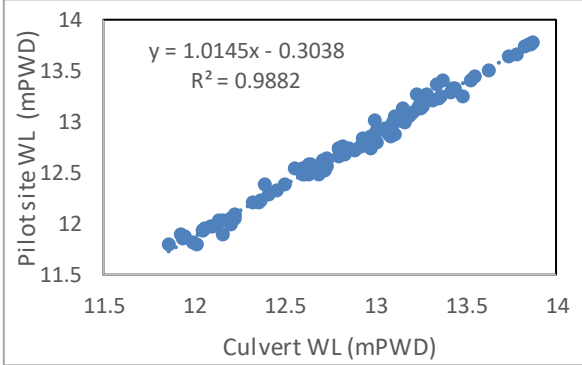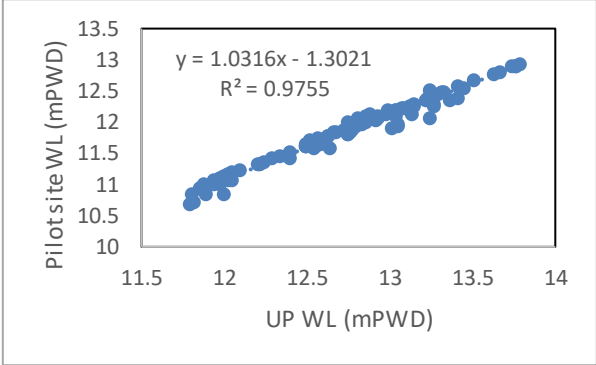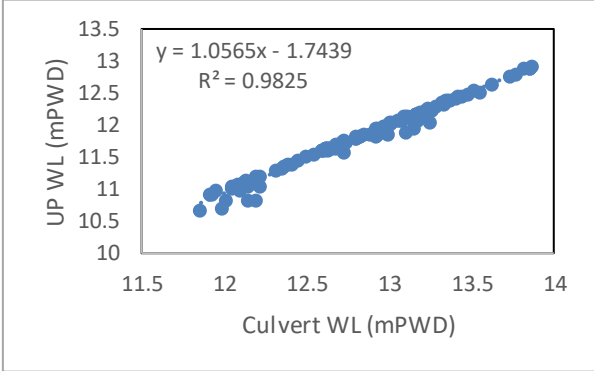


Figure 5.8  Relation among the Water Level of the Gauges in the Ranigram Area

The relation of the flood water level at the gauges with the previous day's floodwater level is also investigated. The relation with the water level of the previous one day, two days, and three days is analyzed. The $R^2$ value at Union Parishad is found from 0.94 to 0.64 for the previous one to three days water level. The $R^2$ value at Culvert and Pilot Site is found from 0.93 to 0.63 and from 0.93 to 0.62, respectively.

### 5.2.1.2    Relation of Gauge Water Level with the Water Level of the Jamuna River

The water level of each gauge at the Ranigram area was plotted with the Jamuna's water level at Sirajganj station. The relation of water level at this gauge location in Ranigram with the Jamuna river water level is investigated. Furthermore, from this analysis, a statistical relation between the water level of the Jamuna River and the water level at the location of gauges are established according to equation (4.6). The relation and error in the model were analyzed using the equations (4.8), (4.9), and (4.10).

The statistical relation found between the water level at the location of Union Parishad and the Jamuna River water level at Sirajganj is given below:

$$Y_{UP} = 1.1093X - 0.9437 \text{--------------- (5.1)}$$

Here, Y is the water level at Union Parishad, and X is the water level in the Jamuna River at Sirajganj for the corresponding day.

In the regression and Nash–Sutcliffe Efficiency (NSE) analysis, the R² value is found to be 0.79 (Figure 5.9), and the NSE is found to be 0.795, which refers to a good relationship. In the Mean Absolute Error (MAE) and the Root Mean Square Error (RMSE) analysis, the MAE is found to be 0.20 m, and RMSE is found to be 0.236 m. The Residual Range is from 0.267 to -0.298 m.
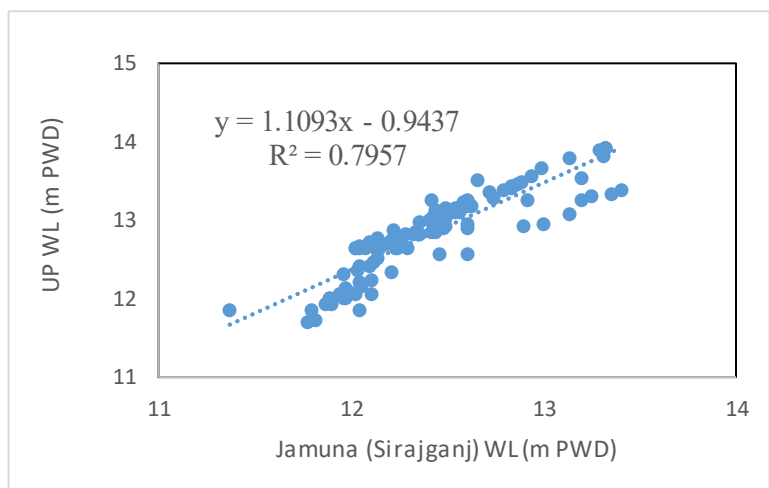


Figure 5.9: Relation of the Jamuna River Water Level with the Water Level at Union Parishad in the Ranigram for 2018.

The statistical relation found between the water level at the location of Culvert and the Jamuna River water level at Sirajganj is given below:

$$Y_{Culvert} = 1.0635X - 0.3715 \text{------------- (5.2)}$$

Here, Y is the water level at Culvert, and X is the water level in the Jamuna River at Sirajganj for the corresponding day.

In the regression and NSE analysis, the R² value is found to be 0.83 (Figure 5.10), and NSE is found to be 0.831, which refers to a good relationship. In the Mean Absolute Error and the Root Mean Square Error analysis, the MAE is found 0.15 m, and RMSE is 0.201 m. The Residual Range is from 0.276 to -0.176 m.
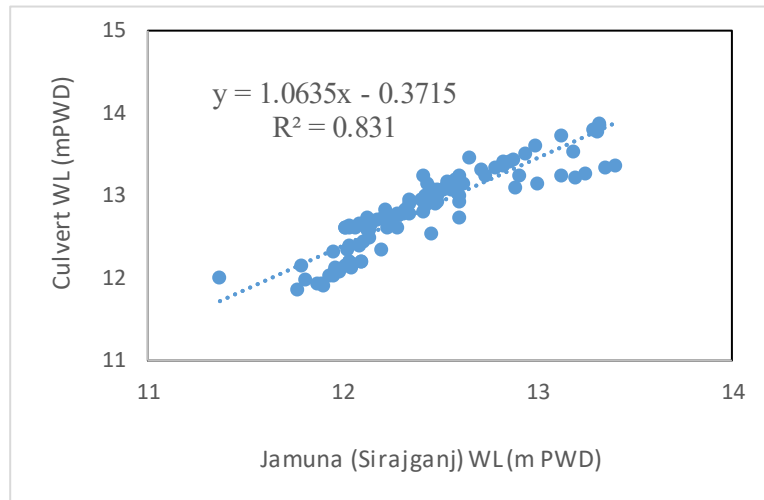


Figure 5.10: Relation of the Jamuna River Water Level with the Water Level at Culvert in the Ranigram for 2018.

The statistical relation found between the water level at the location of Pilot Site and the Jamuna River water level at Sirajganj is given below:

$$Y_{PilotSite} = 1.1072X - 1.0313 \text{--------- (5.3)}$$

Here, Y is the water level at Pilot Site, and X is the water level in the Jamuna River at Sirajganj for the corresponding day.

In the regression and NSE analysis, the R² value is found to be 0.86 (Figure 5.11), and NSE is found to be 0.864, which refers to a good relationship. In the Mean Absolute Error and the Root Mean Square Error analysis, the MAE is found 0.14 m, and RMSE is 0.184 m. The Residual Range is from 0.334
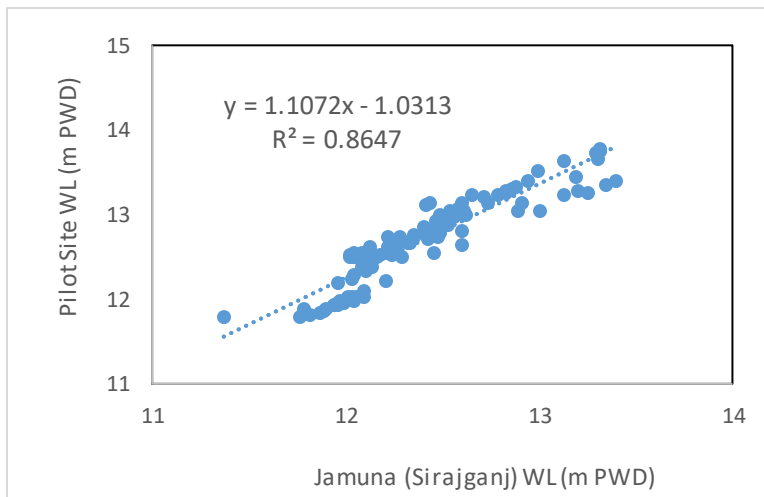


Figure 5.11: Relation of the Jamuna River Water Level with the Water Level at Pilot Site in the Ranigram for 2018.

to -0.240 m. Table 5.1 summarizes the findings of the above statistical analyses.

Table 5.1 Statistical Relation and Error of Gauge Water Level with the Jamuna River Water Level in Simple Regression Model for 2018 Flood

|  | R² | NSE | MAE (m) | RMSE (m) | Residual Range (m) |
|---|---|---|---|---|---|
| **UP** | 0.79 | 0.80 | 0.2 | 0.24 | 0.267 to -0.298 |
| **Culvert** | 0.83 | 0.83 | 0.15 | 0.20 | 0.276 to -0.176 |
| **Pilot Site** | 0.86 | 0.86 | 0.14 | 0.18 | 0.334 to -0.240 |

### 5.2.1.2.1 Residual from Statistical Model of Simple Regression

Residual in the three water level gauge locations for the 2018 flood season is calculated for each day. The measured water level is subtracted from the water level of the statistical model. The residual from the model for each day in the three water level gauges is shown in Figure 5.12. The residual is higher at the beginning and end of the flood period. When the flood is stabilized, the residual is very low.
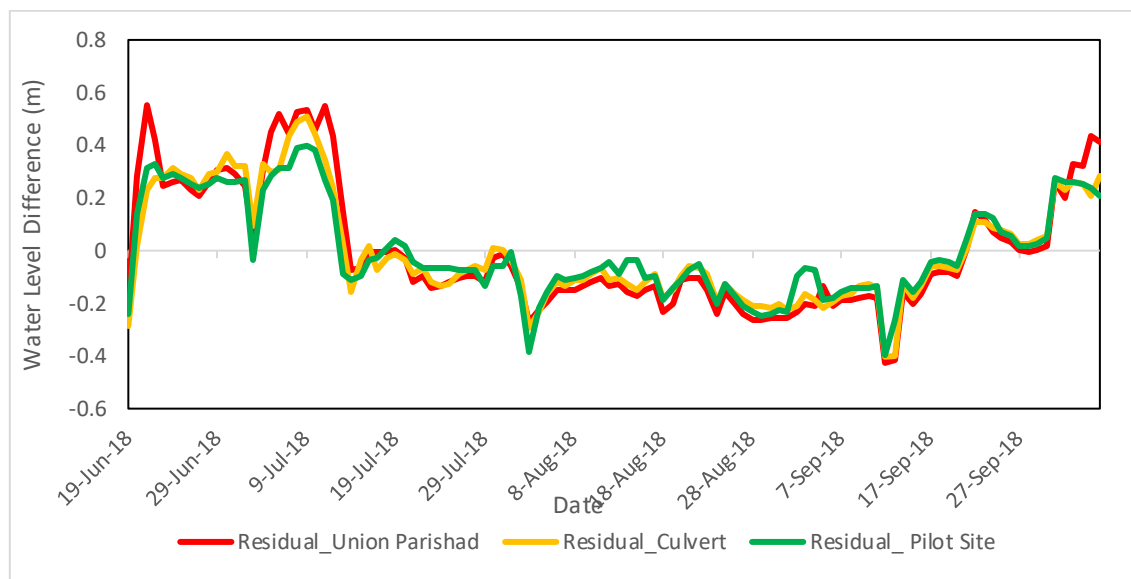


Figure 5.12 Residual from Statistical Model using Simple Regression for 2018 Flood

### 5.2.1.2.2 The Difference in Daily Flood Water Level 2018

The daily water level difference in each gauge from the previous day's water level is calculated for the Jamuna River. Then, the difference in daily water level for the gauges and the Jamuna River is plotted for the corresponding date in Figure 5.13.
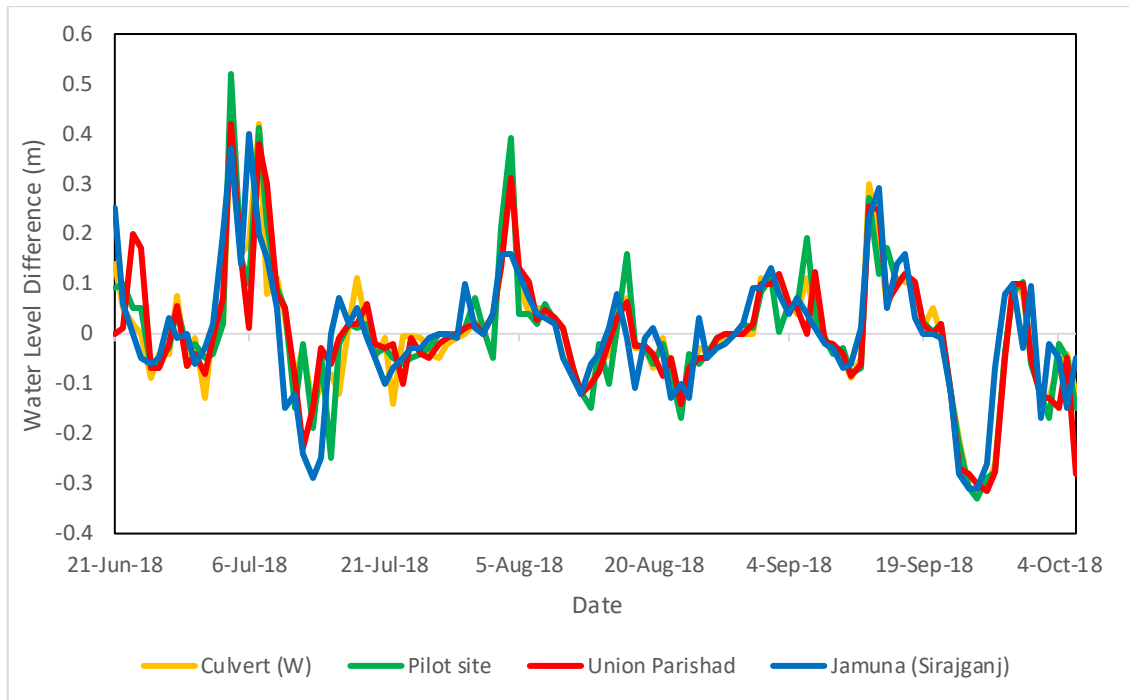


Figure 5.13 The Difference in Daily Flood Water Level in 2018

The value of the water level difference in the gauges is plotted with the difference in Jamuna water level. In the linear regression analysis, the $R^2$ value is found from 0.54 to 0.64 (Figure 5.14), which shows some relation in the daily difference in water level. When the floodwater level increases or decreases at the Jamuna River, it also directly impacts the floodwater in the Ranigram area.
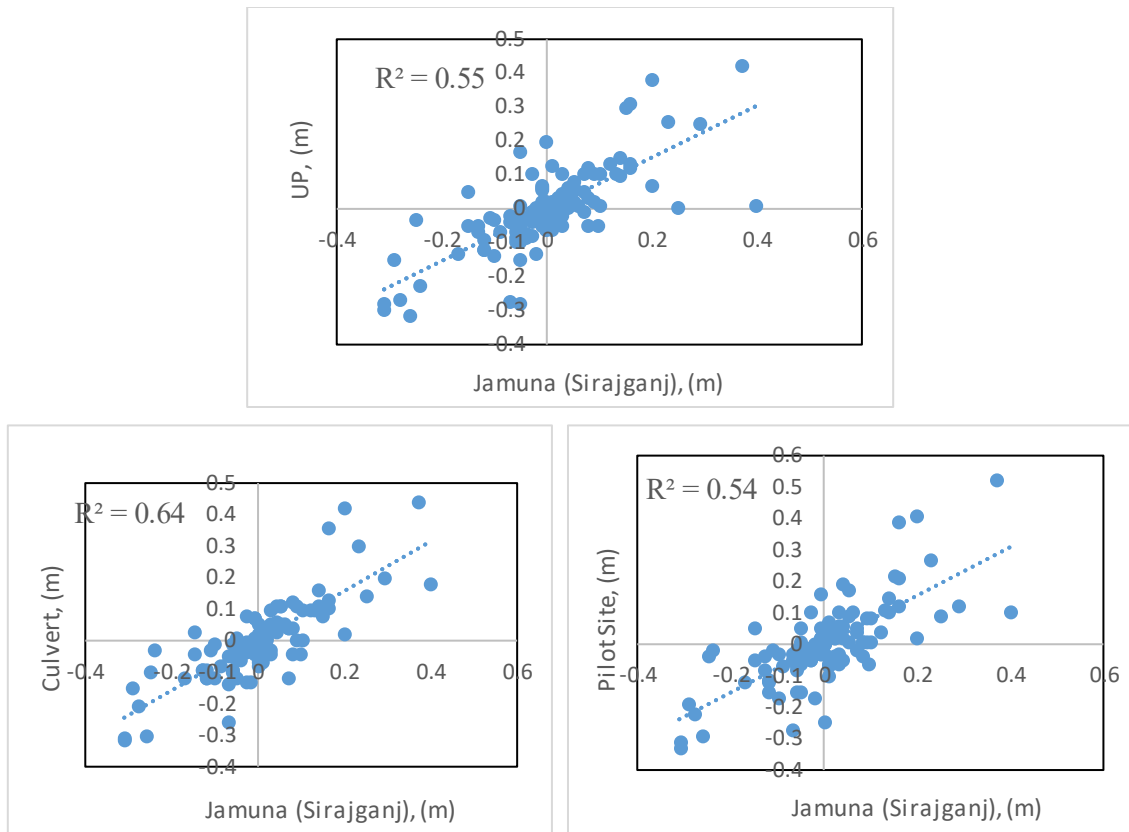
Figure 5.14 Relation in Daily Water Level Difference between the Gauges in Ranigram and the Jamuna River

### 5.2.1.3 Relation of Gauges Water level with Previous Day's Water Level of the Jamuna River

The relation of water level gauges with the previous day's water level of the Jamuna at Sirajganj also shows some co-relation having $R^2$ value from 0.86 to 0.41 for the previous one to three days water level. For the relation of the previous one to three days water level at the Jamuna, the $R^2$ value is found from 0.79 to 0.41 at Union Parishad. The $R^2$ value at Culvert and Pilot Site is found from 0.83 to 0.43 and from 0.86 to 0.45, respectively.

### 5.2.2 Multiple Regression with the Jamuna River Water Level at Sirajganj

As there is some relation with the previous day's water level, a multiple regression relationship is established for the gauge location in the Ranigram. The water level at the gauges is established with three dependent variables. The previous day's water level at

that gauge location, the Jamuna River water level for the corresponding day, and the previous day are used as independent variables. Depending on these three variables, the water level for the location of gauges was calculated. The accuracy of this multiple regression equation is also investigated.

$$X_{UP}= 0.739*Y_{Jamuna} -0.695*(Y-1)_{Jamuna}+ 0.964*(X-1)_{UP} -0.086 \text{ ----------} \quad (5.4)$$

Here X is the water level at Union Parishad gauge location, Y is the water level at the Jamuna for the corresponding day, and (X-1) and (Y-1) is the previous day's water level at Union Parishad location and the Jamuna River, respectively.

In the regression and NSE analysis for this multiple regression relation, the $R^2$ value is found to be 0.97, and NSE is found to be 0.97, which refers to a good relationship. In the Mean Absolute Error and the Root Mean Square Error analysis, the MAE is found 0.055 m, and RMSE is 0.082 m. The Residual Range is from 0.267 to -0.298m.

$$X_{Culvert}= 0.762*Y_{Jamuna} -0.717*(Y-1)_{Jamuna}+ 0.960*(X-1)_{Culvert} -0.045 \text{ --------------} \quad (5.5)$$

Here X is the water level at Culvert gauge location, Y is the water level at the Jamuna for the corresponding day, and (X-1) and (Y-1) is the previous day's water level at the Culvert location and the Jamuna River, respectively.

In the regression and NSE analysis for this multiple regression relation, the $R^2$ value is found to be 0.98, and NSE is found to be 0.98, which refers to a good relationship. In the Mean Absolute Error and the Root Mean Square Error analysis, the MAE is found 0.047 m, and RMSE is 0.071 m. The Residual Range is from 0.276 to -0.176 m.

$$X_{Pilot\ Site}= 0.811*Y_{Jamuna} -0.736*(Y-1)_{Jamuna}+ 0.932*(X-1)_{Pilot\ Site} -0.08 \text{ ---------------} \quad (5.6)$$

Here X is the water level at the Pilot Site gauge location and Y is the water level at the Jamuna for the corresponding day, and (X-1) and (Y-1) is the previous day's water level at the Pilot Site location and the Jamuna River, respectively.

In the regression and NSE analysis for this multiple regression relation, the $R^2$ value is found to be 0.98, and NSE is found to be 0.98, which refers to a good relationship. In the Mean Absolute Error and the Root Mean Square Error analysis, the MAE is found 0.05 m, and RMSE is 0.077 m. The Residual Range is from 0.334 to -0.24 m. Table 5.2 summarizes the different statistical parameters of the above analyses. From the analysis,

the multiple regression equation also seems to represent the floodwater level of the location with deficient error.

Table 5.2  Statistical Relation and Error of Gauge Water Level with the Jamuna River Water Level in Multiple Regression Model for 2018 Flood

|  | R² | NSE | MAE (m) | RMSE (m) | Residual Range (m) |
|---|---|---|---|---|---|
| **UP** | 0.97 | 0.98 | 0.055 | 0.082 | 0.267 to -0.298 |
| **Culvert** | 0.98 | 0.98 | 0.047 | 0.071 | 0.276 to -0.176 |
| **Pilot Site** | 0.98 | 0.98 | 0.05 | 0.077 | 0.334 to -0.24 |

### 5.2.2.1  Residual from Statistical Model of Multiple Regression

Residual in the three water level gauge locations for the 2018 flood season is calculated for each day. The measured water level is subtracted from the water level of the multiple regression statistical model. The residual from the model for each day in the three water level gauges is shown in Figure 5.15. The residual range is lower for the multiple regression equation than the simple regression equation.
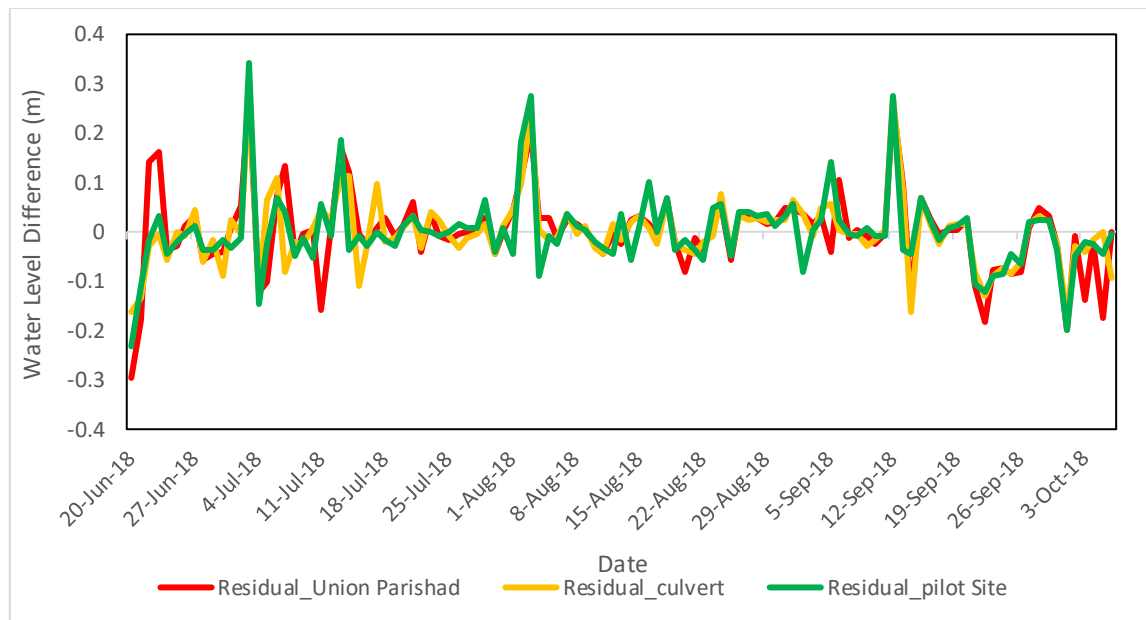


Figure 5.15 Residual from the Multiple Regression Statistical Model for 2018 Flood

## 5.2.3 Flood Data Analysis of 2020:

The flood depth data at each water level gauge in the Ranigram village was collected during the flood season of 2020 also which is shown in Figure 5.16. The floodwater level for the corresponding depth was calculated. The water level at the Ranigram area is plotted with the water level of the Jamuna at Sirajganj station. The measured data of the 2020 flood will be used to validate the equation developed with the 2018 data.
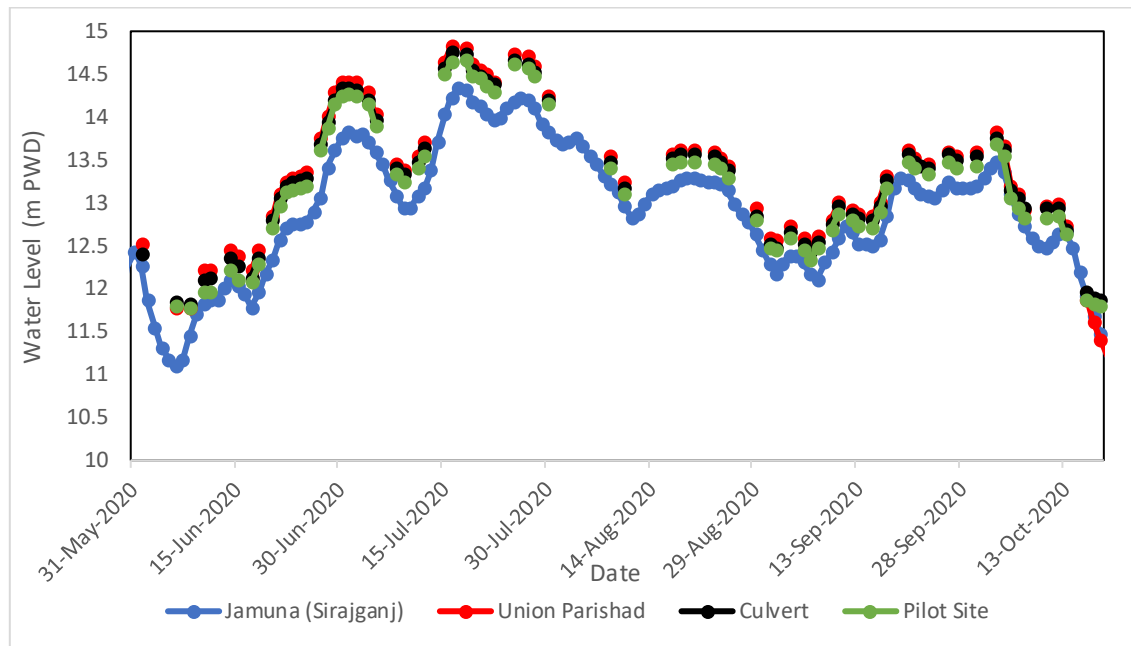


Figure 5.16 Flood Water Level Data at the Gauges in the Ranigram and Sirajganj Station of Jamuna River in 2020

The water level of each gauge at the Ranigram area was plotted (Figure 5.17) with Jamuna's water level at Sirajganj station. The relation of water level at this gauge location in Ranigram with the Jamuna river water level is investigated. And from the analysis for 2020, an excellent relationship is found as like the 2018 flood.



$y = 1.0771x - 0.5964$
$R^2 = 0.975$
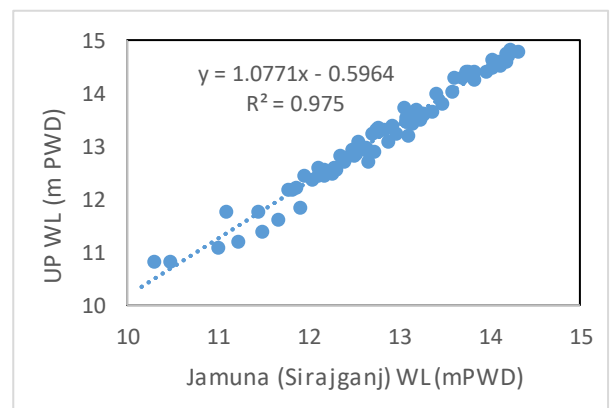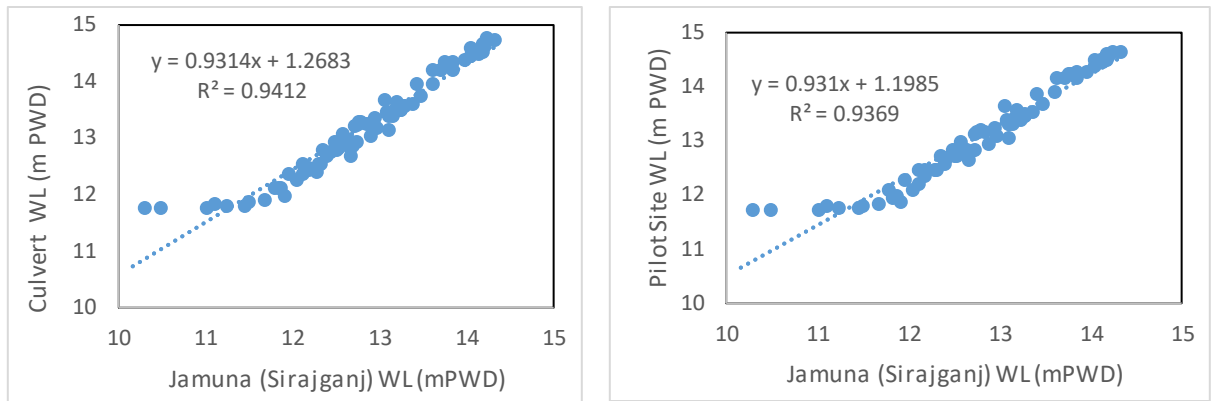
Figure 5.17 Relation of the Jamuna River Water Level with the Water Level at gauges in the Ranigram for 2020.

### 5.2.3.1 Statistical Model Validation with Measured Data of 2020

Equations (5.1), (5.2), and (5.3) developed with the data of 2018 were validated using the measured data of 2020. First, the daily data of the Jamuna River of 2020 was input as the independent variable for each equation. Furthermore, from these equations, the water level for each gauge for the 2020 flood was found. Then the water level from this statistical model is plotted with the measured floodwater level of 2020. Figure 5.18, 5.19, and 5.20 shows the plot of the model and measured water levels at Union Parishad, Culvert, and Pilot Site, respectively. The $R^2$, NSE, MAE, RMSE, and error range were analyzed for this statistical model validation.

Figure 5.18 The Simple Regression Model Water Level and Measured Water Level for 2020 at Union Parishad

In the regression and NSE analysis, the R² value is found to be 0.98, and NSE is found to be 0.97. In the Mean Absolute Error and the Root Mean Square Error analysis, the MAE is found 0.14 m, and RMSE is 0.17 m. The Residual Range is from 0.418m to -0.392m.

Figure 5.19 The Simple Regression Model Water Level and Measured Water Levels
for 2020 at Culvert

In the regression and NSE analysis, the R² value is found to be 0.94, and NSE is found
to be 0.92. In the Mean Absolute Error and the Root Mean Square Error analysis, the
MAE is found 0.16 m and RMSE 0.27 m. The Residual Range is from 1.228 to -0.370m.



Figure 5.20 The Simple Regression Model Water Level and Measured Water Level for
2020 at Pilot Site

In the regression and NSE analysis, the R² value is found to be 0.94, and NSE is found to be 0.78. In the Mean Absolute Error and the Root Mean Square Error analysis, the MAE is found 0.18 m, and RMSE is 0.30 m. The Residual Range is from 1.355 m to - 0.406 m.

Table 5.3 Statistical Relation and Error of Gauge Water Level with Jamuna River Water Level in Simple Regression Model Validation for 2020 Flood

|  | R² | NSE | MAE (m) | RMSE (m) | Residual Range (m) |
|---|---|---|---|---|---|
| **UP** | 0.98 | 0.97 | 0.14 | 0.17 | 0.418m to -0.392m |
| **Culvert** | 0.94 | 0.92 | 0.16 | 0.27 | 1.228m to -0.370m |
| **Pilot Site** | 0.94 | 0.78 | 0.18 | 0.30 | 1.355m to -0.406m |

### 5.2.3.2 Multiple Regression Validation for 2020

The multiple regression equations (5.4), (5.5), and (5.6) developed with the data of 2018 were validated using the measured data of 2020. First, Jamuna River water level data of 2020 for the corresponding day and the previous day's water level at that gauge location was input as the independent variable for each equation. Furthermore, from these equations, the water level for each gauge for the 2020 flood was found. Then the water level from this statistical model is plotted with the measured floodwater level of 2020. Figure 5.21, 5.22, and 5.23 shows the plot of the multiple regression model and measured

water levels at Union Parishad, Culvert, and Pilot Site, respectively. The $R^2$, NSE, MAE, RMSE, and error range were analyzed for this statistical model validation.
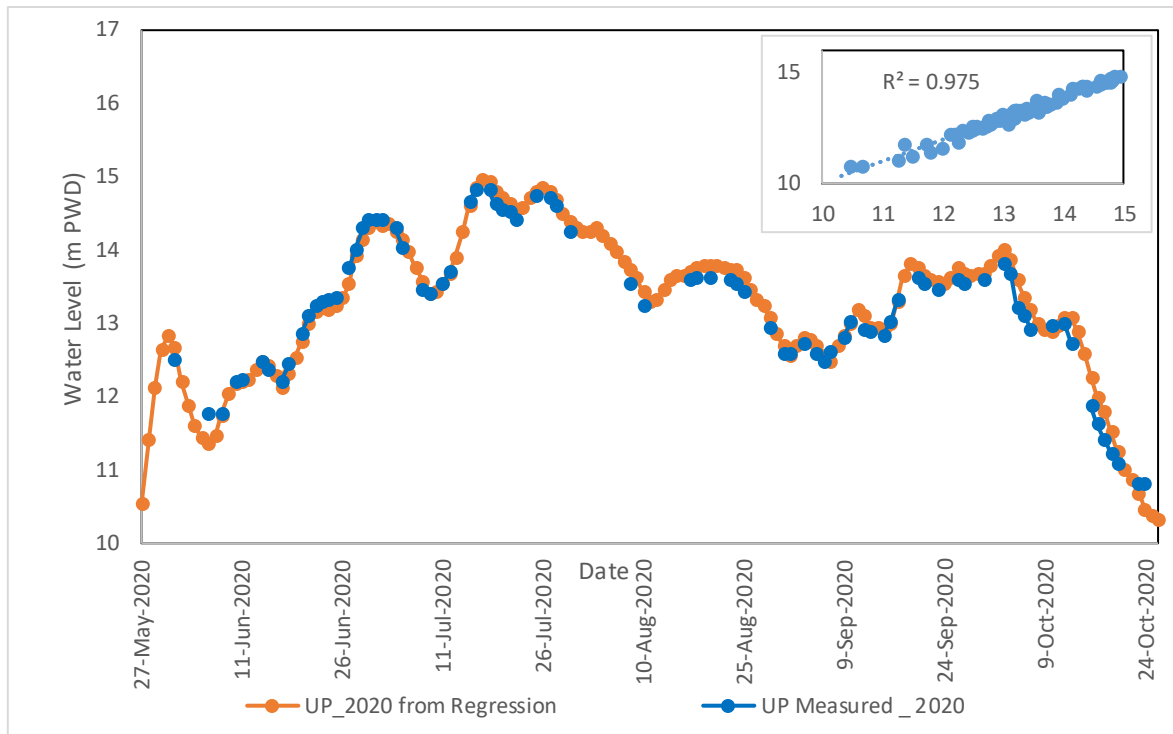


Figure 5.21 The Multiple Regression Model Water Level and Measured Water Level for 2020 at Union Parishad

In the regression and NSE analysis, the R² value is found to be 0.85, and NSE is found to be 0.83 at Union Parishad. In the Mean Absolute Error and the Root Mean Square Error analysis, the MAE is found 0.32 m, and RMSE is 0.40 m. The Residual Range is from 0.736 m to -0.881 m.
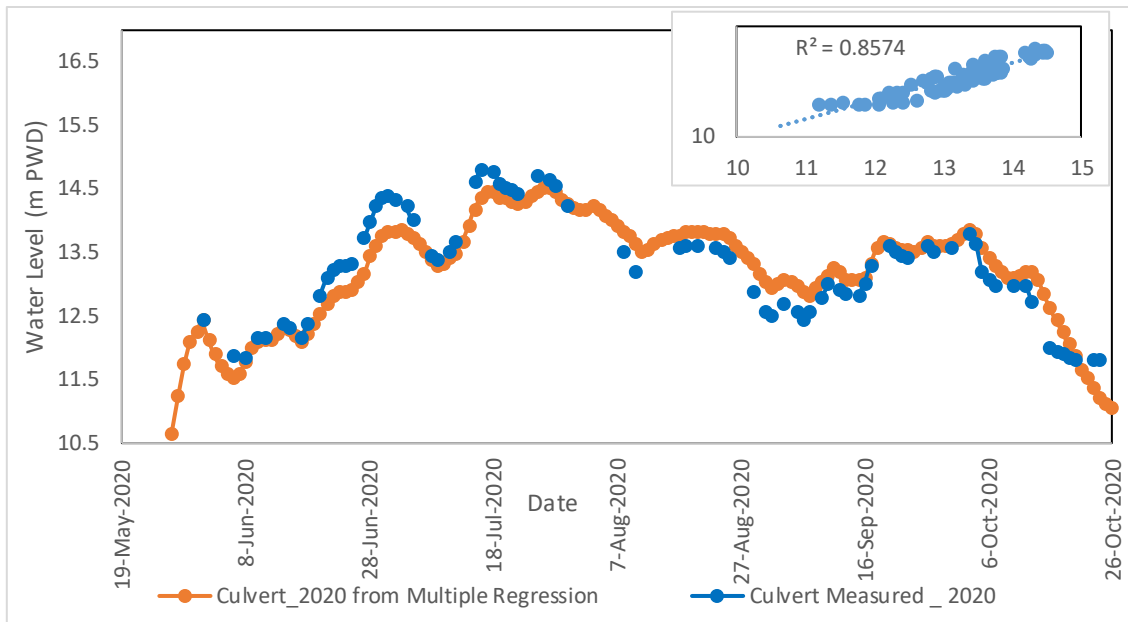
Figure 5.22 The Multiple Regression Model Water Level and Measured Water Level for 2020 at Culvert
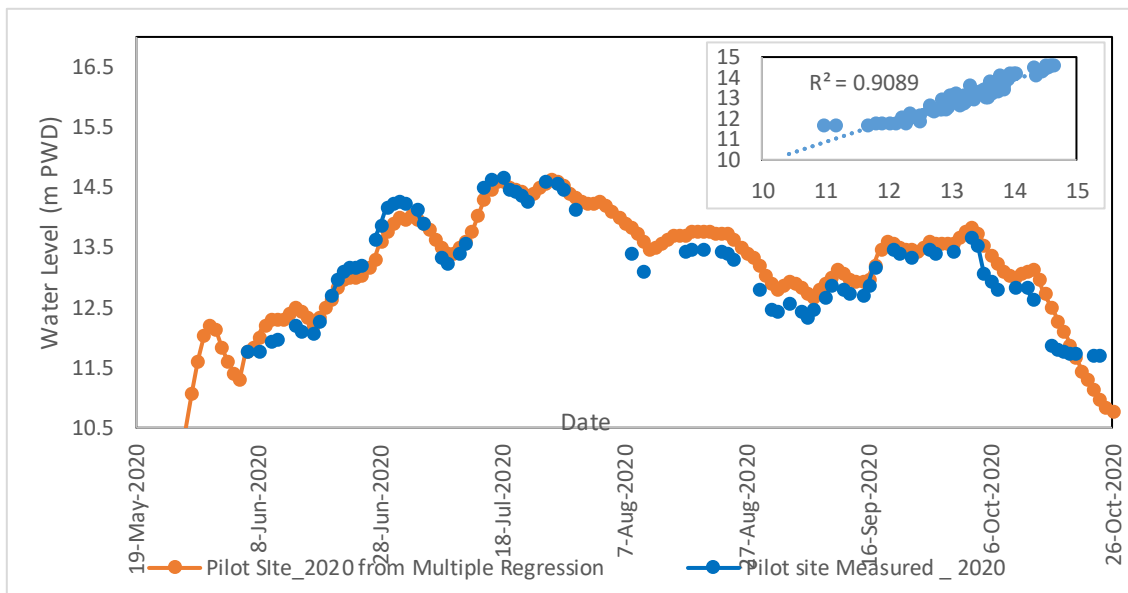


Figure 5.23 The Multiple Regression Model Water Level and Measured Water Level for 2020 at Pilot Site

In the regression and NSE analysis, the $R^2$ value is found to be 0.8, and NSE is found to be 0.85 at Culvert. In the Mean Absolute Error and the Root Mean Square Error analysis, the MAE is found 0.27 m, and RMSE is 0.32 m. The Residual Range is from 0.613 m to -0.621 m.
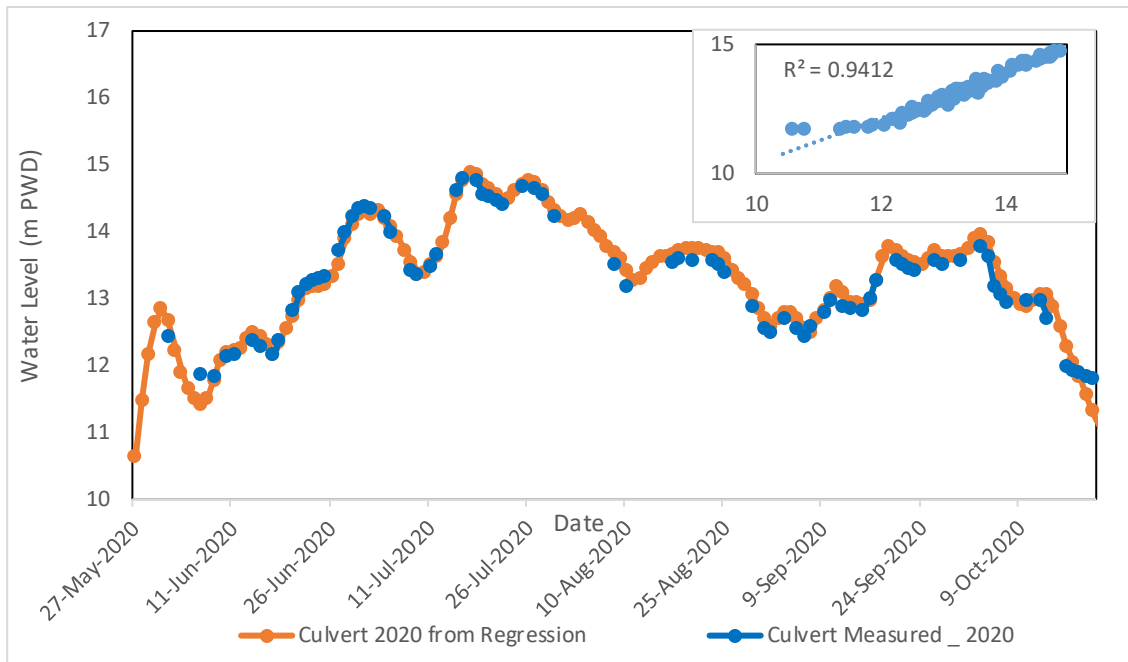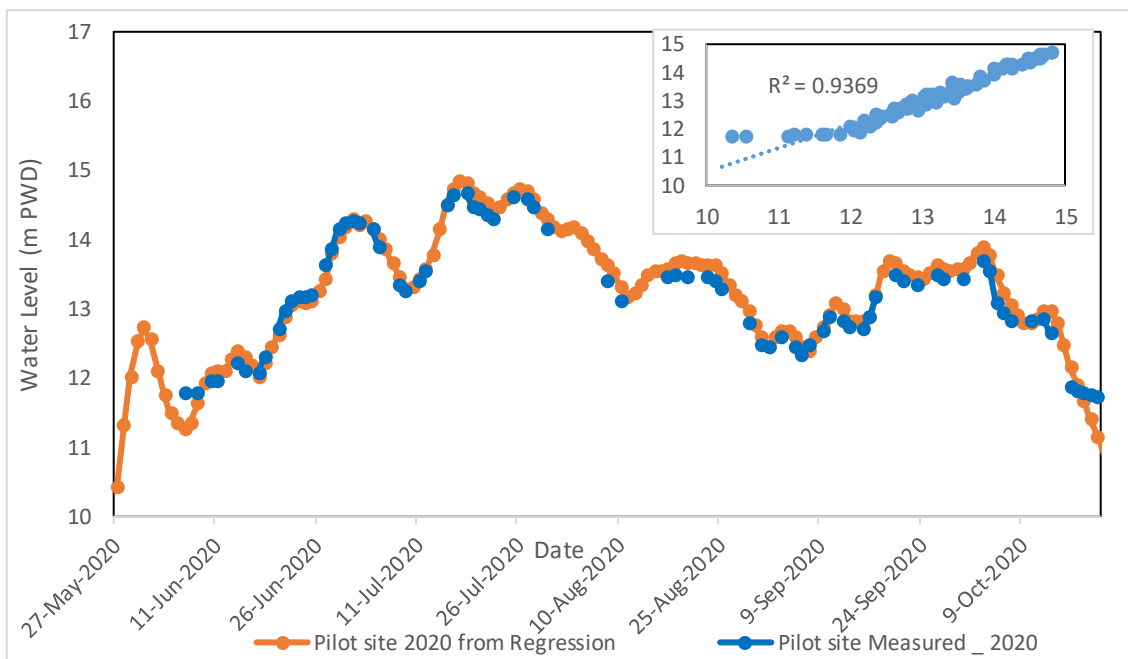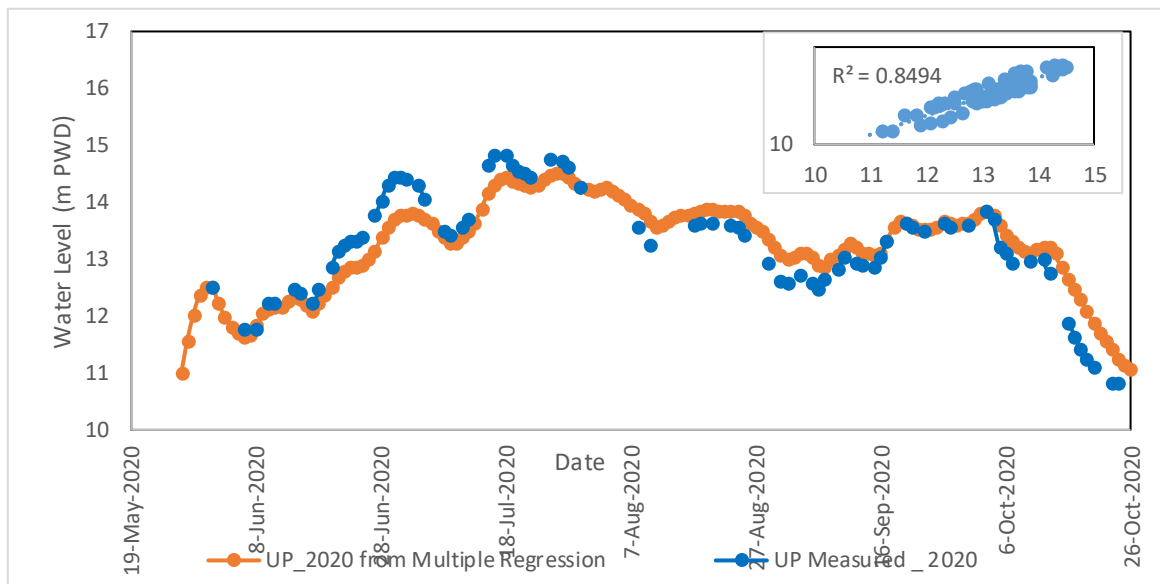
In the regression and NSE analysis, the R² value is found to be 0.91, and NSE is found to be 0.89 at Pilot Site. In the Mean Absolute Error and the Root Mean Square Error analysis, the MAE is found 0.24 m, and RMSE is 0.28 m. The Residual Range is from 0.748 m to -0.633 m.

Table 5.4 Statistical Relation and Error of Gauge Water Level with Jamuna River Water Level in Multiple Regression Model Validation for 2020 Flood

|  | R² | NSE | MAE (m) | RMSE (m) | Residual Range (m) |
|---|---|---|---|---|---|
| **UP** | 0.85 | 0.83 | 0.32 | 0.40 | 0.7363 to -0.881 |
| **Culvert** | 0.86 | 0.85 | 0.27 | 0.32 | 0.613 to -0.621 |
| **Pilot Site** | 0.91 | 0.89 | 0.24 | 0.28 | 0.748 to -0.633 |

From both the simple and multiple regression analysis, though the multiple regression model was performed better during calibration, the error during validation is higher than the simple regression model. The simple regression model is found more stable, and the error in both calibration and validation is found moderate. So, from the observation, we have taken the simple statistical model to best fit for representing the floodwater level.

## 5.3 HEC-RAS 2D Model Results

The statistical model is very good at predicting the floodwater level and depth in the floodplain of Ranigram. The other flood characteristics, like flood arrival time, duration, extent, and velocity, are also fundamental to forecast flood in the local area. A two-dimensional hydrodynamic model performs very well in representing flood propagation in the floodplain. Therefore, the HEC-RAS 2D model is selected to model the flood in the floodplain of Ranigram. A two-dimensional HEC-RAS model incorporated with high-resolution DTM was developed, and the simulation results were calibrated and validated with the measured data of 2018 and 2020, respectively. The water level at the Union Parishad was used as a boundary condition. The water levels at the Culvert and Pilot Site were used to calibrate and validate the model.

## 5.3.1  Calibration with the 2018 Data

After the simulation in HCE-RAS, the computational cell at the Culvert water level gauge location was selected in the RAS Mapper. The daily water surface elevation data of the cell was collected from the model result. The floodwater level data of the model was plotted with the gauges' measured floodwater level data.  Figure 5.24 and 5.25 shows the plot of HEC-RAS simulated and measured water level at Culvert and Pilot Site.



Figure 5.24 The HEC-RAS Model Water Level and Measured Water Level for 2018 at Culvert

In the regression and NSE analysis of the measured and HEC-RAS model water level for 2018, the $R^2$ value is found to be 0.98, and NSE is found to be 0.97, which refers to very much good co-relation. In the Mean Absolute Error and the Root Mean Square Error analysis, the MAE is found 0.043 m, and RMSE is 0.068 m at Culvert. The Residual Range is from 0.34 to -0.07 m.

After the simulation in HCE-RAS, the computational cell at the location of the Pilot Site water level gauge was selected in the RAS Mapper. The daily water surface elevation data of the cell was collected from the model result. The floodwater level data of the model was plotted with the Pilot Site gauge's measured floodwater level data.

Figure 5.25 The HEC-RAS Model Water Level and Measured Water Level for 2018 at Pilot Site

In the regression and NSE analysis of the measured and HEC-RAS model water level for 2018, the $R^2$ value is 0.97, and NSE is 0.91, which refers to very much good co-relation. In the Mean Absolute Error and the Root Mean Square Error analysis, the MAE is found 0.131 m, and RMSE is 0.141 m at the Pilot Site. The Residual Range is from 0.167 to -0.271 m. The results are summarized in Table 5.5.

From the model result, it is found that the model water level matches the measured water level very well. The error in the model is about 30 cm, which is comparatively low. Thus, for the set-up, the model performs very well for the floodplain in Sirajganj.

Table 5.5 Relation and Error of Gauge Water Level with the Jamuna River Water Level in HEC-RAS Model Calibration for 2018 Flood

| Site | $R^2$ | NSE | MAE (m) | RMSE (m) | Residual Range (m) |
|---|---|---|---|---|---|
| **Culvert** | 0.98 | 0.97 | 0.043 | 0.068 | 0.34 to -0.07 |
| **Pilot Site** | 0.97 | 0.91 | 0.131 | 0.141 | 0.17 to -0.27 |

So, from the calibration, it appears that the HEC-RAS model incorporated with high-resolution DTM performs very well when compared with the measured water level in the Ranigram area. Though there is some residual in the model, the error is not very high. So, we can say that the model is well-set for representing the flood scenario in the floodplain of Ranigram.

### 5.3.2    Validation with the 2020 data

Again, the model was run with the boundary condition of the water level of 2020 for validation. The water level data for 2020 at the Union Parishad derived from equation (4.6) using the FFWC Jamuna River water level for Sirajganj station was used for boundary conditions. The 2D HEC-RAS model was run with this water level of 2020 as the boundary condition at the Union Parishad location. After the simulation in HCE-RAS, the computational cell at the Culvert water level gauge location was selected in the RAS Mapper. The daily water surface elevation data of the cell was collected from the model result. The water level at the culvert gauge from the model result was plotted with the measured floodwater level of the culvert gauge of 2020. Figure 5.26 and 5.27 shows the plots of HEC-RAS simulated and measured water level in 2020 at the Culvert and Pilot Site locations in Ranigram.
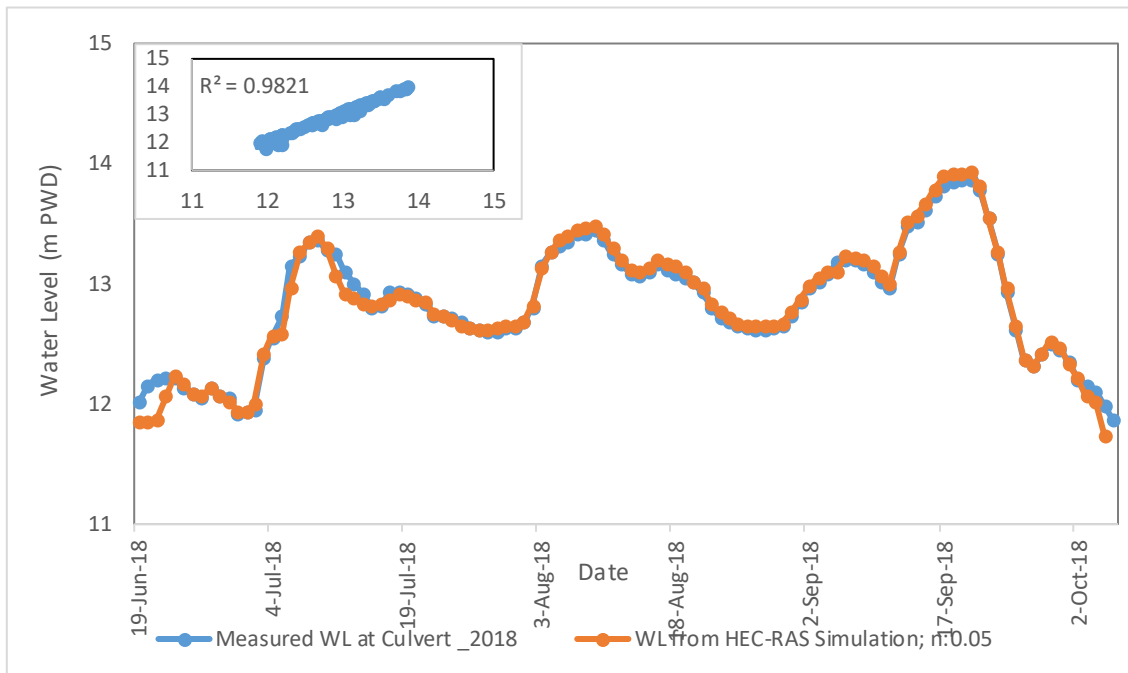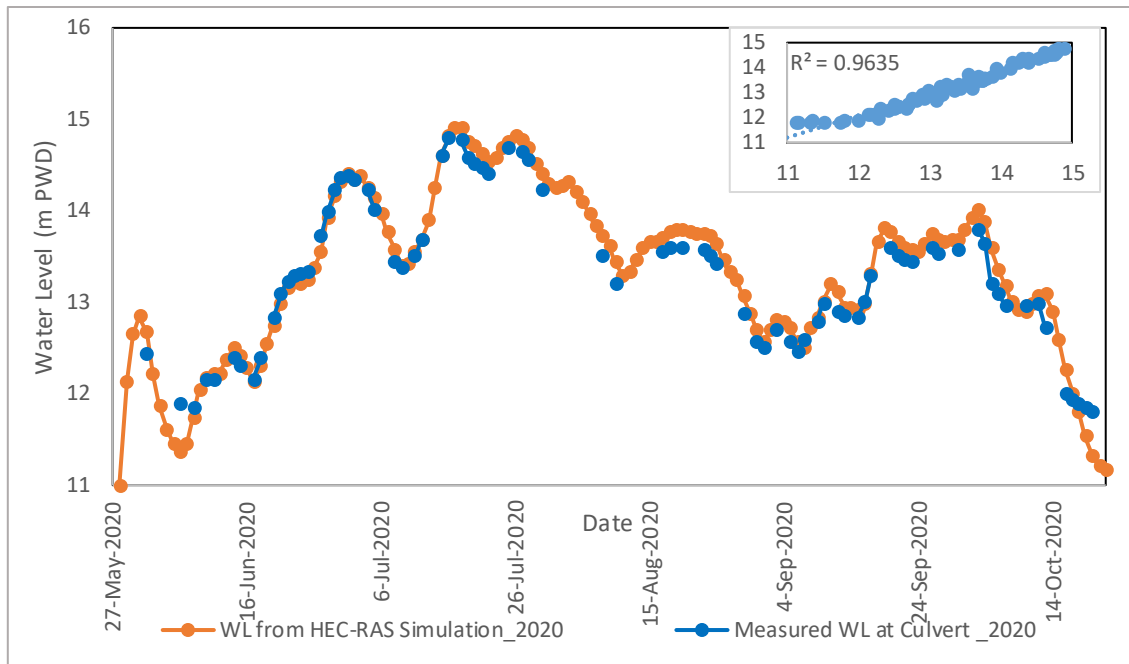
Figure 5.26 The HEC-RAS Model Water Level and Measured Water Level for 2020 at Culvert

In the regression and NSE analysis of the measured and HEC-RAS model water level for 2020, the R² value is 0.96, and NSE is 0.82, which refers to very much good co-relation. The MAE is found 0.10 m and RMSE 0.12 m at the culvert in the Mean Absolute Error and the Root Mean Square Error analysis. The Residual Range is from 0.691 to -0.08 m.

After the simulation in HCE-RAS, the computational cell at the location of the Pilot Site gauge was selected in the RAS Mapper. The daily water surface elevation data of the cell was collected from the model result. The water level at the Pilot Site from the model result was plotted with the measured floodwater level of the Pilot Site gauge of 2020.
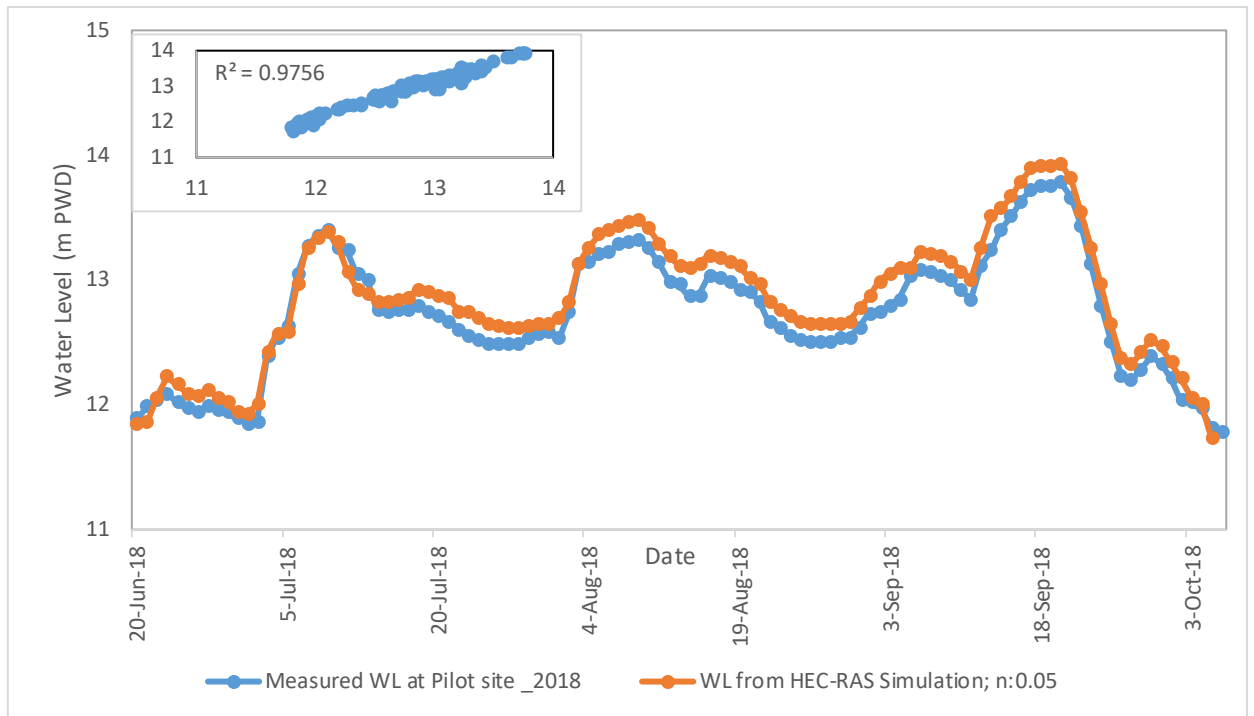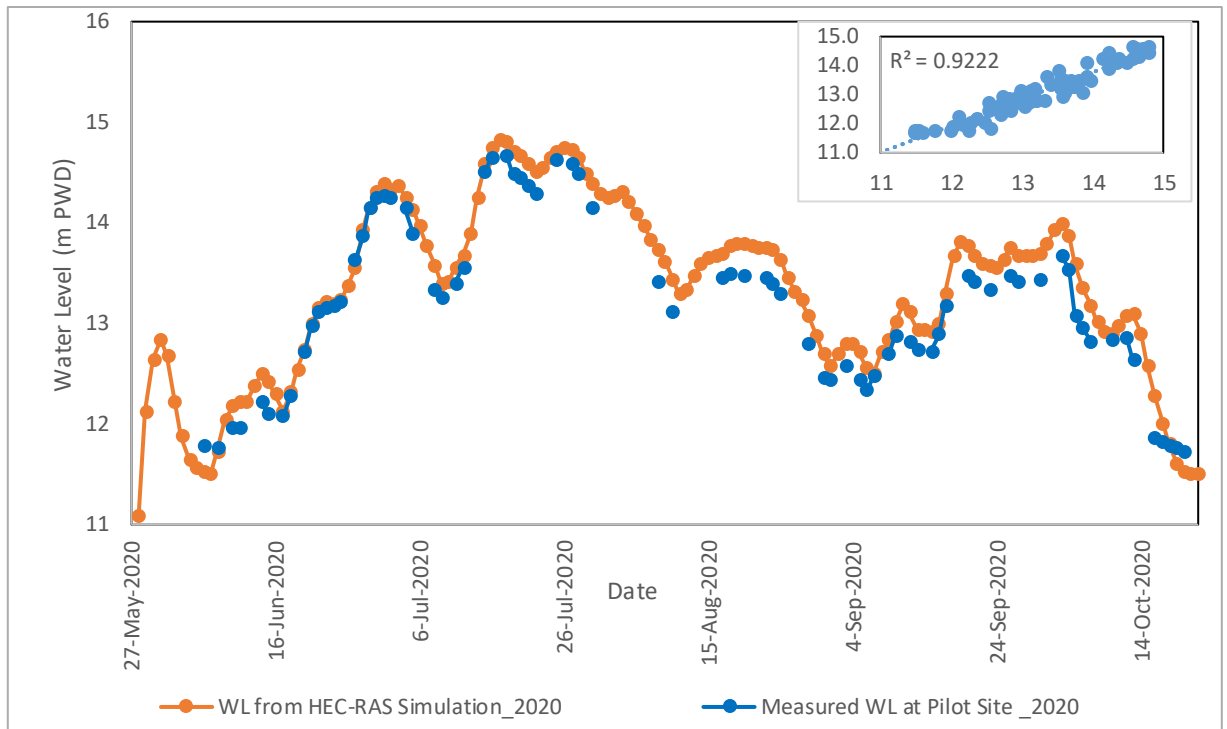
Figure 5.27 The HEC-RAS Model Water Level and Measured Water Levels for 2020 at Pilot Site

In the regression and NSE analysis of the measured and HEC-RAS model water level for 2020, the $R^2$ value is 0.92, and NSE is 0.87, which refers to a very good co-relation. The MAE is found 0.189 m and RMSE 0.227 m at the Pilot Site in the Mean Absolute Error and the Root Mean Square Error analysis. The Residual Range is from 0.338 to -0.667 m. The results are summarized in Table 5.6.

Table 5.6 Relation and Error of Gauge Water Level with the Jamuna River Water Level in HEC-RAS Model Validation for 2020 Flood

|            | R²   | NSE  | MAE (m) | RMSE (m) | Residual Range (m) |
|------------|------|------|---------|----------|--------------------|
| **Culvert**    | 0.96 | 0.82 | 0.10    | 0.12     | 0.691 to -0.08 m   |
| **Pilot Site** | 0.92 | 0.87 | 0.189   | 0.227    | 0.338 to -0.667    |

From the analysis, it is seen that the simulated water level matches with the pattern of the measured water level at both Culvert and Pilot Site and it is found that the model performs very well when validated with the measured data of 2020. The residual is high at the beginning and end of the flood period as in those days there is a sudden rise or fall

in the water level in the Jamuna River. So, from the validation, it appears that the HEC-RAS model incorporated with high-resolution DTM performs very well when compared with the measured water level in the Ranigram area. Though there is some residual in the model, the error is not very high. So, we can say that the model is validated and can represent the real flood scenario in the floodplain of Ranigram.

### 5.3.2.1 HEC-RAS Flood Maps Comparison with Real-time Flood Photos in Important Locations

The result of the HEC-RAS model was also compared with an actual flood event in 2020. The flood photos were collected from some crucial locations in the Ranigram for a few days during the flood. Then flood inundation maps were extracted from the HEC-RAS model for the specific dates for which the flood photos were collected from the Ranigram area. Photos of flood scenario for 28th June, 8th July, 15th July, and 29th August, 2020 were collected, and the model result was compared.

On the 28th of June, photos were taken from the locations at the local market beside the Union Parishad, retrofitted house, Pilot Site, and Culvert. The exported HEC-RAS inundation maps for the 28th of June of 2020 were compared at the locations of the photos taken at Ranigram (Figure 5.28).

On the 8th of July, photos were taken from the Union Parishad gauge and Pilot site locations. The exported HEC-RAS inundation maps for the 8th of July of 2020 were compared at the locations of the photos taken at Ranigram (Figure 5.29).
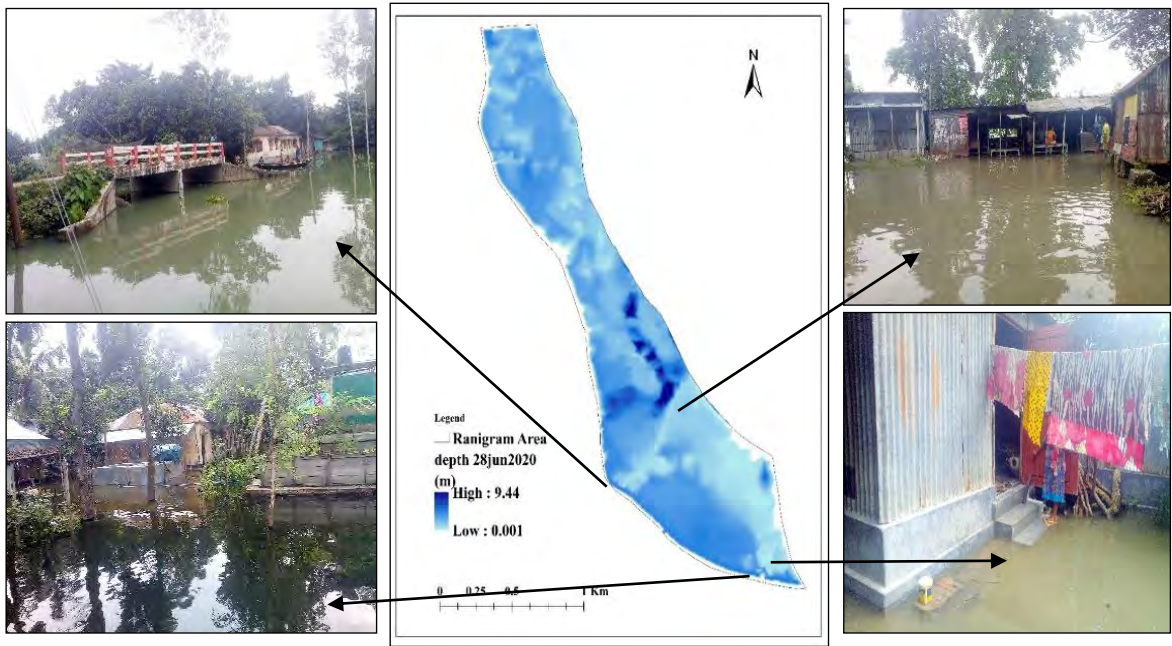
Figure 5.28 Flood Maps for the 28th June, 2020 with Real-time Flood Photos in the Floodplain of Ranigram.
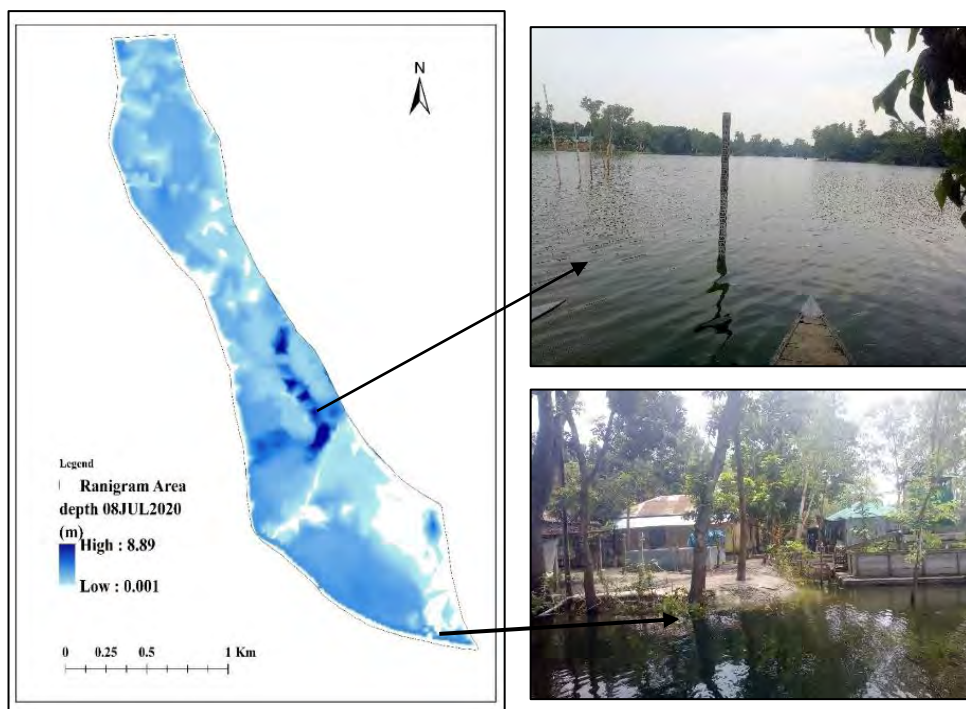


Figure 5.29 Flood Maps for the 08th July, 2020 with Real-time Flood Photos in the Floodplain of Ranigram.

On the 15th of July 2020, photos were taken from the locations at the house behind the Union Parishad, retrofitted house, Pilot Site, and embankment-bend before Culvert. The

exported HEC-RAS inundation maps for the 15th of June of 2020 were compared at the locations of the photos taken at Ranigram (Figure 5.30).
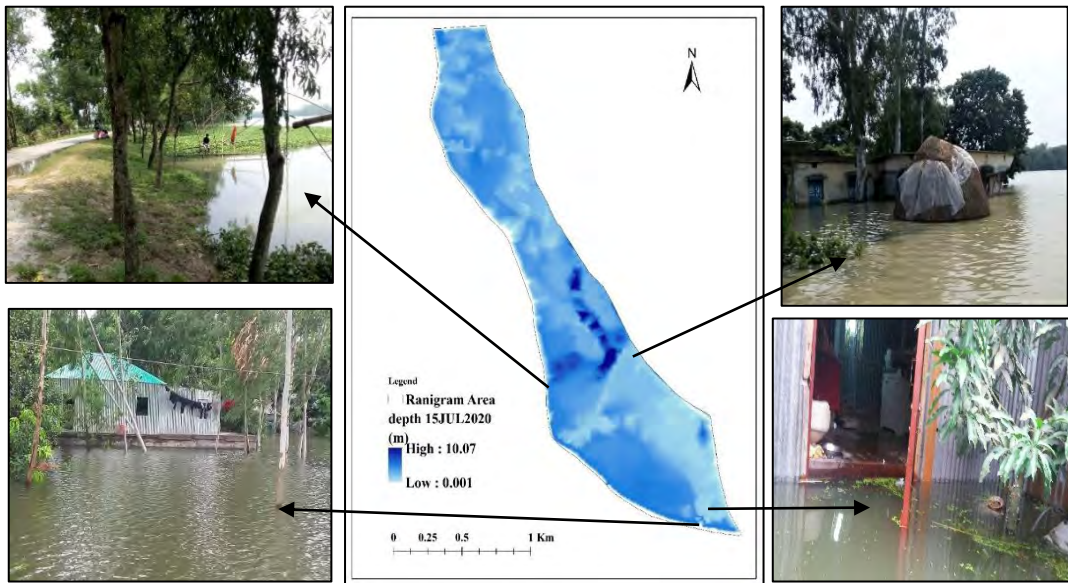


Figure 5.30 Flood Maps for the 15th July 2020 with Real-time Flood Photos in the Floodplain of Ranigram
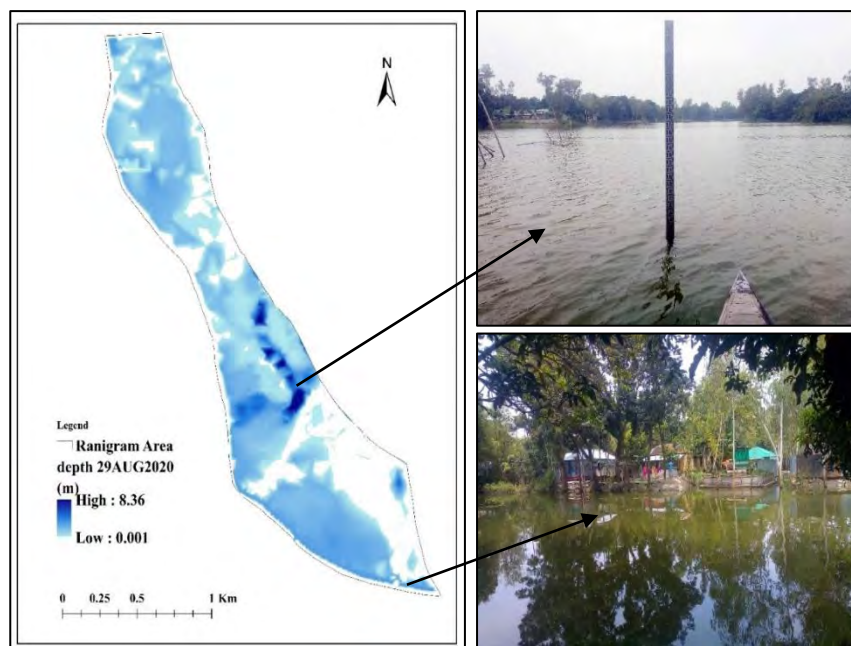


Figure 5.31 Flood Maps for the 29th August 2020 with Real-time Flood Photos in the Floodplain of Ranigram

On the 29th of August 2020, photos were taken from the locations at the Union Parishad gauge covering the whole outside area and the Pilot site from the embankment. The exported HEC-RAS inundation maps for the 29th of August of 2020 were compared at the locations of the photos taken at Ranigram (Figure 5.31).

The model-simulated flood maps show a similar flood scenario when compared with the photos of actual floods. Thus, the model incorporated with the high-resolution DTM can represent the real flood scenario at the locality in the floodplain.

### 5.3.2.2 Flood Propagation Dynamics in the HEC-RAS Model

The dynamics of flood in the HEC-RAS model also follows the real flood propagation pattern. At first the floodwater propagates from the breaching location beside UP toward the culvert location in the western part of the village. HEC-RAS model also shows in Figure 5.32(a) that the floodwater is blocked by the elevated lands, road from the UP to the culvert and so water couldn't overtop the elevated areas. So, water only after reaching the culvert location, then bellow the culvert it passes through to the Southern part of the Ranigram area.
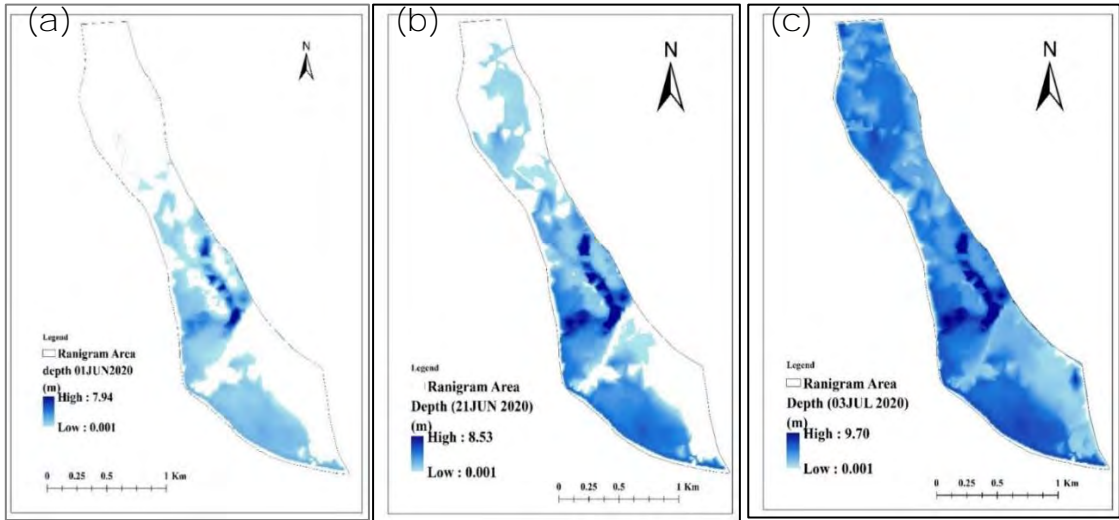


Figure 5.32 Flood Propagation Dynamics in the HEC-RAS Model for (a) low, (b) medium, and (c) high flood in Ranigram Area

Also, in the Northern part the water at first only passes through the canal beside the breaching location as there was some high elevated housing land in both side of the canal. Figure 5.32(a) shows water can reach to the Northern part of the village after passing

through the canal. Flood water propagates in the whole lower Northern area after reaching through the canal (Fig. 5.32(b)). Finally, when the flood water level increased the water overtop the elevated lands from those area and the whole Ranigram area gets flooded (Fig. 5.32(c)).

### 5.3.3    Satellite-based  Flooded Area Comparison with HEC-RAS Results

During the monsoon, the images from the satellite are mostly clouded in the Bangladesh region.  Even in the pre-monsoon, there are few clouds. Google Earth Engine Platform was used to calculate the flood inundated areas by automatic threshold method from the selected Sentinel 1 Satellite image for the specific dates of the 2020 flood season. The algorithm has been used to separate the flooded and non-flooded areas in a series of Sentinel 1 images. The maps on the right in Figure 5.32, 5.33, 5.34, 5.35 and 5.36 show result from satellite images. It shows where water is and where water in the Ranigram area is not for the specific date. The maps on the left in Figures 5.33, 5.34, 5.35, 5.36 and 5.37 show the flood inundation from the HEC-RAS model for the corresponding date of satellite images.
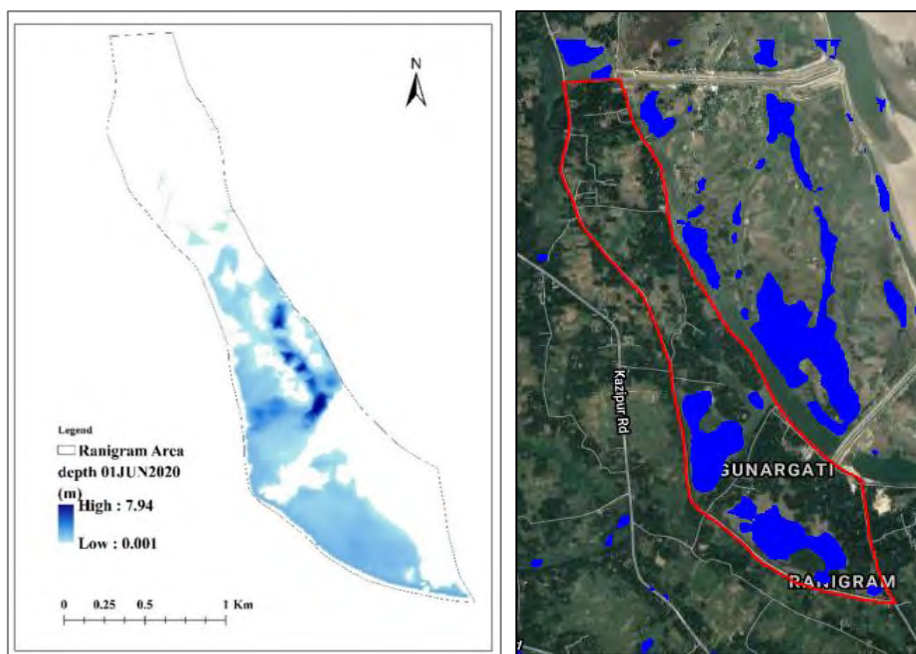


Figure 5.33 Comparison of HEC-RAS Flood Maps with Satellite-based Flooded Areas on 1st June, 2020

Figure 5.33 shows the HEC-RAS flood map and the Satellite-based flood map for 1st June, 2020. Both the HEC-RAS flood map and the Satellite-based flood map show inundation in the lower elevation indicating cultural lands in the Ranigram area.

Figure 5.34 shows the HEC-RAS flood map and the Sentinel flood map for 21st June, 2020. For the 21st of June, both the HEC-RAS flood map and the Sentinel flood map show inundation in the lower elevation indicating cultural lands in the Ranigram area. In the northern portion of the Ranigram, the HEC-RAS map shows total flooding, whereas the Satellite-based maps show discontinuing flooding.
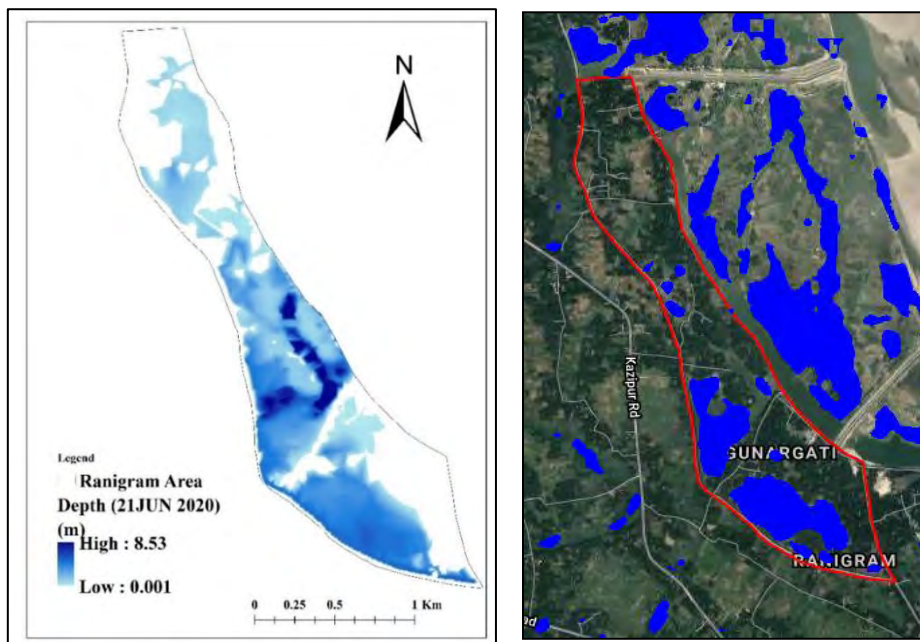


Figure 5.34 Comparison of HEC-RAS Flood Maps with Satellite-based Flooded Areas on 21st June, 2020

Figure 5.35 shows the HEC-RAS flood map and the Sentinel 1 flood map for 3rd July, 2020. The HEC-RAS flood map shows that the whole Ranigram area is flooded, whereas the satellite-based flood map shows inundation for only the lower elevated agricultural lands. The inundation in the tree canopy area in the northern and southern portions of the Ranigram is not captured by the satellite-based flood map.
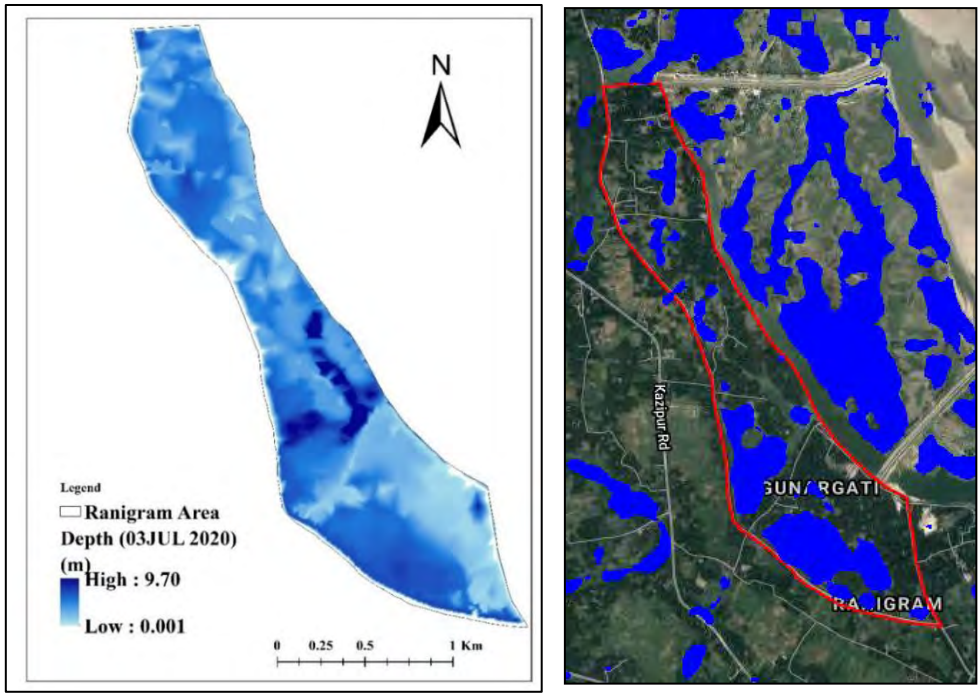
Figure 5.35 Comparison of HEC-RAS Flood Maps with Satellite-based Flooded Areas on 3rd July, 2020

Figure 5.36 shows the HEC-RAS flood map and the Sentinel 1 flood map for 15th July, 2020. The result is similar to the result of the 3rd of July. The HEC-RAS flood map shows that the whole Ranigram area is flooded, whereas the satellite-based flood map shows inundation for only the lower elevated agricultural lands. The inundation in the tree
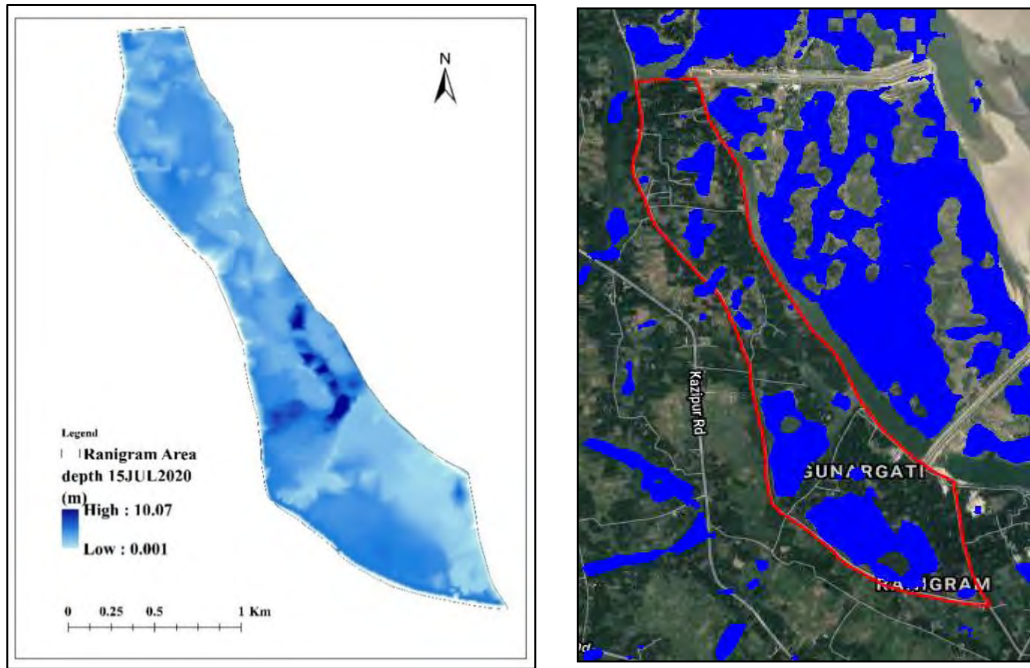
Figure 5.36 Comparison of HEC-RAS Flood Maps with Satellite-based Flooded Areas on 15th July, 2020

canopy area in the northern and southern portions of the Ranigram is not captured by the satellite-based flood map.

Figure 5.37 shows the HEC-RAS flood map and the Sentinel 1 flood map for 20th August, 2020. The result is similar to the result of the 3rd of July and 15th of July.
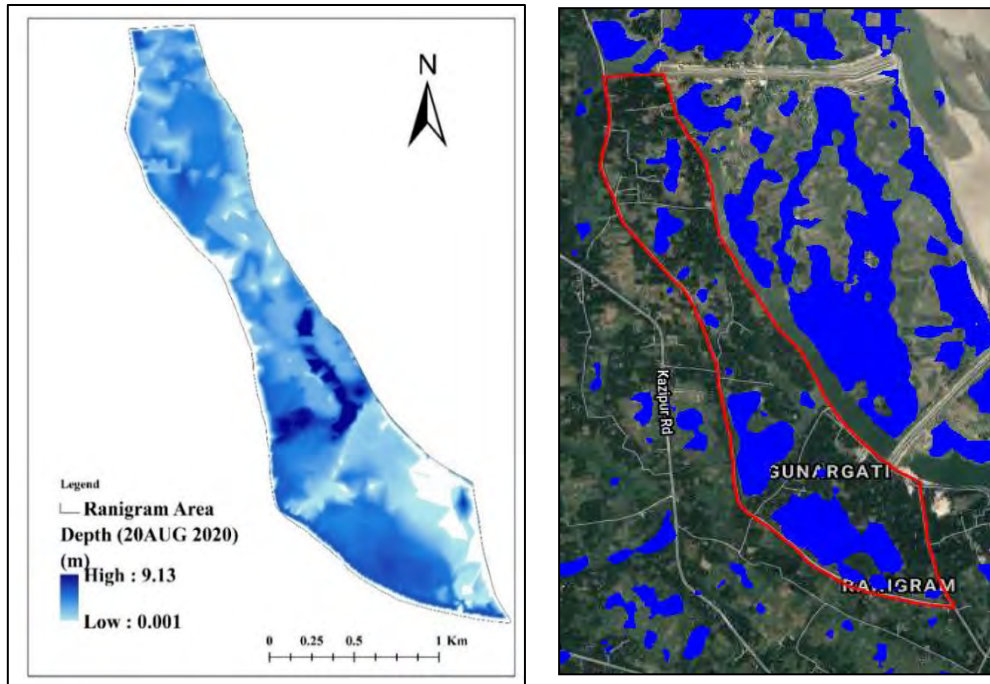
Figure 5.37 Comparison of HEC-RAS Flood Maps with Satellite-based Flooded Areas on 20th August, 2020

The satellite-based Sentinel 1 flood maps give a good result in a very detailed level for low flood (1st and 21st June, 2020) when only the agricultural lands were flooded. The satellite-based Sentinel-1 flood inundation map and UAV-based HEC-RAS flood give a similar pattern of the result. However, the flooding in the tree-canopy area cannot be captured with the remotely sensed satellite images. As the tree blocks the light and so it cannot reach the ground to find the flooding. When the whole area is flooded for high floods, the sentinel flood maps show inundation only in the non-canopy areas. The satellite images cannot detect the flooding in the tree-canopy area. Also because of the low resolution of the satellite images, all the physical phenomena is not captured in these flood maps which can be captured by high resolution model.

## 5.3.4 Maps of Different Flood Parameters with UAV-based DTM

From the above analysis, it seems that the HEC-RAS 2D model incorporated with UAV-based high-resolution DTM performs very well in representing the flood scenario of the floodplain of the Ranigram area. Therefore, the necessary flood parameters like flood

Arrival Time, Duration, Percentage of inundated time, and maximum Depth and Extent for the floodplain of the Ranigram area are extracted from the model.

Figure 5.38 shows the Arrival Time, Duration, Percent Time Inundated, and Maximum Depth and Extent for the 2018 Flood.
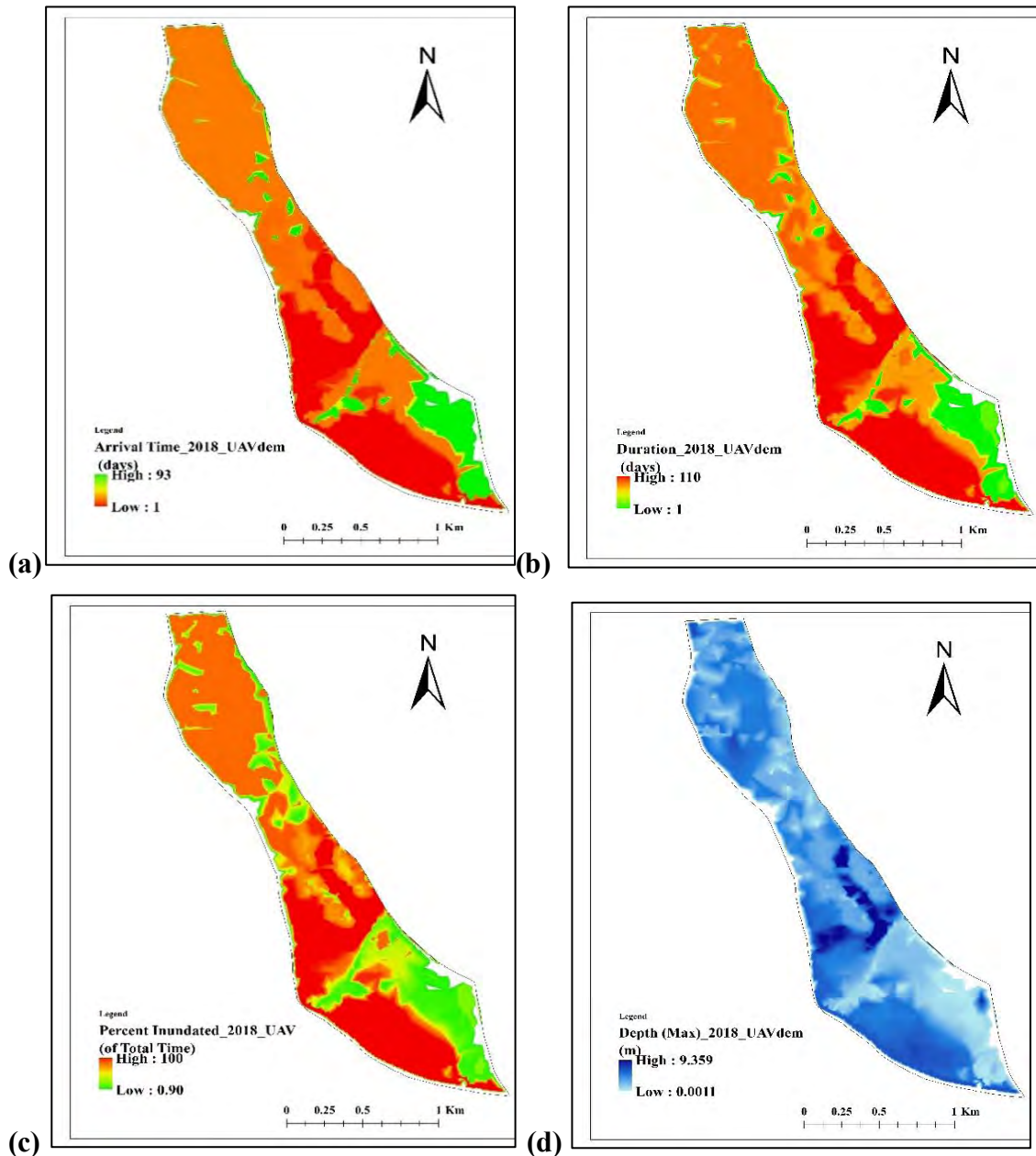


Figure 5.38 Flood Maps of (a) Arrival Time, (b) Duration, (c) Percent Time Inundated and (d) Maximum Depth and Extent for the Flood Events of 2018, respectively.

Flood arrived very quickly in the lower agricultural lands of the central Ranigram area. After overtopping the breach, floodwater arrived in the agricultural lands within one day,

and in northern agricultural lands and medium elevated housing lands within a week in 2018. In contrast, the high elevated housing in southern Ranigram faced inundation after three months at the end of the flood period. The lower agricultural lands of the central Ranigram area faced flooding for the whole flood period and were inundated for three months and 20 days. The elevated housing lands in the southern part were less affected and were inundated for about two weeks. In 2018 the whole Ranigram was inundated except the embankment. The agricultural lands were inundated with a depth of about 3 m to 4m, and the housing were inundated with a depth of about 1 m to 1.5 m.

Figure 5.39 shows the Arrival Time, Duration, Percent Time Inundated, and Maximum Extent and Depth for the 2020 Flood.

Like 2018, the flood in 2020 also arrived very quickly in the lower agricultural lands of the central Ranigram area and stayed a very long period this year. After overtopping the breach, floodwater arrived in the agricultural lands within one day, and in the northern agricultural lands and medium elevated housing lands within a week in 2020, and the high elevated housing in southern Ranigram faced inundation in three weeks. The lower agricultural lands of the central Ranigram area faced flooding for the whole flood period and were inundated for about five months. The elevated housing lands in the southern part were affected more this year and were inundated for about two months. In 2020 like 2018, the whole Ranigram was inundated except the embankment. The agricultural lands were inundated with a depth of about 3 m to 4 m, and the housing was inundated with a depth of about 1 m to 1.5 m. In the 2020 flood, the suffering of the Ranigram was very severe due to the early flood and more extended flood period.
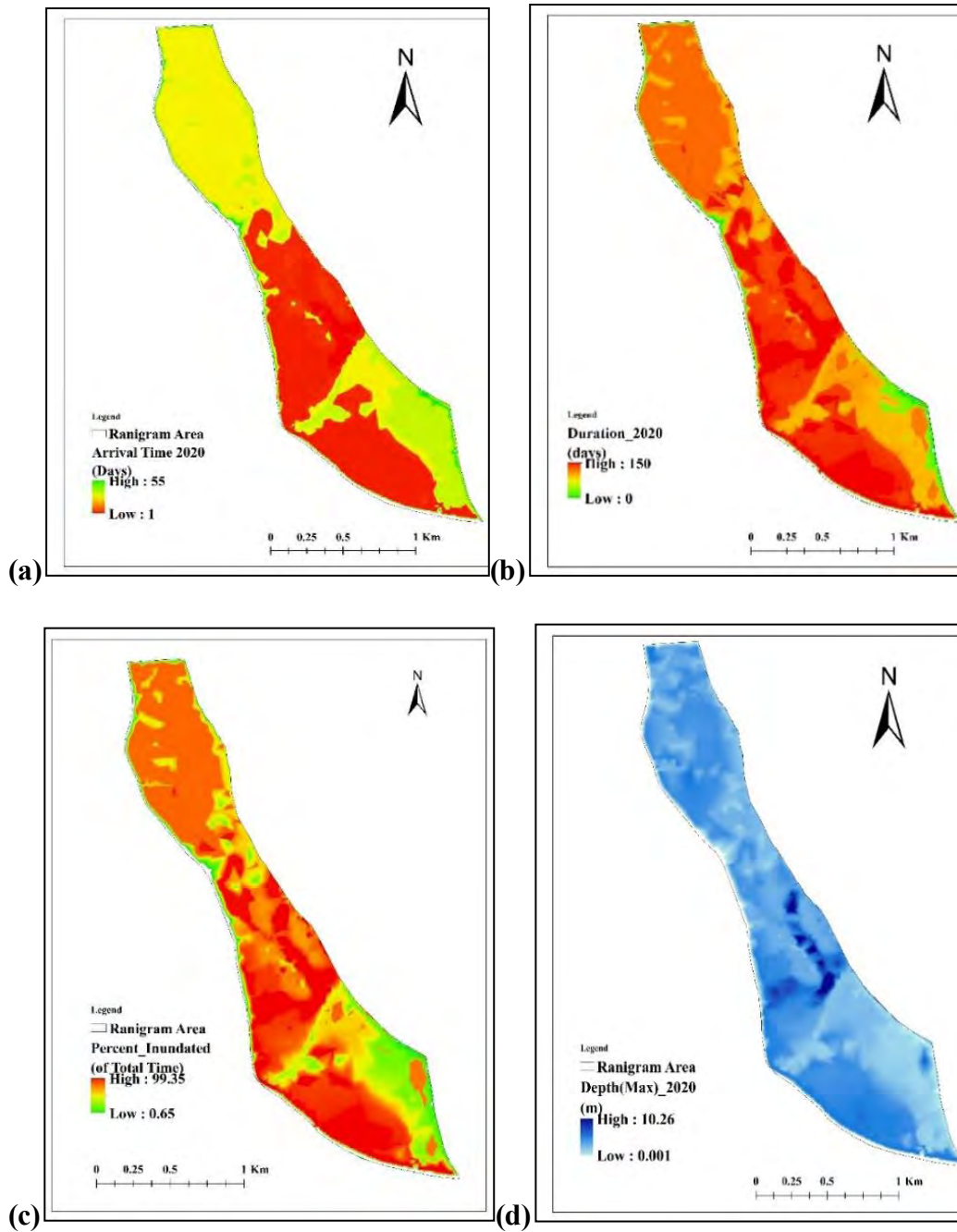
Figure 5.39 Flood Maps of (a) Arrival Time, (b) Duration, (c) Percent Time Inundated and (d) Maximum Extent and Depth for the Flood Events of 2020, respectively.

## 5.3.5 Suitability of Different DEMs in HEC-RAS Modeling

This model was again simulated using different DEMs to investigate the influence and performance of other globally available comparatively lower-resolution DEMs. The result of Arrival Time, Duration, Percent Time Inundated and Maximum Depth and

Extent for the 2020 flood is compared for UAV-based DTM, WorldDEM™, ALOS PALSAR, SRTM 30m, and ASTER DEM.

### 5.3.5.1 Arrival Time

Figure 5.40 shows the Arrival Time map of the 2020 Flood for UAV-based DTM, WorldDEM™, ALOS PALSAR, SRTM 30m and ASTER DEM.
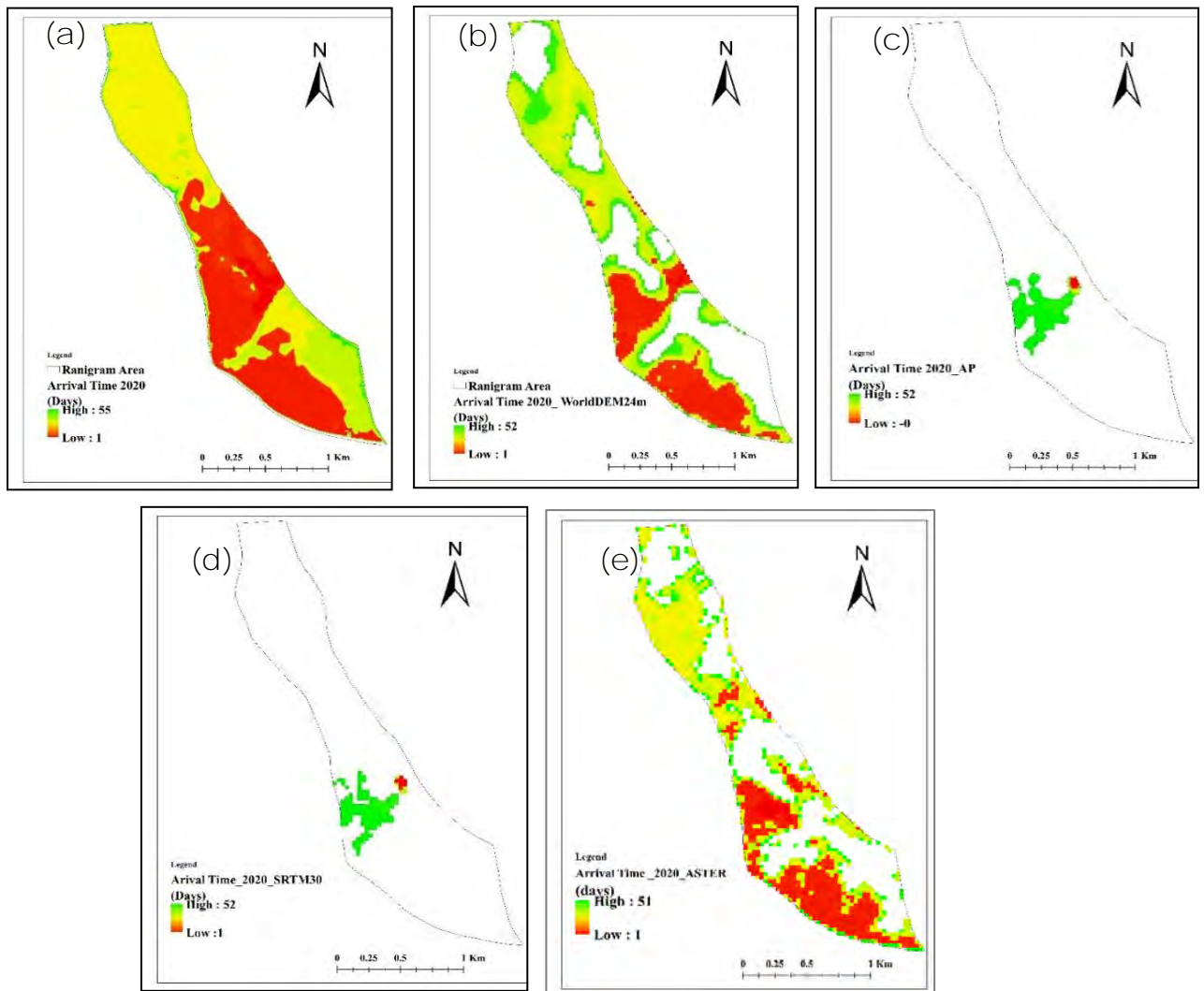


Figure 5.40 Arrival Time of 2020 Flood from the HEC-RAS simulation using (a) UAV-based DTM, (b) WorldDEM™, (c) ALOS PALSAR, (d) SRTM 30m and (e) ASTER DEM

From the Arrival Time maps, we can see that SRTM and ALOS PALSAR DEM result is only floodwater arriving in the agricultural lands near the breaching point and could not even arrive at the other lower lands passing culvert. On the other hand, the result from WorldDEM and ASTER DEM shows the floodwaters arriving in the agricultural

lands following the result of UAV-based DTM though here the floodwater did not arrive in the elevated housing lands.

### 5.3.5.2 Flood Duration

Figure 5.41 shows the Duration map of the 2020 flood for UAV-based DTM, WorldDEM™, ALOS PALSAR, SRTM 30m and ASTER DEM.
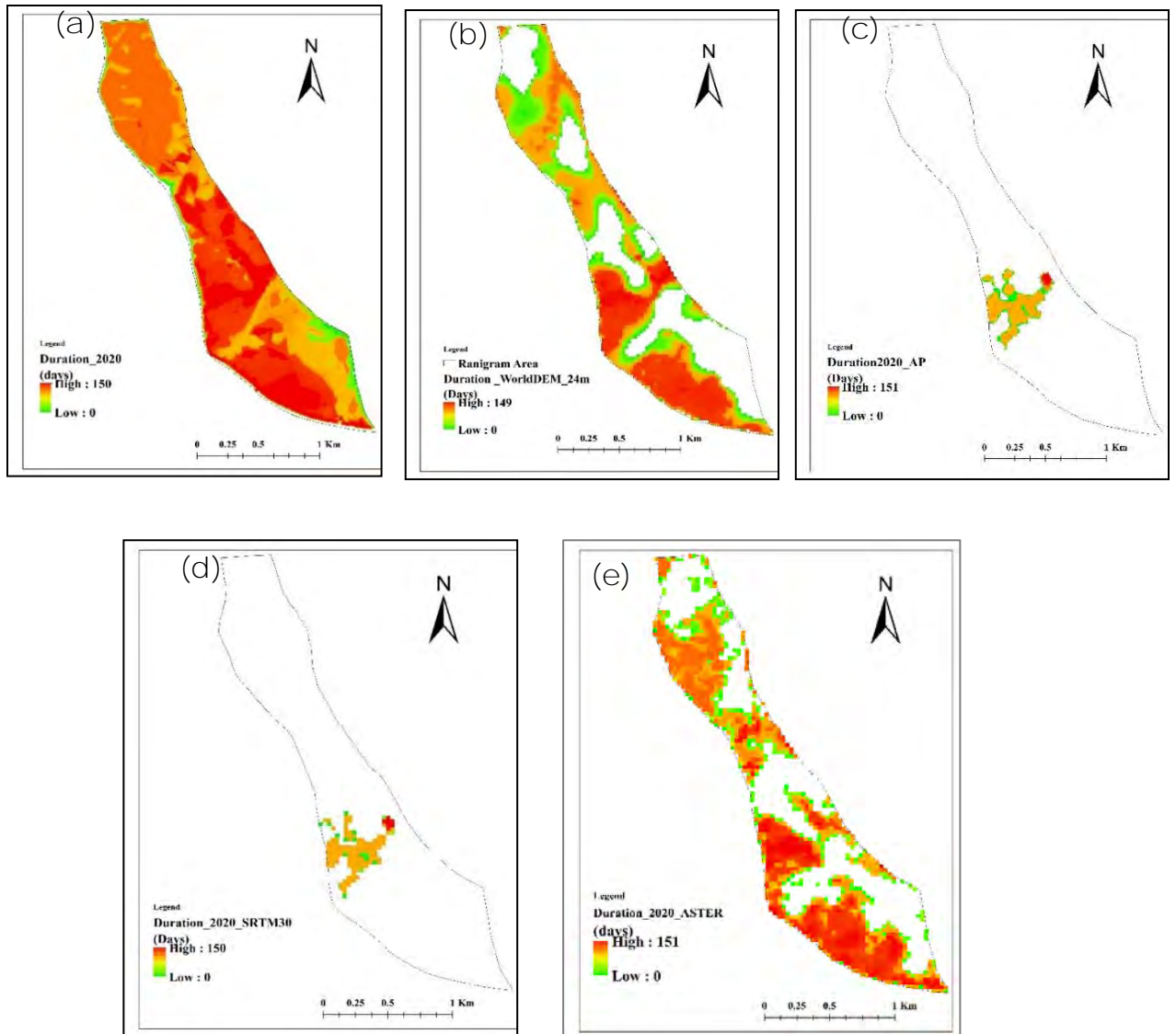


Figure 5.41 Duration of 2020 Flood from the HEC-RAS simulation using (a) UAV-based DTM, (b) WorldDEM™, (c) ALOS PALSAR, (d) SRTM 30m and (e) ASTER DEM

From the Duration maps, we can see that WorldDEM and ASTER DEM show the flood duration in the lower agricultural lands the same as the UAV-based DTM though no flood is shown in the elevated housing lands. On the other hand, SRTM and ALOS

PALSAR DEM show that floods only stayed in the agricultural lands near the breaching point and could capture two-thirds of the UAV-based DEM result.

### 5.3.5.3 Percentage Time Inundated

Figure 5.42 shows the Percentage Time Inundated Map of 2020 flood for UAV-based DTM, WorldDEM™, ALOS PALSAR, SRTM 30m and ASTER DEM.



Figure 5.42 Percentage of Time Inundated of 2020 Flood from the HEC-RAS Simulation Using (a) UAV-based DTM, (b) WorldDEM™, (c) ALOS PALSAR, (d) SRTM 30m and (e) ASTER DEM

The result of the Percentage of Time Inundated shows a similar result as the flood duration.

## 5.3.5.4 Maximum Flood Extent and Depth

Figure 5.43 shows the Maximum flood extent and depth Map of 2020 flood for UAV-based DTM, WorldDEM$^{TM}$, ALOS PALSAR, SRTM 30m and ASTER DEM
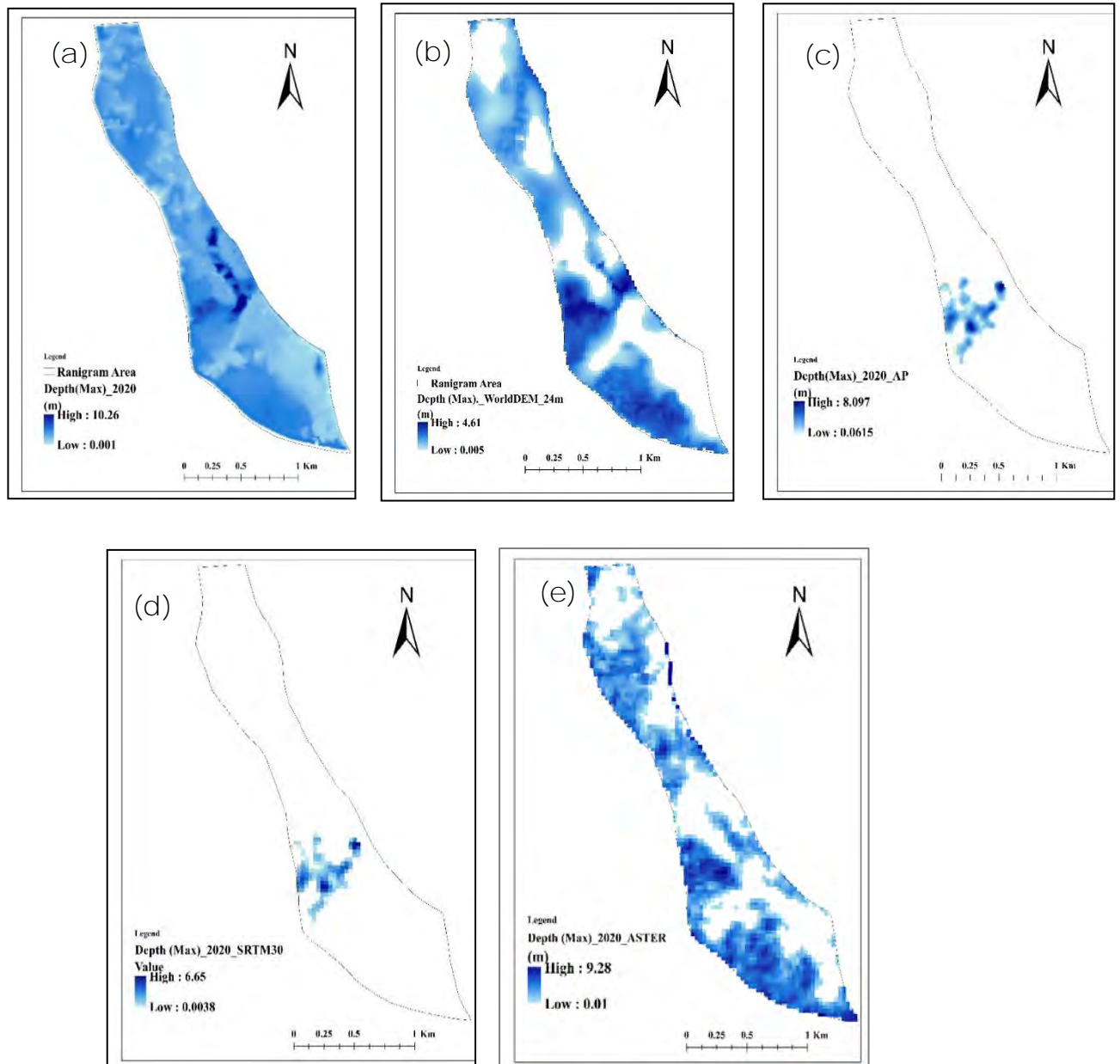


Figure 5.43 Maximum Extent and Depth of 2020 Flood from the HEC-RAS Simulation Using (a) UAV-based DTM, (b) WorldDEM$^{TM}$, (c) ALOS PALSAR, (d) SRTM 30m and (e) ASTER DEM

From the Maximum flood extent and depth maps, it is observed that the result from WorldDEM and ASTER DEM shows the flood extent only in the lower agricultural lands, but no flood is in the elevated housing lands. On the other hand, SRTM and ALOS PALSAR DEM show flood extent only in the agricultural lands near the breaching point.

However, when comparing the flood depth, the result of ASTER DEM is not following the result of the UAV-based DTM, though the result of WorldDEM is following the result of the UAV-based DTM in the lower agricultural area. The maximum flood depth in the lower agricultural land is 2 m to 4m in both WorldDEM and UAV-based DTM, whereas the ASTER DEM shows a flood depth of 4 m to 9 m.

The result from the SRTM and ALOS PALSAR DEM is very much deviated from the real field scenario. The water flow below the culvert is not possible with these DEM as it needs manual hydraulic correction. So, the flooding in the Southern part of Ranigram cannot be captured by these DEMs. Also the canal, through which water reach to the northern part of Ranigram from the breaching location, is missing in both DEMs because of their very low spatial resolution. And so, the flooding in the Northern Ranigram is also not captured by SRTM and ALOS PALSAR DEM.

From the above discussion, the performance of SRTM and ALOS PALSAR DEM at the very local level is found to be not good and not suitable for flood modeling for the locality. On the other hand, WorldDEM and ASTER DEM perform well in the non-canopy area. Though in the tree-canopy area, WorldDEM and ASTER DEM cannot represent the actual scenario. Overall, the result of the WorldDEM is the closest to the UAV-based DTM and can be used for the non-canopy area.

### 5.3.5.5 Difference in Vertical Elevation of Satellite-based DEMs with UAV-based DTM

The difference in vertical elevation of different global DEMs is compared with the UAV-based high-resolution DTM for the Ranigram area. The negative value represents that the elevation in those areas is higher than the UAV-based DTM, and the positive value represents that the elevation in those areas is lower than the UAV-based DTM. Figure 5.44 shows the difference in vertical elevation of WorldDEM[TM], ALOS PALSAR, SRTM 30m, and ASTER DEM compared with the UAV-based high-resolution DTM.

The difference in vertical elevation of WorldDEM with UAV-based DTM is the lowest compared to the other DEMs. The difference in the tree-canopy area is 2m to 5m and in the non-canopy agricultural land is within 1 m. The difference with ALOS PALSAR DEM is very high, ranging from 4 m to 10 m in the tree-canopy area and 1 m to 4m in

the non-canopy agricultural land. The difference with SRTM DEM is about the same as ALOS PALSAR. The difference with MERIT DEM is 1 m to 4m in the whole area and does not follow any pattern. The difference with ASTER DEM ranges from 4 m to 7 m in the tree-canopy area and -2 m to 2 m in the non-canopy agricultural land.



(a)

(b)

(c)

(d)

**(e)**
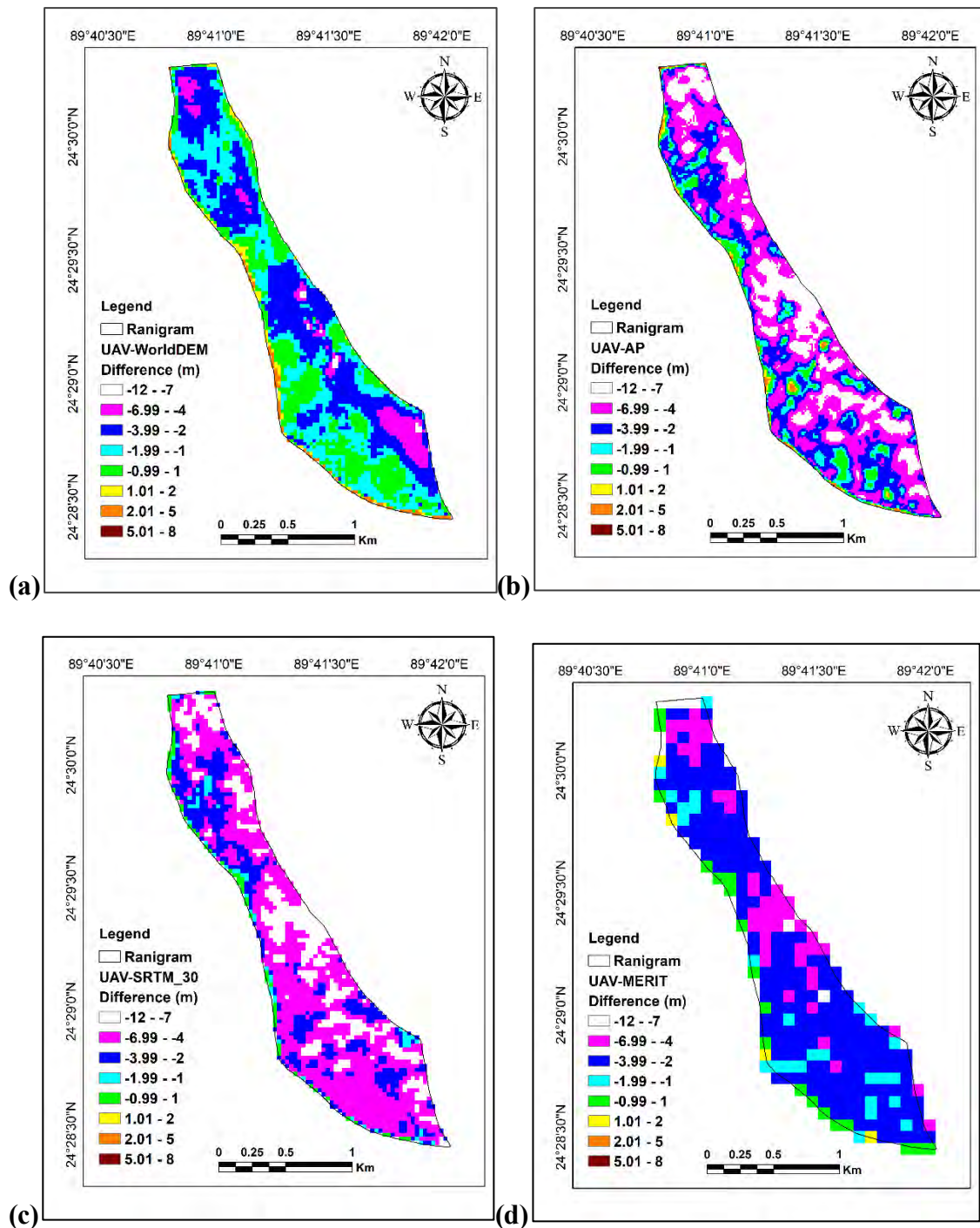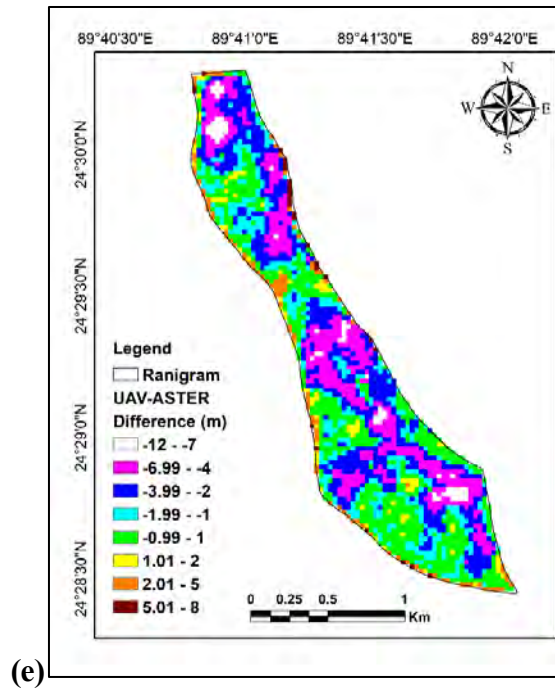
Figure 5.44 Difference in Vertical Elevation of (a) WorldDEM$^{TM}$, (b) ALOS PALSAR, (c) SRTM 30m DEM, (d) MERIT DEM and (e) ASTER, DEM with the UAV-based High-resolution DTM for Ranigram Area.

The opening below culvert is not present in any of these DEM as it is not seen from remote sensing and needs manual hydraulic correction. Also the canal, through which water reach to the northern part of Ranigram from the breaching location, is missing in SRTM and ALOS PALSAR DEMs because of their low spatial resolution. The embankment is missing in the MERIT DEM because of its very low spatial resolution. The difference in vertical elevation shows that most of the global DEMs are highly elevated compared to the UAV-based DTM, and the value is higher in the tree-canopy area because of the captured surface elevation by remotely sensed satellite images. In most results, the portion low elevated is the embankment area that the global DEMs do not include because of low horizontal resolution. So, we conclude that to have a flood model to represent the local level flood scenario, the UAV-based high-resolution DTM incorporated with measured field bathymetry is essential. Other global DEMs like WorldDEM performs well in some areas but have limitation in the canopy area and cannot represent accurate flood scenario because of their low horizontal resolution.

## 5.3.6 Flood Inundation Maps for Different Return Periods

From this model using the boundary condition of different return period water levels of the Jamuna River at Sirajganj station, we can predict the flood scenario in the Ranigram area. The flood maps of Ranigram for different return period floods are generated using the developed HEC-RAS model. Figure 5.45 shows the flood depth and extent maps of the Ranigram for 1, 2, 10, 20, 50, and 100-year return periods.
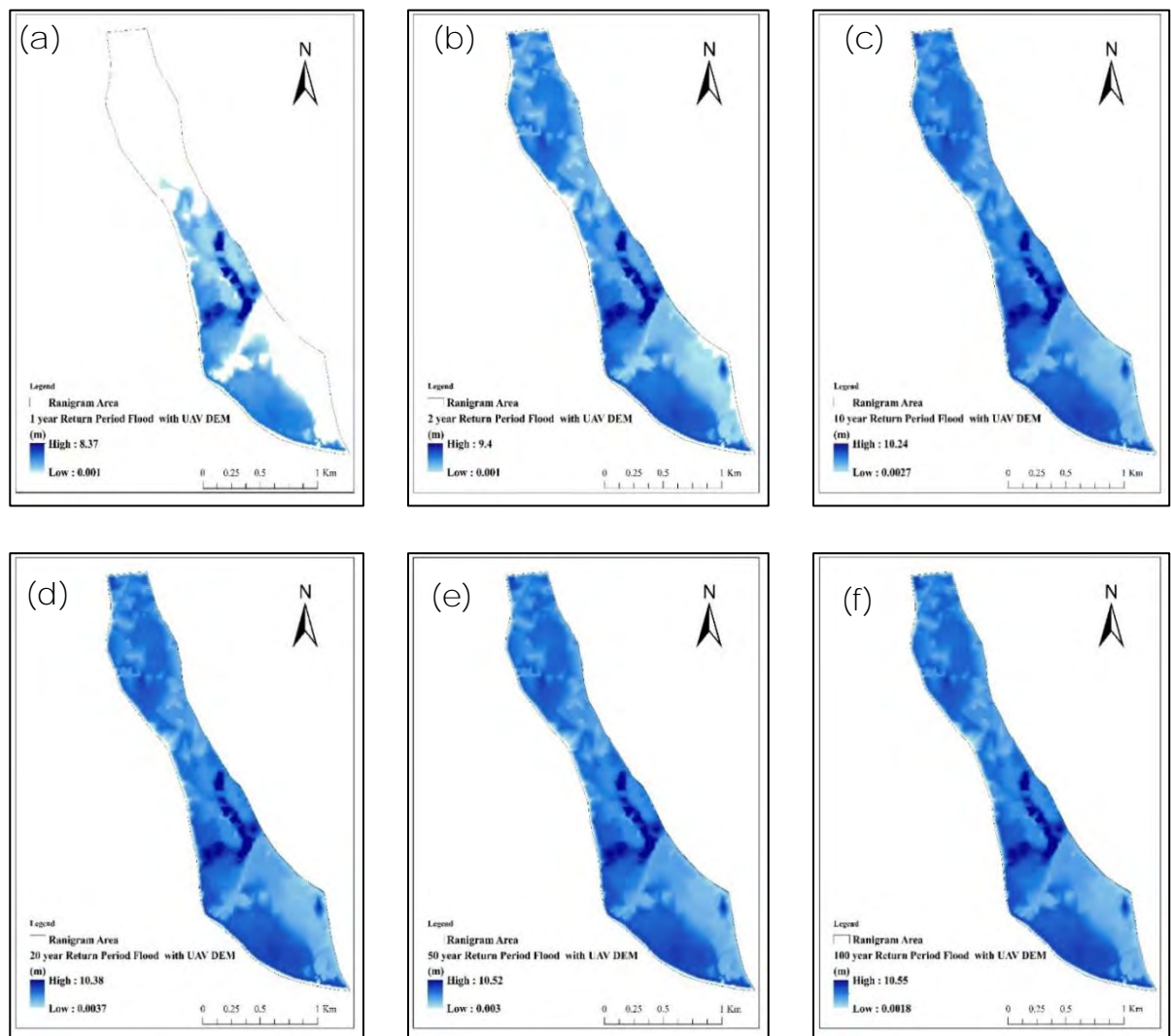


Figure 5.45 Flood Depth and Extent Map for (a) 1 year, (b) 2 years, (c) 10 years, (d) 20 years, (e) 50 years and (f) 100 years of Return Period in Ranigram Area

The From the HEC-RAS model using UAV-based DTM, we can see that the lower lands of the Ranigram village are inundated for 1 year return period flood having a maximum flood depth of 8.37 m beside the Union Parishad. For a 2-year return period flood, the whole village is inundated, having a maximum flood depth of 9.40 m, and the high-

elevated housing-lands have an inundation depth of about 0.5 m. For a 5-year return period flood, the whole Ranigram village is inundated, having a maximum flood depth of 9.93 m, and the high lands are inundated less than 1 m. For a 10-year return period flood, the Ranigram village is inundated, having a maximum flood depth of 10.24 m, and the high-elevated housing lands are inundated for more than 1.25 m. For a 50-year return period flood, the maximum flood depth in the Ranigram village is 10.52 m, and the high-elevated housing lands are inundated for less than 1.5 m. Finally, for a 100-year return period flood, the maximum flood depth in the Ranigram village is 10.55 m, and the high-elevated housing lands are inundated for more than 1.5 m.

From the analysis, it is found that the agricultural lowlands get flooded every year. Already for a 2-year return period flood, the complete flooding of the Ranigram area is observed. During a 10-year flood event, the mounds with elevated houses are inundated for a depth of about 1 m, and during a 50-year return period, the high elevated lands are flooded for a depth of more than 1.5 m.

## 5.4 Flood Forecasting in Ranigram using FFWC River Forecast

This model can be used to forecast floods in the Ranigram area. The model's boundary condition can be developed from the FFWC's forecasted water level in the Jamuna River. Moreover, the result of the model will represent the forecasted flood scenario in the Ranigram area for the corresponding FFWC forecast.

### 5.4.1 Analysis of FFWC Forecasted Water Level at Sirajganj Station

At first, the accuracy of the 1-day to 5-day forecast in the Jamuna River is investigated. During the 2020 flood, the FFWC forecasted water level in the Jamuna River is collected regularly. The 24-hour, 48-hour, 72-hour, 96-hour, and 120-hour water level forecast is collected, and the measured water level for the Jamuna River for the corresponding dates is also collected. Figure 5.46 shows the measured water level of the Jamuna River plotted with the forecasted water level for the 2020 flood.
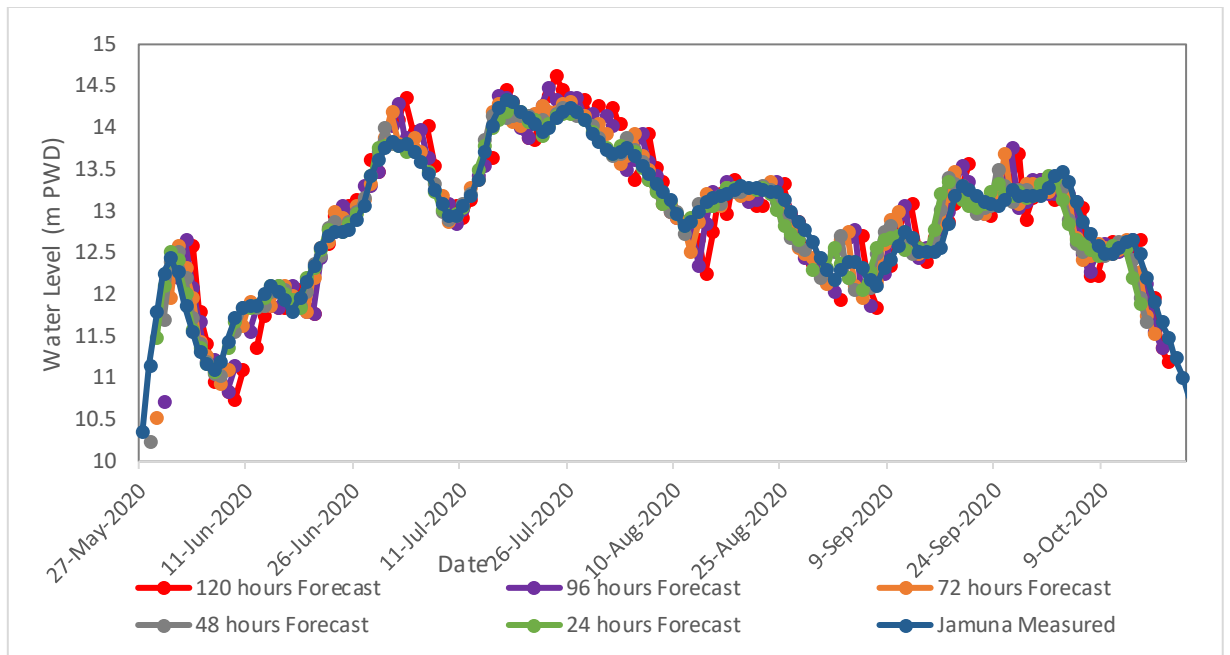
Figure 5.46 FFWC Forecasted 24-hour, 48-hour, 72-hour, 96-hour, and 120-hour Water Level with the Measured Water Level at the Sirajganj Station of the Jamuna River

The Different Lead-time forecasted water level is plotted with the measured water level of the Jamuna River for the 2020 flood period. The accuracy of the FFWC forecast was analyzed with the measured water level at the Sirajganj station.
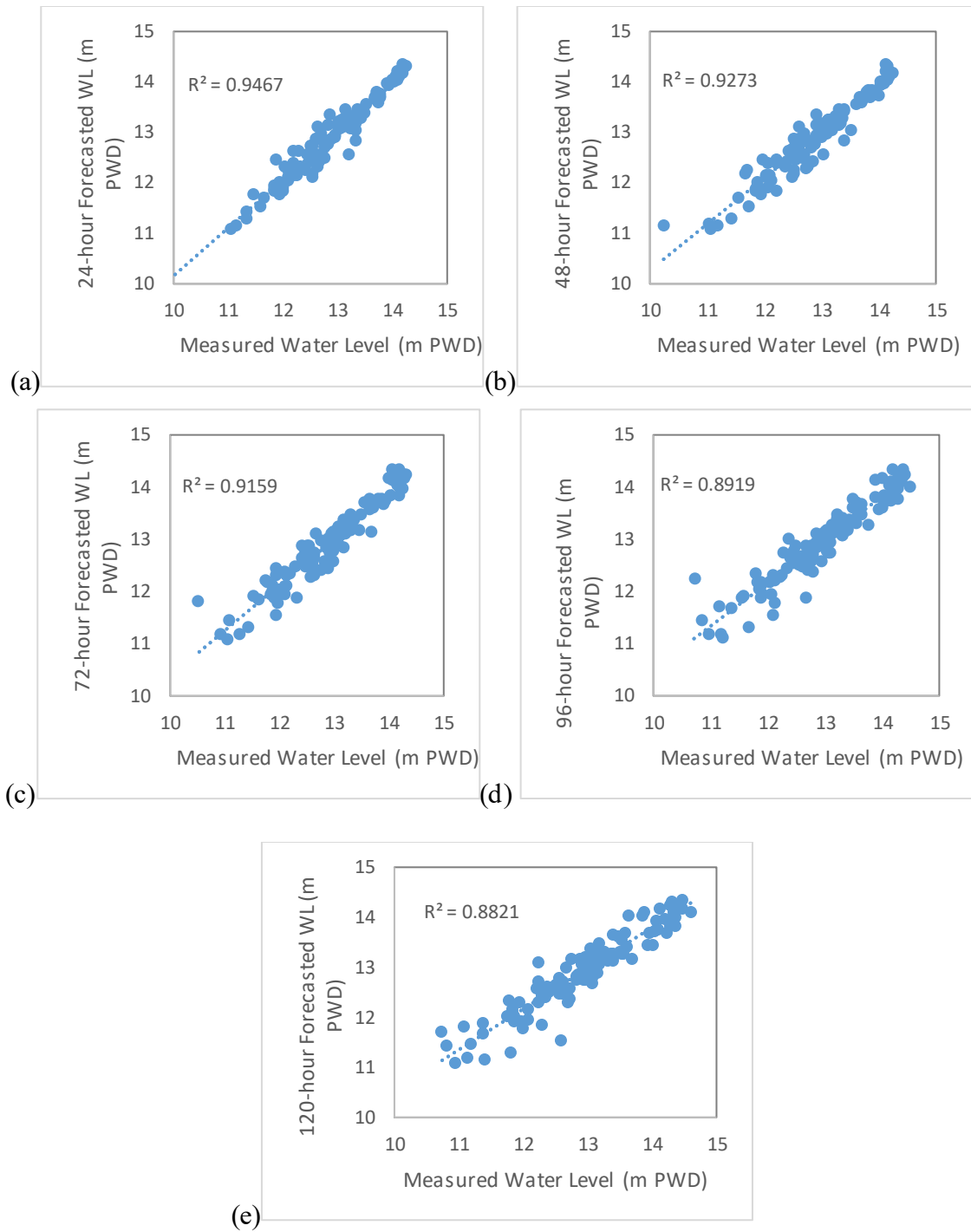
Figure 5.47 Statistical Relation of FFWC Forecast with the Measured Water Level at the Sirajganj Station of the Jamuna River

The regression and NSE were analyzed for the 24-hour, 48-hour, 72-hour, 96-hour, and 120-hour forecasts in the Jamuna River at the Sirajganj station. The $R^2$ (Figure 5.46) and NSE values are found in the range of 0.95 to 0.82 for the different day forecasts. In the Mean Absolute Error and the Root Mean Square Error analysis, the MAE is found

between 0.107 m to 0.234 m, and RMSE is between 0.168 m to 0.296 m for different day forecasts. The Residual Range is from 1.54 to -1.03 m. Table 5.7 summarizes the results.

Table 5.7 Statistical Relation and Error of Different Lead-time FFWC Forecast with the Measured Jamuna River Water Level for 2020 Flood

| FFWC 2020 | R² | NSE | MAE (m) | RMSE (m) | Residual Range (m) |
|-----------|------|------|---------|----------|--------------------|
| 24 hours | 0.95 | 0.95 | 0.107 | 0.168 | 0.52 to -0.64 |
| 48 hours | 0.93 | 0.92 | 0.136 | 0.196 | 0.91 to -0.55 |
| 72 hours | 0.91 | 0.89 | 0.164 | 0.231 | 1.26 to -0.55 |
| 96 hours | 0.89 | 0.84 | 0.203 | 0.280 | 1.54 to -0.79 |
| 120 hours | 0.88 | 0.82 | 0.234 | 0.296 | 0.97 to -1.03 |

From the above analysis, it is found that the forecasted water level at the Sirajganj station of the Jamuna River is very close to the measured water level.

## 5.4.2    Application of FFWC Forecast for Flood Forecasting in Floodplain

The forecasted data for the Jamuna River from FFWC is next used to generate the boundary condition for the model, and then the model was run to forecast flood in the floodplain of Ranigram.

At first, using the simple statistical equation, the water level at the Union Parishad location is established for the 24-hour, 48-hour, 72-hour, 96-hour, and 120-hour forecasts. Figure 5.48 shows the water level boundary condition at the Union Parishad developed using the FFWC forecast. For the downstream boundary condition, the normal depth value established with 2018 data is used.
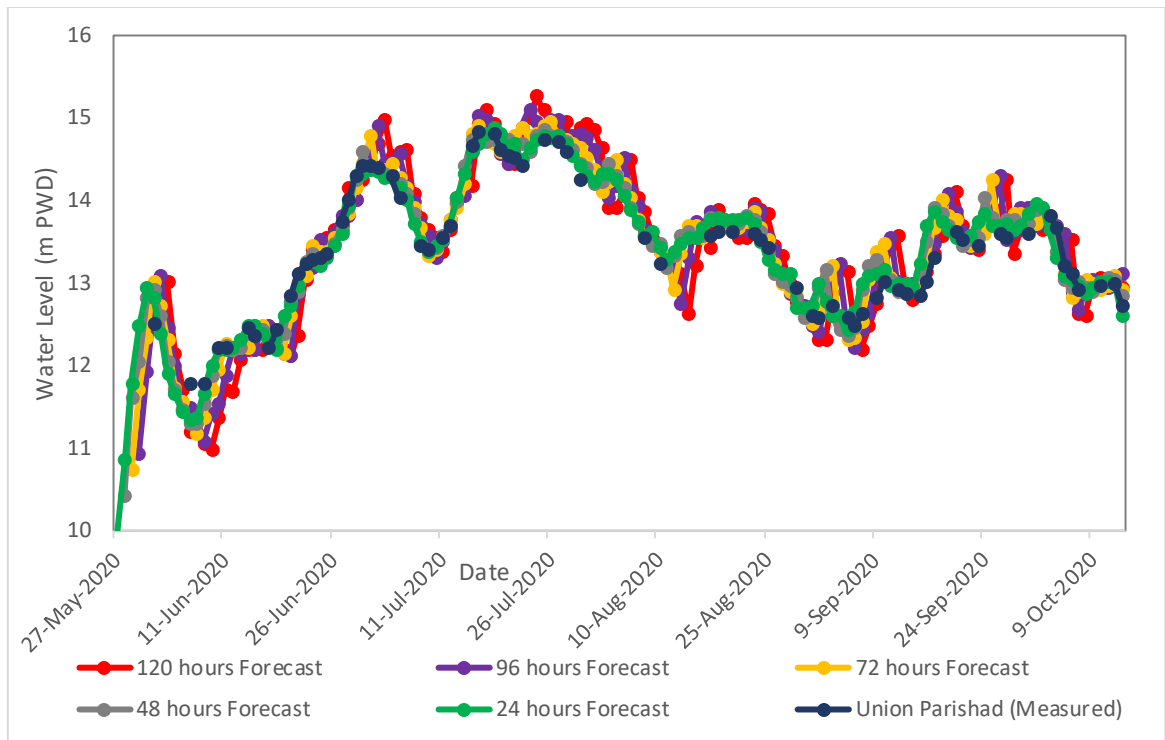
Figure 5.48 Water Level Boundary Condition at the Union Parishad Developed Using the FFWC Forecast.

After the simulation with the forecasted boundary condition, the computational cell at the location of the Culvert and Pilot Site water level gauge was selected in the RAS Mapper. The daily water surface elevation data of the cell was collected from the model result. The floodwater level data of the model was plotted with the Culvert and Pilot Site gauges' measured floodwater level data.

Figure 5.49 shows the 24-hour, 48-hour, 72-hour, 96-hour, and 120-hour forecasted water level at Culvert location in Ranigram with the measured water level for 2020 flood.
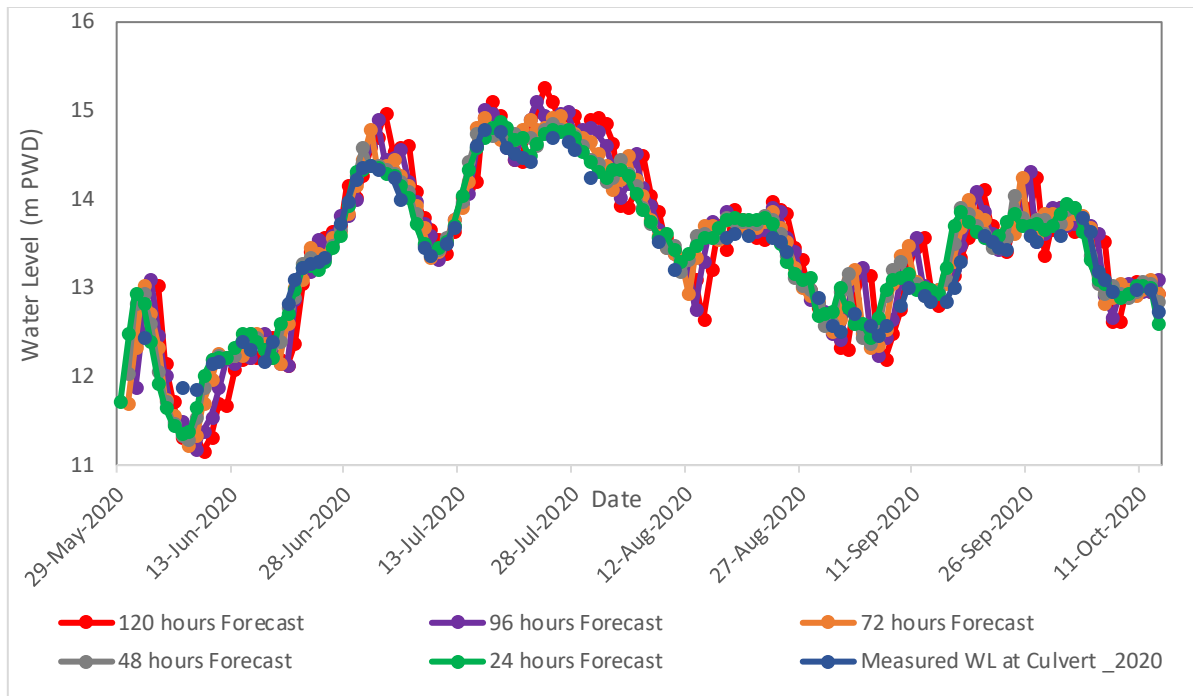
Figure 5.49 Forecasted 24-hour, 48-hour, 72-hour, 96-hour, and 120-hour Water Level at the Culvert Gauge Location in Ranigram with the Measured Water Level for the 2020 Flood

The $R^2$ and NSE values for the forecasted Culvert water levels are found in the range of 0.94 to 0.78 for different day forecasts. In the Mean Absolute Error and the Root Mean Square Error analysis, the MAE is found between 0.14 m to 0.27 m, and RMSE is between 0.20 m to 0.34 m for different day forecasts. The Residual Range is from 0.83 to -0.72 m. Table 5.8 summarizes the results.

Table 5.8 Relation and Error of Different Lead-time FFWC Forecast by HEC-RAS Model with the Measured Water Level at Culvert for 2020 Flood

|  | R² | NSE | MAE (m) | RMSE (m) | Residual Range (m) |
|---|---|---|---|---|---|
| **24 hours** | 0.94 | 0.92 | 0.14 | 0.20 | 0.53 to -0.69 |
| **48 hours** | 0.94 | 0.92 | 0.14 | 0.20 | 0.56 to -0.62 |
| **72 hours** | 0.94 | 0.9 | 0.17 | 0.22 | 0.52 to -0.59 |
| **96 hours** | 0.92 | 0.85 | 0.24 | 0.3 | 0.70 to -0.71 |
| **120 hours** | 0.89 | 0.78 | 0.27 | 0.34 | 0.83 to -0.72 |

Figure 5.50 shows the 24-hour, 48-hour, 72-hour, 96-hour, and 120-hour forecasted water level at the Pilot Site location in Ranigram with the measured water level for the 2020 flood.
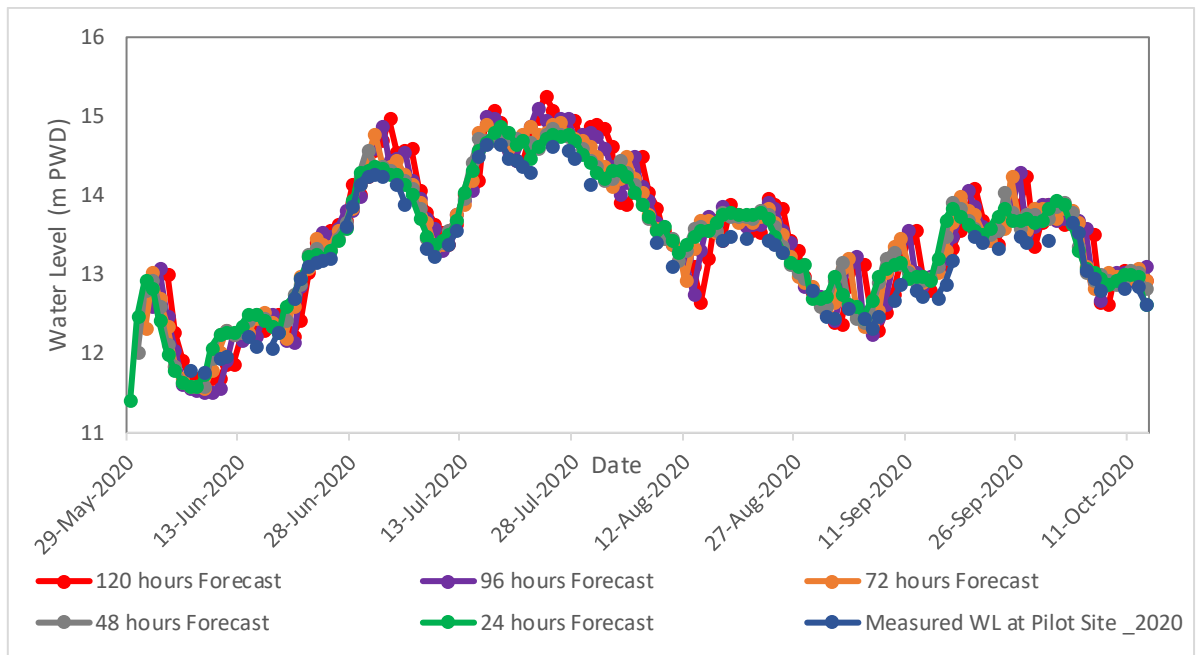


Figure 5.50 Forecasted 24-hours, 48-hours, 72-hours, 96-hours, and 120-hours Water Level at Pilot Site Gauge Location in Ranigram with the Measured Water Level for the 2020 Flood

The $R^2$ and NSE values for forecasted Pilot Site water levels are found in the range of 0.95 to 0.83 for different day forecasts. In the Mean Absolute Error and the Root Mean Square Error analysis, the MAE is found between 0.14 m to 0.24 m, and RMSE is between 0.19 m to 0.30 m for different day forecasts. The Residual Range is from 0.67 to -0.71 m. Table 5.9 summarizes the results.

Table 5.9 Relation and Error of Different Lead-time FFWC Forecast by HEC-RAS Model with the Measured Water Level at Pilot Site for 2020 Flood

| | $R^2$ | NSE | MAE (m) | RMSE (m) | Residual Range (m) |
|---|---|---|---|---|---|
| 24 hours | 0.95 | 0.93 | 0.14 | 0.19 | 0.32 to -0.69 |
| 48 hours | 0.95 | 0.93 | 0.14 | 0.19 | 0.27 to -0.62 |
| 72 hours | 0.95 | 0.91 | 0.16 | 0.21 | 0.27 to -0.59 |

| | | | | | |
|---|---|---|---|---|---|
| **96 hours** | 0.92 | 0.87 | 0.21 | 0.27 | 0.67 to -0.71 |
| **120 hours** | 0.90 | 0.83 | 0.24 | 0.30 | 0.65 to 0.72 |

From the above discussion, it is observed that the model run with the boundary condition derived from the FFWC forecasted water level of Sirajganj station in the Jamuna River is very good at representing flood propagation scenarios in the Ranigram area. The 2D hydrodynamic model following the above methodology can predict the location-specific flood water level inside the floodplain of Ranigram.

### 5.4.3   Framework for Flood Forecasting Methodology in the Floodplain

This method can be used to forecast location-specific flood scenarios in the floodplain (Figure 5.51). In the 2D model, the boundary condition will be developed from the FFWC's forecasted water level in the river. Furthermore, the result of the model will represent the forecasted flood scenario in the floodplain for the corresponding FFWC forecast. Therefore, the essential element in the methodology is to use a high-resolution DTM of the floodplain that can accurately represent the topography of the floodplain, which will provide location-specific flood information.

Figure 5.51 shows the methodological framework proposed for forecasting floods in the floodplain.
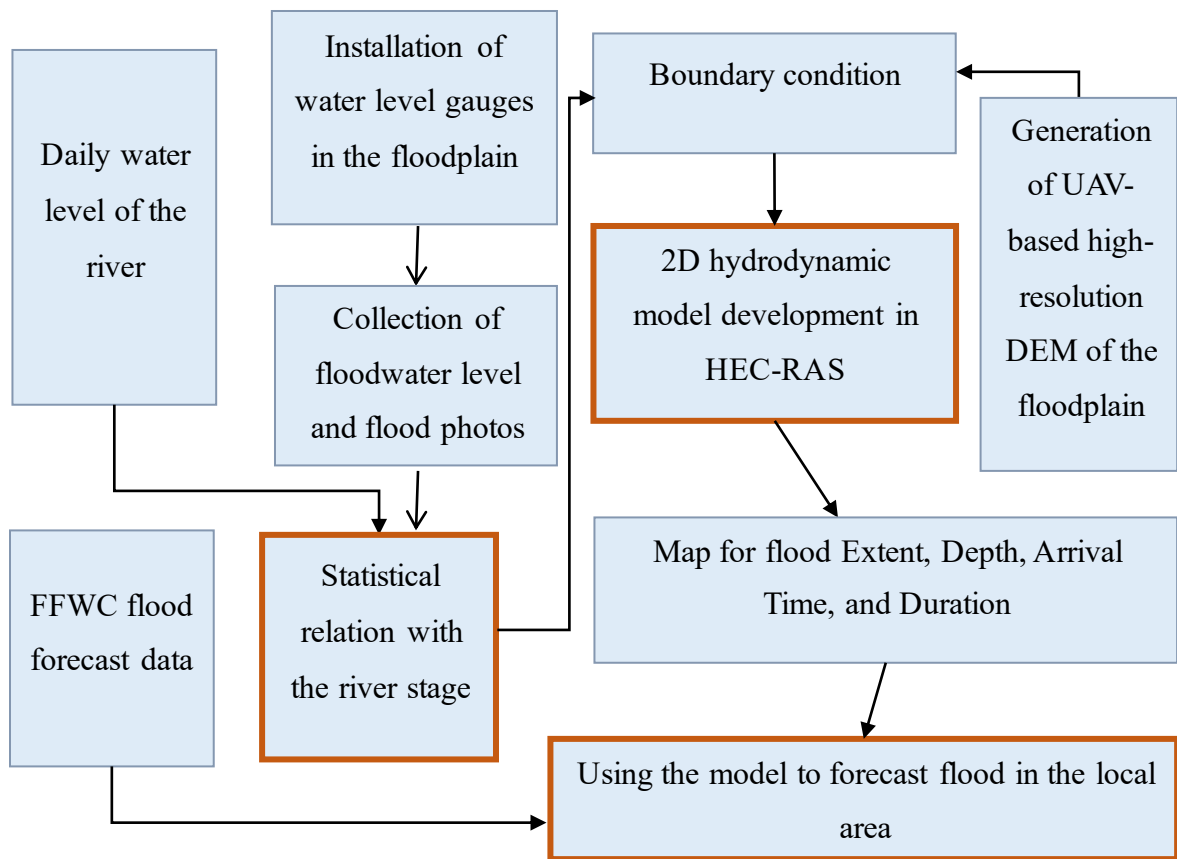
Figure 5.51 Methodological Framework for Forecasting Floods in the Floodplain

### 5.4.4 Potential Options for Dissemination of the Flood Forecasts

It is necessary to deploy both traditional and modern communication channels for disseminating flood forecast information in the community. Local Government organizations like the Union Parishad and Community-Based Organizations like mosques and temples can play an essential role in circulating the forecasts to the community. Presently, Bangladesh has almost 100% coverage of mobile phone networks, and about 80% of people have mobile phones. Recent studies have shown the usefulness of mobile phones in communicating flood forecasts and warnings (Cumiskey, 2013; FFWC, 2017). Also, people nowadays are very active on Facebook, and so the Facebook page can also be used to disseminate the flood forecasts targeting the audience for the specific disaster-prone area. Therefore, technological tools can be the fastest devices to disseminate the information in the community.

# CHAPTER SIX
# CONCLUSIONS AND RECOMMENDATIONS

## 6.1    Conclusions

The flooding in the Jamuna riverside Ranigram village is mainly dominated by the overtopping river water and are highly influenced by the fluctuation of the river water level. The observed floodwater level shows an excellent dynamic relation with the water level at Sirajganj station of the Jamuna River, with $R^2$ and NSE values of 0.78 to 0.98 and a maximum error of 33 cm.

The statistical relation between the water levels of the floodplain and Jamuna River derived from 2018 data was validated with the observed data of 2020. The regression model is found to be very much effective in predicting the flood water levels in the Ranigram area with the dependent variable of Jamuna River water level. However, to understand flood more inclusively, the other flood propagation parameters like flood arrival time, duration, and flood entering and exiting phenomena are necessary.

A two-dimensional hydrodynamic model was developed to understand the flood propagation in the floodplain of Ranigram and to have an accurate flood model that can represent the real flood scenario in the locality. A HEC-RAS 2D model was developed using UAV-based high-resolution DTM, and boundary condition generated using the Jamuna River water level. The model was calibrated and validated with the observed floodwater level data in the floodplain. The high-resolution DTM was generated using a drone survey, and measured elevation and bathymetry data. The results of the HEC-RAS model incorporated with UAV-based DTM showed an excellent agreement with the observed water level and collected flood photos of the Ranigram Area.

When compared with satellite-based flood inundation maps, the model result was better even in the tree-canopy area. The model was run with the globally available DEMs, and the WorldDEM$^{TM}$, ALOS PALSAR, SRTM 30m, MERIT, and ASTER DEMs are found to be unsuitable in the detailed local level modeling.

So, we found that a high-resolution DTM and frequent field-measured data can significantly improve the 2D hydrodynamic model. This level of detailed information

representing real flood scenarios in the floodplain is crucial for location-specific flood information.

In this model, using the boundary condition of FFWC forecasted river water level instead of daily river water level, we can get corresponding forecasted flood information in the associated floodplain. As FFWC measure water level in 3 hour interval, the location-specific forecast in floodplain can be generated in 3 hour interval at 5day to 1day lead time. This methodology of flood modeling can be used at any riverside area for flood forecasting concerning the FFWC river forecast. The information of flood arrival time, duration, and maximum depth and extent for the floodplain area can be extracted from the 2D hydrodynamic model. The flood forecasting information for any specific location of the floodplain can be obtained from the flood maps. This information will help the local people to take the necessary precautions and evacuations before floodwater enters their lands. Presently people of the locality only get river forecast and use their indigenous knowledge to just assume when water can enter the important locations. By getting location specific forecasting they will be able to harvest their crops and evacuate houses before floodwater enters or destroy their valuables. Furthermore, the outcomes of this study will also be helpful in forecasting and assessing flood risk and damage for the floodplain areas.

## 6.2   Recommendations for Future Study

Based on the findings of this study and the experiences gained during the study, the following recommendations are provided for future studies.

- This study can be replicated in any riverside floodplain that has interaction with the river.
- The model can be developed with a large flow area to examine the applicability for the large area. The cost of the drone survey for large-scale can be reduced by buying own drone and surveying instead of contract with any survey farm.
- For future studies, 1D-2D coupling model can be developed, instead of only 2D model as this will reduce cost and time.

- In this study, forecast model has been developed on a daily basis. As riverside community is the first to be affected, forecast model can be developed for a 3hr interval in further studies if relevant data are available.

- This study considered hydrodynamic analysis only. For future studies, the hydrological and hydro-morphological analysis can be added.

- The effect of any change in the morphological and land-use due to human factor, can be analyzed in future studies.

- The embankment breaching analysis can be done in the future studies. The flood propagation due to embankment breaching and its associated impacts in the floodplain can also be analyzed.

# REFERENCES

Agrawala, S., Ota, T., Ahmed, A., Smith, J., & Aalst, M. (2003). *Development and climate change in Bangladesh: focus on coastal flooding and the Sundarbans*. Environment Directorate and Development Co-Operation Directorate, OECD, France. Retrieved from https://www.academia.edu/2266268/Development_and_climate_change_in_Banglades h_focus_on_coastal_flooding_and_the_Sundarbans

Airbus (2018). WorldDEM™ Technical product specification - Digital Surface Model, Digital Terrain Model Version 2.4.

Akter, J., Sarker, M. H., Popescu, I., & Roelvink, D. (2016). Evolution of the Bengal delta and its prevailing processes. Journal of Coastal Research, 321, 1212–1226. doi:10.2112/jcoastres-d-14-00232.1

Ali, M., Bhattacharya, B., Islam, A., Islam, G., Hossain, M., & Khan, A. (2018). Challenges for flood risk management in flood-prone Sirajganj region of Bangladesh. *Journal of Flood Risk Management, 12*(1), e12450. doi: 10.1111/jfr3.12450

Anusha, N., & Bharathi, B. (2020). Flood detection and flood mapping using multi-temporal synthetic aperture radar and optical data. *The Egyptian Journal of Remote Sensing and Space Science*, *23*(2), 207-219. doi: 10.1016/j.ejrs.2019.01.001

ASF (2021). ALOS PALSAR – Radiometric Terrain Correction. Retrieved 12 November 2021, from https://asf.alaska.edu/data-sets/derived-data-sets/alos-palsar-rtc/alos-palsar-radiometric-terrain-correction/

Avinash, S. (2014). "Flood related disasters: Concerned to urban flooding in Bangalore, India". *International Journal of Research in Engineering and Technology,* 03 (28): 76-83. doi:10.15623/ijret.2014.0328013

Azizian, A., & Brocca, L. (2019). Determining the best remotely sensed DEM for flood inundation mapping in data sparse regions. *International Journal of Remote Sensing*, *41*(5), 1884-1906. doi: 10.1080/01431161.2019.1677968

Bazzoffi, P. (2015). Measurement of rill erosion through a new UAV-GIS methodology. *Italian Journal of Agronomy*, *10*(1s). doi: 10.4081/ija.2015.708

BBS (2016). Economic Census 2013 - District Report: Sirajganj. Reproduction, Documentation & Publication (RDP) Section, Bangladesh Bureau of Statistics, Bangladesh.

Becek, K., Koppe, W., & Kutoğlu, Ş. (2016). Evaluation of vertical accuracy of the WorldDEM™ using the runway method. *Remote Sensing*, *8*(11), 934. doi: 10.3390/rs8110934

Ben Khalfallah, C., & Saidi, S. (2018). Spatiotemporal floodplain mapping and prediction using HEC-RAS - GIS tools: Case of the Mejerda river, Tunisia. Journal of African Earth Sciences, 142, 44–51. doi:10.1016/j.jafrearsci.2018.03.004

Bhuiyan, S. (2006). Flood forecasting, warning and response system. In: Options for flood risk and damage reduction in Bangladesh. Dhaka, The University Press Limited.

Biswas, A. K. (2008). Management of Ganges-Brahmaputra-Meghna system: way forward. Management of Transboundary Rivers and Lakes, In: *Management of Transboundary Rivers and Lakes,* 143–164. doi:10.1007/978-3-540-74928-8_6

Biswas, S. (2020). Assessing the impacts of the Padma River stabilization and its embankment failure through a combined 1d and 2d hydrodynamic model simulation. M. Sc. Thesis, Institute of Water and Flood Management, Bangladesh University of Engineering and Technology.

Brammer, H. (2010). After the Bangladesh flood action plan: Looking to the future. *Environmental Hazards,* 9 (1): 118-130. doi:10.3763/ehaz.2010.si01.

BWDB (1999). Annual flood report 1998, Flood Forecasting and Warning Centre, BWDB, Dhaka.

Chiabrando, F., D'Andria, F., Sammartano, G., & Spanò, A. (2018). UAV photogrammetry for archaeological site survey. 3D models at the Hierapolis in Phrygia (Turkey). *Virtual Archaeology Review*, *9*(18), 28. doi: 10.4995/var.2018.5958.

Chowdhury, A., Reshad, S., & Kumruzzaman, M. (2021). Hydrodynamic flood modelling for the Jamuna River using HEC-RAS & MIKE 11. *5th International*

*Conference on Advances in Civil Engineering (ICACE-2020)*. WRE 188-195, CUET, Chattogram.

Chu, T., & Lindenschmidt, K. (2017). Comparison and validation of digital elevation models derived from InSAR for a flat inland delta in the high latitudes of northern Canada. *Canadian Journal of Remote Sensing*, *43*(2), 109-123. doi: 10.1080/07038992.2017.1286936

Costabile, P., Costanzo, C., Ferraro, D., Macchione, F., & Petaccia, G. (2020). Performances of the new HEC-RAS version 5 for 2D Hydrodynamic-based rainfall-runoff simulations at basin scale: Comparison with a state-of-the art model. *Water*, 12(9), 2326. doi:10.3390/w12092326

Coveney, S., & Roberts, K. (2017). Lightweight UAV digital elevation models and orthoimagery for environmental applications: data accuracy evaluation and potential for river flood risk modelling. *International Journal of Remote Sensing*, *38*(8-10), 3159-3180. doi: 10.1080/01431161.2017.1292074

Cowan, D., & Cooper, G. (2005). The Shuttle Radar Topography Mission—A new source of near-global digital elevation data. *Exploration Geophysics*, *36*(4), 334-340. doi: 10.1071/eg05334

Cumiskey, L. (2013). Flood warning communication using mobile services in flash flood communities of Bangladesh. MSc Thesis, UNESCO-IHE Institute for Water Education, Delft. https://cdm21063.contentdm.oclc.org/digital/collection/masters2/id/53997

Das, A., Agrawal, R., & Mohan, S. (2014). Topographic correction of ALOS-PALSAR images using InSAR-derived DEM. *Geocarto International*, 30(2), 1-9. doi: 10.1080/10106049.2014.883436

DeWitt, J., Warner, T., & Conley, J. (2015). Comparison of DEMs derived from USGS DLG, SRTM, a statewide photogrammetry program, ASTER GDEM and LiDAR: implications for change detection. *Giscience & Remote Sensing*, *52*(2), 179-197. doi: 10.1080/15481603.2015.1019708

Farooq, M., Shafique, M., & Khattak, M. (2019). Flood hazard assessment and mapping of River Swat using HEC-RAS 2D model and high-resolution 12-m TanDEM-X DEM (WorldDEM). *Natural Hazards*, *97*(2), 477-492. doi: 10.1007/s11069-019-03638-9

Farooq, M., Shafique, M., & Khattak, M. S. (2019). Flood hazard assessment and mapping of River Swat using HEC-RAS 2D model and high-resolution 12-m TanDEM-X DEM (WorldDEM). Natural Hazards, 97 (2): 477-492. doi:10.1007/s11069-019-03638-9

Farr, T., Rosen, P., Caro, E., Crippen, R., Duren, R., Hensley, S., Kobrick, M., Paller, M., Rodriguez, E., Roth, L., Seal, D., Shaffer, S., Shimada, J., Umland, J., Werner, M., Oskin, M., Burbank, D. & Alsdorf, D. (2007). The Shuttle Radar Topography Mission. *Reviews of Geophysics*, *45*(2). doi: 10.1029/2005rg000183

FFWC (2018). Annual flood report 2018. Processing and Flood Forecasting Circle, Bangladesh Water Development Board, Government of the People's Republic of Bangladesh.

Franci, F., Bitelli, G., Mandanici, E., Hadjimitsis, D., & Agapiou, A. (2016). Satellite remote sensing and GIS-based multi-criteria analysis for flood hazard mapping. *Natural Hazards*, *83*(S1), 31-51. doi: 10.1007/s11069-016-2504-9

Freund, R.J., Wilson, W. J., & Sa, P. (2006). *Regression Analysis*. 2nd ed. Boston: Academic Press.

Gafurov, A. (2021). The methodological aspects of constructing a high-resolution DEM of large territories using low-cost UAVs on the example of the Sarycum Aeolian Complex, Dagestan, Russia. *Drones*, *5*(1), 7. doi: 10.3390/drones5010007

Gallien, T., Schubert, J., & Sanders, B. (2011). Predicting tidal flooding of urbanized embayments: A modeling framework and data requirements. *Coastal Engineering*, *58*(6), 567-577. doi: 10.1016/j.coastaleng.2011.01.011

Gesch, D., Oimoen, M., Zhang, Z., Meyer, D., & Danielson, J. (2012). Validation of the Aster global digital elevation model version 2 over the Conterminous United States. *The International Archives of the Photogrammetry, Remote Sensing and Spatial Information Sciences*, *XXXIX-B4*, 281-286. doi: 10.5194/isprsarchives-xxxix-b4-281-2012

Giustarini, L., Chini, M., Hostache, R., Pappenberger, F., & Matgen, P. (2015). Flood hazard mapping combining hydrodynamic modeling and multi annual remote sensing data. *Remote Sensing*, 7(10), 14200–14226. doi:10.3390/rs71014200

GoB (2021). Sirajganj District. Retrieved 12 November 2021, from http://www.sirajganj.gov.bd/en/site/page/lSin-%E0%A6%AD%E0%A7%8C%E0%A6%97%E0%A6%B2%E0%A6%BF%E0%A6%95-%E0%A6%AA%E0%A6%B0%E0%A6%BF%E0%A6%9A%E0%A6%BF%E0%A6%A4%E0%A6%BF

González-Moradas, M., & Viveen, W. (2020). Evaluation of ASTER GDEM2, SRTMv3.0, ALOS AW3D30 and TanDEM-X DEMs for the Peruvian Andes against highly accurate GNSS ground control points and geomorphological-hydrological metrics. *Remote Sensing of Environment*, *237*, 111509. doi: 10.1016/j.rse.2019.111509

Grimaldi, S., Li, Y., Pauwels, V., & Walker, J. (2016). Remote sensing-derived water extent and level to constrain hydraulic flood forecasting models: opportunities and challenges. *Surveys in Geophysics*, *37*(5), 977-1034. doi: 10.1007/s10712-016-9378-y

Guan, L., Pan, H., Zou, S., Hu, J., Zhu, X., & Zhou, P. (2020). The impact of horizontal errors on the accuracy of freely available digital elevation models (DEMs). *International Journal of Remote Sensing*, *41*(19), 7383-7399. doi: 10.1080/01431161.2020.1759840

Gutierrez Andres, J. and Lhomme, J. and Weisgerber, A. and Cooper, A. and Gouldby, B.P. & Mulet-Marti, J. (2008). Testing and application of a practical new 2D hydrodynamic model. In: FLOOD risk 2008, 30 September - 2 October 2008, Keble College, Oxford, UK.

Hafiz, R.B. (2019). A study on water quality parameters due to withdrawal and flow augmentation in the Dhaka peripheral river system. MSc Thesis, Department of Water Resources Engineering, Bangladesh University of Engineering and Technology, Dhaka.

Hashemi-Beni, L., Jones, J., Thompson, G., Johnson, C., & Gebrehiwot, A. (2018). Challenges and opportunities for UAV-based digital elevation model generation for flood-risk management: a case of Princeville, North Carolina. *Sensors*, *18*(11), 3843. doi: 10.3390/s18113843

Hassan, A., & Shah, M. A. R. (2008). "A participatory model for flood early warning dissemination". *Third South Asia Water Research Conference on Innovative Modeling Approaches for IWRM*. BUET, Dhaka, Bangladesh.

Hirano, A., Welch, R., & Lang, H. (2003). Mapping from ASTER stereo image data: DEM validation and accuracy assessment. *ISPRS Journal of Photogrammetry and Remote Sensing*, *57*(5-6), 356-370. doi: 10.1016/s0924-2716(02)00164-8

Hofer, T., & Messerli, B. (2006). Floods in Bangladesh: History, dynamics and rethinking the role of the Himalayas. United Nations University Press, Tokyo, Japan.

Horritt, M., & Bates, P. (2002). Evaluation of 1D and 2D numerical models for predicting river flood inundation. *Journal of Hydrology*, *268*(1-4), 87-99. doi: 10.1016/s0022-1694(02)00121-x

Hossain, A. (2003). *Bangladesh: Flood Management*. World Meteorological Organization. Retrieved from http://www.floodmanagement.info/publications/casestudies/cs_bangladesh_full.pdf

Hostache, R., Chini, M., Giustarini, L., Neal, J., Kavetski, D., Wood, M., Corato, G., Pelich, R. and Matgen, P. (2018). Near-Real-Time assimilation of SAR-derived flood maps for improving flood forecasts. *Water Resources Research*, *54*(8), 5516-5535. doi: 10.1029/2017wr022205

Huang, M., & Jin, S. (2020). Rapid flood mapping and evaluation with a supervised classifier and change detection in Shouguang using Sentinel-1 SAR and Sentinel-2 optical data. *Remote Sensing*, 12(13), 2073. doi:10.3390/rs12132073

Hydrologic Engineering Center (2018). HEC-RAS 5.0 - Hydraulic Reference Manual. http:// www.hec.usace.army.mil/software/hec-ras/documentation.aspx.

IFRC. (2014). Emergency appeal operations update Bangladesh: Floods. International Federation of Red Cross and Red Crescent Societies (IFRC) Dhaka. Retrieved from https://reliefweb.int/sites/reliefweb.int/files/resources/MDRBD014OU1.pdf

Internetgeography (2021). Human and physical factors causing river flooding. Retrieved on 16 November, 2021, from https://www.internetgeography.net/topics/human-and-physical-factors-causing-river-flooding/

Islam, A. S., Haque, A., & Bala, S. K. (2010). Hydrologic characteristics of floods in Ganges–Brahmaputra–Meghna (GBM) delta. *Natural Hazards*, 54(3), 797–811. Doi:10.1007/s11069-010-9504-y

Islam, M. A. (1995). Environment land use and natural hazards in Bangladesh. University of Dhaka, Dhaka.

Islam, S., & Miah, S. (2012). Banglapedia: National Encyclopedia of Bangladesh. Dhaka: Asiatic Society of Bangladesh.

Jackson, A. (2021). Flooding. Retrieved on 16 November, 2021, from https://geographyas.info/rivers/flooding/

Jacob, X., Bisht, D., Chatterjee, C., & Raghuwanshi, N. (2019). Hydrodynamic modeling for flood hazard assessment in a data scarce region: a case study of Bharathapuzha River basin. *Environmental Modeling & Assessment, 25*(1), 97-114. doi: 10.1007/s10666-019-09664-y

Jain, S., Mani, P., Jain, S., Prakash, P., Singh, V., Tullos, D., Kumar, S., Agarwal, S. and Dimri, A. (2018). A Brief review of flood forecasting techniques and their applications. *International Journal of River Basin Management, 16*(3), 329-344. doi: 10.1080/15715124.2017.1411920

Jakob, M., Holm, K., Lazarte, E., & Church, M. (2014). A flood risk assessment for the City of Chilliwack on the Fraser River, British Columbia, Canada. *International Journal of River Basin Management, 13*(3), 263-270. doi: 10.1080/15715124.2014.903259

Jakovljevic, G., Govedarica, M., Alvarez-Taboada, F., & Pajic, V. (2019). Accuracy assessment of deep learning based classification of LiDAR and UAV points clouds for DTM creation and flood risk mapping. *Geosciences, 9*(7), 323. doi: 10.3390/geosciences9070323

JPL (2021). ASTER global digital elevation map. Retrieved on 12 November, 2021, from https://asterweb.jpl.nasa.gov/gdem.asp

Jung, Y., Kim, D., Kim, D., Kim, M., & Lee, S. (2014). Simplified flood inundation mapping based on flood elevation-discharge rating curves using satellite images in gauged watersheds. *Water, 6*(5), 1280-1299. doi: 10.3390/w6051280.

Kardasz, P., & Doskocz, J. (2016). Drones and possibilities of their using. *Journal of Civil & Environmental Engineering, 6*(3). doi: 10.4172/2165-784x.1000233

Kellndorfer, J., Walker, W., LaPoint, E., Kirsch, K., Bishop, J., & Fiske, G. (2010). Statistical fusion of LiDAR, InSAR, and optical remote sensing data for forest stand height characterization: A regional-scale method based on LVIS, SRTM, Landsat ETM+, and ancillary data sets. *Journal of Geophysical Research: Biogeosciences*, *115*(G2). doi: 10.1029/2009jg000997

Khan, MSA. (2008). Disaster preparedness for sustainable development in Bangladesh. *Disaster Prevention and Management: An International Journal*, *17*(5), 662-671. doi: 10.1108/09653560810918667.

Kumar, H., Rajan, S., & Shukla, A. (2012). Development of lithium-ion batteries from micro-structured to nanostructured materials: its issues and challenges. *Science Progress*, *95*(3), 283-314. doi: 10.3184/003685012x13421145651372

Kumar, N., Kumar, M., Sherring, A., Suryavanshi, S., Ahmad, A., & Lal, D. (2019). Applicability of HEC-RAS 2D and GFMS for flood extent mapping: a case study of Sangam area, Prayagraj, India. *Modeling Earth Systems and Environment*, *6*(1), 397-405. doi: 10.1007/s40808-019-00687-8

Kundu, S., Aggarwal, S., Kingma, N., Mondal, A., & Khare, D. (2014). Flood monitoring using microwave remote sensing in a part of Nuna river basin, Odisha, India. *Natural Hazards*, *76*(1), 123-138. doi: 10.1007/s11069-014-1478-8

Kundzewicz, Z. (2002). Non-structural flood protection and sustainability. *Water International*, *27*(1), 3-13. doi: 10.1080/02508060208686972

Langhammer, J., Bernsteinová, J., & Miřijovský, J. (2017). Building a high-precision 2D hydrodynamic flood model using UAV photogrammetry and sensor network monitoring. *Water*, *9*(11), 861. doi: 10.3390/w9110861

Learn on Internet (2021). Rivers - Discharge - Storm Hydrograph. Retrieved on 16 November, 2021, from http://geography.learnontheinternet.co.uk/topics/discharge.html

Liang, J., & Liu, D. (2020). A local thresholding approach to flood water delineation using Sentinel-1 SAR imagery. *ISPRS Journal of Photogrammetry and Remote Sensing*, *159*, 53-62. doi: 10.1016/j.isprsjprs.2019.10.017

Liu, Y., & De Smedt, F. (2005). Flood modeling for complex terrain using GIS and remote sensed information. *Water Resources Management*, *19*(5), 605-624. doi: 10.1007/s11269-005-6808-x

Mahmud. (2017). Seasonal variation of hydrodynamic parameters of Padma River, B.Sc thesis, Department of Water Resources Engineering, Bangladesh University of Engineering and Technology, Dhaka.

Mali, V., Veeranna, B., Parik, A., & Kuiry, S. (2020). Experimental and numerical study of flood dynamics in a river-network-floodplain set-up. *Journal of Hydroinformatics*, *22*(4), 793-814. doi: 10.2166/hydro.2020.160.

Masood, M., & Takeuchi, K. (2011). Assessment of flood hazard, vulnerability and risk of mid-eastern Dhaka using DEM and 1D hydrodynamic model. *Natural Hazards*, *61*(2), 757-770. doi: 10.1007/s11069-011-0060-x

Mehta D. J., Yadav S. M., and Waikhom S. (2013). Geomorphic channel design and analysis using HEC-RAS hydraulic design functions. *Global Research Analysis*, 2(4):90–93

Mehta, D. J., & Yadav, S. (2019). Hydrodynamic simulation of river Ambica for riverbed assessment: a case study of Navsari region. *Lecture Notes in Civil Engineering*, 127-140. doi: 10.1007/978-981-13-8181-2_10

Meire, D., De Doncker, L., Declercq, F., Buis, K., Troch, P., & Verhoeven, R. (2010). Modelling river-floodplain interaction during flood propagation. *Natural Hazards*, *55*(1), 111-121. doi: 10.1007/s11069-010-9554-1

MERIT DEM (2021). Multi-Error-Removed Improved-Terrain DEM. Retrieved on 12 November, 2021, from http://hydro.iis.u-tokyo.ac.jp/~yamadai/MERIT_DEM/

Merwade, V., Cook, A., & Coonrod, J. (2008). GIS techniques for creating river terrain models for hydrodynamic modeling and flood inundation mapping. *Environmental Modelling & Software*, 23(10-11), 1300–1311. doi:10.1016/j.envsoft.2008.03.005

Miller, J., & Hutchins, M. (2017). The impacts of urbanisation and climate change on urban flooding and urban water quality: a review of the evidence concerning the United

Kingdom. *Journal of Hydrology: Regional Studies*, *12*, 345-362. doi: 10.1016/j.ejrh.2017.06.006.

Mirza, MMQ. (2002). Global warming and changes in the probability of occurrence of floods in Bangladesh and implications. *Global Environmental Change*, *12*(2), 127-138. doi: 10.1016/s0959-3780(02)00002-x

Moftakhari, H., Schubert, J., AghaKouchak, A., Matthew, R., & Sanders, B. (2019). Linking statistical and hydrodynamic modeling for compound flood hazard assessment in tidal channels and estuaries. *Advances in Water Resources*, *128*, 28-38. doi: 10.1016/j.advwatres.2019.04.009

Mondal, MS, Islam, A.K.M. S., Haque, A., Islam, M. R., Biswas, S., & Mohammed, K. (2021). Assessing high-end climate change impacts on floods in major rivers of Bangladesh using multi-model simulations. *Global Science and Technology Journal,* 6 (2), 1-14. https://zantworldpress.com/wp-content/uploads/2018/10/1.Mondal.pdf.

Mosquera-Machado, S., & Ahmad, S. (2006). Flood hazard assessment of Atrato River in Colombia. *Water Resources Management*, *21*(3), 591-609. doi: 10.1007/s11269-006-9032-4

Mozumder, P. (2005). Exploring flood mitigation strategies in Bangladesh. MSc Thesis, Water Resources Program, University of New Mexico.

Mukherjee, S., Joshi, P., Mukherjee, S., Ghosh, A., Garg, R., & Mukhopadhyay, A. (2013). Evaluation of vertical accuracy of open source digital elevation model (DEM). *International Journal of Applied Earth Observation and Geoinformation*, *21*, 205-217. doi: 10.1016/j.jag.2012.09.004

Munir, B., & Iqbal, J. (2016). Flash flood water management practices in Dera Ghazi Khan City (Pakistan): a remote sensing and GIS prospective. *Natural Hazards*, *81*(2), 1303-1321. doi: 10.1007/s11069-015-2136-5

Ninno, C. D., Dorosh, P. A., Smith, L. C., & Roy, D. K. (2001). The 1998 Floods in Bangladesh: Disaster Impacts, Household Coping Strategies, and Response. Research report no.: 122, International Food Policy Research Institute., Washington D.C.

NIRAPAD (2016). Bangladesh: flood situation analysis - August 31, 2016. Retrieved on 16 November, 2021, from https://reliefweb.int/report/bangladesh/bangladesh-flood-situation-analysis-august-31-2016.

NIRAPAD. (2007). Bangladesh Flood 2007. Situation report no. 09, 02 August 2007, Dhaka, Retrieved from https://reliefweb.int/sites/reliefweb.int/files/resources/957021ABD1074225492573520025D75A-Full_Report.pdf

NIRAPAD. (2010). Bangladesh: Flood and River Erosion. Situation report no.184, Dhaka. Retrieved from https://reliefweb.int/sites/reliefweb.int/files/resources/853E383E6938C6FFC1257751001D02CC-Full_Report.pdf

Pinel, S., Bonnet, M., S. Da Silva, J., Sampaio, T., Garnier, J., Catry, T., Calmant, S., Fragoso, C., Moreira, D., Motta Marques, D. and Seyler, F. (2020). Flooding dynamics within an Amazonian floodplain: water circulation patterns and inundation duration. *Water Resources Research*, *56*(1). Doi: 10.1029/2019wr026081

Quirogaa, V. M., Kurea, S., Udoa, K., & Manoa, A. (2016). Application of 2D numerical simulation for the analysis of the February 2014 Bolivian Amazonia flood: Application of the new HEC-RAS version 5. *Ribagua*, 3(1), 25–33. Doi:10.1016/j.riba.2015.12.001

Quirogaa, V. M., Kurea, S., Udoa, K., & Manoa, A. (2016). Application of 2D numerical simulation for the analysis of the February 2014 Bolivian Amazonia flood: Application of the new HEC-RAS version 5. Ribagua, 3(1), 25–33. doi:10.1016/j.riba.2015.12.001

Rabus, B., Eineder, M., Roth, A., & Bamler, R. (2003). The shuttle radar topography mission—a new class of digital elevation models acquired by spaceborne radar. *ISPRS Journal of Photogrammetry and Remote Sensing*, *57*(4), 241-262. Doi: 10.1016/s0924-2716(02)00124-7

Rahman, M. M. (2015). Modeling flood inundation of the Jamuna River. M. Sc. Thesis, Department of Water Resources Engineering, Bangladesh University of Engineering and Technology.

Rahman, M., and Ali, M. (2016). Modeling flood inundation in floodplain of the Jamuna River using HEC-RAS and HEC-GeoRAS. Journal of Civil Engineering (IEB), 44 (1) (2016) 41-51.

Rahman, M., Goel, N., & Arya, D. (2012). Study of early flood warning dissemination system in Bangladesh. *Journal of Flood Risk Management*, *6*(4), 290-301. Doi: 10.1111/jfr3.12012

Rahman, R. & Salehin, M. (2013). *Flood risks and reduction approaches in Bangladesh. In: Disaster Risk Reduction, 65–90.* Springer. doi:10.1007/978-4-431-54252-0_4.

Rahman, R., Haque, A., Khan, MSA., Salehin, M., & Bala, S.K. (2006). Investigation of hydrological aspects of flood-2004 with special emphasis on Dhaka city. Final Report, Institute of Water and Flood Management, Bangladesh University of Engineering and Technology, Dhaka.

Rouf, T. (2015). Flood inundation map of Serajgonj district using mathematical model. MSc Thesis, Department of Water Resources Engineering, Bangladesh University of Engineering and Technology, Dhaka.

Roy, B. (2019). A study on fluvial flood hazard and risk assessment of Arial khan river floodplain under future climate change scenarios. MSc Thesis, Department of Water Resources Engineering, Bangladesh University of Engineering and Technology, Dhaka.

Roy, B., Khan, M., Islam, A., Mohammed, K., & Khan, M. (2021). Climate-induced flood inundation for the Arial Khan River of Bangladesh using open-source SWAT and HEC-RAS model for RCP8.5-SSP5 scenario. *SN Applied Sciences*, *3*(6). doi: 10.1007/s42452-021-04460-4

Sai, F., Cumiskey, L., Weerts, A., Bhattacharya, B., & Haque Khan, R. (2018). Towards impact-based flood forecasting and warning in Bangladesh: a case study at the local level in Sirajganj district. *Natural Hazards and Earth System Sciences Discussions*, 1–20. doi:10.5194/nhess-2018-26

Saksena, S. (2015). Investigating the role of DEM resolution and accuracy on flood inundation mapping. *World Environmental and Water Resources Congress 2015*. doi: 10.1061/9780784479162.220

Saksena, S., & Merwade, V. (2015). Incorporating the effect of DEM resolution and accuracy for improved flood inundation mapping. *Journal of Hydrology*, *530*, 180-194. doi: 10.1016/j.jhydrol.2015.09.069

Salvia, M., Grings, F., Ferrazzoli, P., Barraza, V., Douna, V., Perna, P., Bruscantini, C., & Karszenbaum, H. (2011). Estimating flooded area and mean water level using active and passive microwaves: the example of Paraná River Delta floodplain. *Hydrology and Earth System Sciences*, *15*(8), 2679-2692. doi: 10.5194/hess-15-2679-2011.

Schumann, G., & Bates, P. (2018). The need for a high-accuracy, open-access global DEM. *Frontiers in Earth Science*, *6*, 225. doi: 10.3389/feart.2018.00225

Şerban, G., Rus, I., Vele, D., Breţcan, P., Alexe, M., & Petrea, D. (2016). Flood-prone area delimitation using UAV technology in the areas hard-to-reach for classic aircrafts: case study in the north-east of Apuseni Mountains, Transylvania. *Natural Hazards*, *82*(3), 1817-1832. doi: 10.1007/s11069-016-2266-4

Sheonty, S.R. (2021). A comparative study between short- and long-reach flow simulations with 1D hydrodynamic model in a floodplain environment. M. Sc. Thesis, Institute of Water and Flood Management, Bangladesh University of Engineering and Technology.

Shrestha, A., Bhattacharjee, L., Baral, S., Thakur, B., Joshi, N., Kalra, A., & Gupta, R. (2020). Understanding Suitability of MIKE 21 and HEC-RAS for 2D Floodplain Modeling. World Environmental and Water Resources Congress 2020. doi:10.1061/9780784482971.024

Silvestro, F., Rossi, L., Campo, L., Parodi, A., Fiori, E., Rudari, R., & Ferraris, L. (2019). Impact-based flash-flood forecasting system: sensitivity to high resolution numerical weather prediction systems and soil moisture. *Journal of Hydrology*, *572*, 388-402. doi: 10.1016/j.jhydrol.2019.02.055

Skakun, S., Kussul, N., Shelestov, A., & Kussul, O. (2013). Flood hazard and flood risk assessment using a time series of satellite images: a case study in Namibia. *Risk Analysis*, *34*(8), 1521-1537. doi: 10.1111/risa.12156

Smith, P., Brown, S., & Dugar, S. (2017). Community-based early warning systems for flood risk mitigation in Nepal. *Natural Hazards and Earth System Sciences*, *17*(3), 423-437. doi: 10.5194/nhess-17-423-2017

Solaimani, K. (2009). Flood forecasting based on geographical information system. *African Journal of Agricultural Research,* 4 (10), 950-956.

Subramanya, K. (2008). *Engineering Hydrology*. 3rd ed., New Delhi: Tata McGraw-Hill.

Sumaiya (2017). Impacts of Dynamic Interaction between Astronomical Tides and Monsoon Wind on Coastal Flooding in Bangladesh. M. Sc. Thesis, Institute of Water and Flood Management, Bangladesh University of Engineering and Technology.

Takaku, J., T. Tadono, and K. Tsutsui, 2014. Generation of high resolution global DSM from ALOS PRISM. The International Archives of the Photogrammetry, Remote Sensing and Spatial Information Sciences, Suzhou, China, Vol. XL-4, pp. 243-248 https://www.researchgate.net/publication/303794517_VALIDATION_OF_AW3D_GLOBAL_DSM_GENERATED_FROM_ALOS_PRISM

Tollan, A. (2002). Land-use change and floods: what do we need most, research or management?. *Water Science and Technology*, *45*(8), 183-190. doi: 10.2166/wst.2002.0176

Tutor2u (2021). The exam performance specialists – Geography. Retrieved on 16 November, 2021, from https://www.tutor2u.net/geography/reference

UNDRO. (1988). Bangladesh - Floods Aug 1988. Situation Reports 1-13. United Nations Disaster Relief Organization (UNDRO), the Netherlands

USGS (2021). Shuttle Radar Topography Mission (SRTM). Retrieved on 16 November, 2021, from https://www.usgs.gov/centers/eros/science/usgs-eros-archive-digital-elevation-shuttle-radar-topography-mission-srtm-1-arc?qt-science_center_objects=0#qt-science_center_objects

Uuemaa, E., Ahi, S., Montibeller, B., Muru, M., & Kmoch, A. (2020). Vertical accuracy of freely available global digital elevation models (ASTER, AW3D30, MERIT, TanDEM-X, SRTM, and NASADEM). *Remote Sensing*, *12*(21), 3482. doi: 10.3390/rs12213482

Van Wesemael, A., Landuyt, L., Lievens, H., & Verhoest, N. (2019). Improving flood inundation forecasts through the assimilation of in situ floodplain water level measurements based on alternative observation network configurations. *Advances in Water Resources*, *130*, 229-243. doi: 10.1016/j.advwatres.2019.05.025

Vaz, A.C. (2020). Coping with floods- the experience of Mozambique. 1st WARFSA/WaterNet Symposium: Sustainable Use of Water Resources, 1-2 November 2000, Maputo.

WARPO. (2001). National Water Management Plan – Vol 2. Ministry of Water Resources, the Government of the People's Republic of Bangladesh.

Watanabe, Y., & Kawahara, Y. (2016). UAV photogrammetry for monitoring changes in river topography and vegetation. *Procedia Engineering*, *154*, 317-325. doi: 10.1016/j.proeng.2016.07.482

Wessel, B., Huber, M., Wohlfart, C., Marschalk, U., Kosmann, D., & Roth, A. (2018). Accuracy assessment of the global TanDEM-X digital elevation model with GPS data. *ISPRS Journal of Photogrammetry and Remote Sensing*, *139*, 171-182. doi: 10.1016/j.isprsjprs.2018.02.017

Westerveld, S. (2020). Comparing two drone based remote sensing approaches to create high resolution DEMs. MSc Thesis, Geo-information Science and Remote Sensing,Wageningen University, The Netherlands.

Wing, O., Sampson, C., Bates, P., Quinn, N., Smith, A., & Neal, J. (2019). A flood inundation forecast of Hurricane Harvey using a continental-scale 2D hydrodynamic model. *Journal of Hydrology X*, *4*, 100039. doi: 10.1016/j.hydroa.2019.100039

Xiong, S., Muller, J., & Li, G. (2017). The application of ALOS/PALSAR InSAR to measure subsurface penetration depths in deserts. *Remote Sensing*, *9*(6), 638. doi: 10.3390/rs9060638

Yalcin, E. (2020). Assessing the impact of topography and land cover data resolutions on two-dimensional HEC-RAS hydrodynamic model simulations for urban flood hazard analysis. *Natural Hazards*, *101*(3), 995-1017. doi: 10.1007/s11069-020-03906-z.

Yamazaki, D., Ikeshima, D., Sosa, J., Bates, P. D., Allen, G., & Pavelsky, T. (2019). MERIT Hydro: A high-resolution global hydrography map based on latest topography datasets. *Water Resources Research*, 55(6). doi:10.1029/2019wr024873

Yamazaki, D., Ikeshima, D., Tawatari, R., Yamaguchi, T., O'Loughlin, F., Neal, J., Sampson, C. C., Kanae, S., & Bates, P. D. et al. (2017). A high-accuracy map of global terrain elevations. *Geophysical Research Letters*, *44*(11), 5844-5853. doi: 10.1002/2017gl072874

Yang, C., & Tsai, C. (2000). Development of a GIS-based flood information system for floodplain modeling and damage calculation. *Journal of the American Water Resources Association*, *36*(3), 567-577. doi: 10.1111/j.1752-1688.2000.tb04287.x

Yarrakula, K., Deb, D., & Samanta, B. (2010). Hydrodynamic modeling of Subernarekha River and its floodplain using remote sensing and GIS techniques. *Journal of Scientific and Industrial Research*, 69, 529-536.

Yin, J., Yu, D., Yin, Z., Wang, J., & Xu, S. (2012). Multiple scenario analyses of Huangpu River flooding using a 1D/2D coupled flood inundation model. *Natural Hazards*, *66*(2), 577-589. doi: 10.1007/s11069-012-0501-1

Zeybek, M. (2018). Nash-Sutcliffe Efficiency approach for quality improvement. *Journal of Applied Mathematics and Computation*, *2*(11). doi: 10.26855/jamc.2018.11.001.